Layer-by-Layer Assembly of Bio-functionalized Carbon Nanotubes for Rapid and Discriminate Detection of Organophosphate Neurotoxins

by

Jeffrey Stephen Kirsch

A thesis submitted to the Graduate Faculty of
Auburn University
in partial fulfillment of the
requirements for the Degree of
Master of Science

Auburn, Alabama
August 3, 2013

Keywords: Layer-by-Layer Assembly, Carbon Nanotubes, Electrochemical Pesticide Sensor, Enzyme Immobilization

Approved by

Aleksandr Simonian, Chair, Professor of Materials Engineering
J.W. Fergus, Professor of Materials Engineering
D.J. Kim, Associate Professor of Materials Engineering

Abstract

Layer-by-layer assembly is a self-assembly nanofabrication technique that has been used to build electrochemical amperometric sensors to detect pesticides. Organophosphorus hydrolase (OPH) is an enzyme which catalyzes the hydrolysis of organophosphate compounds (e.g. pesticides and chemical warfare agents). Acetylcholinesterase (AChE) biosensors are traditionally used to detect neurotoxic compounds, which inhibit its ability to hydrolyze acetylcholine and acetylthiocholine. However, these biosensors suffer from non-selectivity; many different compounds are able to inhibit AChE activity. AChE and OPH have been immobilized onto carbon nanotubes to stabilize the enzymes and provide scaffolding support for sensor construction. Multi-analyte detection has been realized through the layer-by-layer assembly process by using multiple enzymes within the layers such as Glucose Oxidase and AChE. A multi-layered sensor shows the capability to discriminate between organophosphate neurotoxins and non-OP compounds, through comparison of the activity of AChE and the signal response from the products of OPH hydrolysis. Evidence is provided which suggests that OPH could be used in this fashion to protect acetylcholinesterase from OP compounds, preventing significant inhibition of AChE from up to 10^{-4} M paraoxon.

Acknowledgments

This thesis was supported by numerous funding sources including the AUDFS Center for their financial support, and grants NSF CBET-1317635 and USDA-20053439415674A. This material was based on work which supported ALS by the National Science Foundation, while working at the Foundation.

I would like to thank my advisor, Professor Simonian for his advice and mentoring throughout my graduate school experience; my committee members Professor Fergus and Professor Kim; Professor J. Wild and Drs. J. Grimsley and M. Wales from Texas A&M University for generously providing the enzyme OPH, as well as their expertise, hospitality, and guidance when I went to TAMU to train in its use; and Daniel Horn from Professor Virginia Davis' group for his guidance and advice in carbon nanotubes preparation. Xiaoyun "Shawn" Yang provided his advice, expertise and friendship as my fellow group-mate. I would also like to thank my other group-mates over the course of graduate school, Alice Zitova, Yuanyuan "Amy" Zhang, Diego Scouza, and Mary Arugula, as well as all of my friends here at Auburn. I want to thank the late Mr. L.C. Mathison for providing his advice and expertise with building my flow cell, which I could not have done without his help. I want to thank my family and girlfriend for their love and support. And finally I would like to thank my professors for their patience, understanding and guidance all throughout my graduate career, especially Professor Ash Curtiss for his friendship and advice for both graduate school and Biochemistry.

Table of Contents

List of Tables

List of Figures

List of Abbreviations

MWNT	Multi-Walled Carbon Nanotube
SWNT	Single-Walled Carbon Nanotube
OPH	Organophosphorus Hydrolase
OP	Organophosphate
PX	Paraoxon
GOx	Glucose Oxidase
AChE	Acetylcholinesterase
ATCh	Acetylthiocholine
ACh	Acetylcholine
ChOX	Choline Oxidase
FAD	Flavin Adenosine Dinucleotide
EDC	N-ethyl-N-(3-dimethylaminopropyl)carbodiimide hydrochloride
NHS	N-hydroxysuccinimide
Sulfo-NHS	sulfo-N-hydroxysuccinimide
PNP	*p*-nitrophenol
LbL	Layer-by-Layer
LSV	Linear Sweep Voltammetry
CV	Cyclic Voltammetry
emf	electromotive force

A	Absorbance
C	Concentration
I	Intensity
V_0	Velocity (absorbance/min)
FET	Field Effect Transistor
Au	Gold
NP(s)	Nanoparticle(s)
TAMU	Texas A&M University
LD_{50}	Lethal Dose resulting in death of 50% of patients

UNITS

Pa	Paschal
M	Molar (moles/liter)
V	Volt
A	Ampere
A.U.	Arbitrary Units

Publications

Kirsch, J. S., X. Yang, et al. (2012). "Layer-by-Layer Catalytic Interface for Electrochemical Detection of Multiple Substrates Featuring Bio-Functionalized Carbon Nanotubes." ECS Transactions **50**(12): 345-355.

Kirsch, J. S., C. Siltanen, Q. Zhou, et al. (2013). Biosensor Technology: Recent Advances in Threat Agent Detection and Medicine. (RSC Pending)

Conference Presentations

Kirsch, J. S. and A. Simonian (2012). Layer-by-Layer Catalytic Interface for Electrochemical Detection of Multiple Substrates Featuring Bio-Functionalized Carbon Nanotubes. ECS PRiME Honolulu 222, The Electrochemical Society.

Kirsch, J. S., V. A. Davis, et al. (2012). Direct and discriminative detection of organophosphate neurotoxins for food and agriculture products. Sensors, 2012 IEEE, IEEE.

Kirsch, J. S., X. Yang, et al. (2013). Biofunctionalzed Carbon Nanotubes Sensors for Discriminate Detection of Organophosphorus Compounds. ECS Toronto 223, The Electrochemical Society.

Chapter 1: Introduction

Neurotoxic Compounds

There are two main classes of neurotoxic compounds: organophosphorus (OP) and non-organophosphorus. Organophosphorus compounds make up the single largest class of urban and rural pesticides. Over 1500 different OP neurotoxins have been synthesized in the last century, and more than 100 different compounds are currently being commercially utilized.[1] Many chemical warfare agents, notably Tabun (GA), Sarin (GB), Soman (GD), Cyclosarin (GF), and VX, are organophosphorus compounds, and all of these are or were part of the United States domestic inventory.[2] The use of chemical warfare agents has been banned since the Convention on the Prohibition of the Development, Production, Stockpiling and Use of Chemical Weapons and on their Destruction in 1997,[3] although the deliberate release of Sarin has occurred in 1994 and 1995 in a few Japanese cities by terrorist organizations. This demonstrates a concern that the use of these weapons could have significant impact on the lives of hundreds of thousands of people worldwide. Distribution of chemical agents of mass destruction by a terrorist attack is typically thought to occur through a single-source airborne release, and would result in acute exposure through inhalation, dermal sorption, or contamination of foodstuffs and water. There is also environmental concern for exposure to organophosphate pesticides (non-weaponized) through contamination of foodstuffs and ground water, leading to exposure through ingestion.

Neurotoxic pesticides are used due to the fact that most insects and pests of this nature have no vascular system to exploit in delivering poisons to prevent their destruction of crops and invasion of human dwellings. Unfortunately, most of these neurotoxic pesticides are also very

effective at harming pets and humans. Neurotoxic chemical warfare agents differ from pesticides in that they are engineered to be more effective at killing humans through manipulation of the chemical functional groups to make them more environmentally robust and lethal. The G-agents are all viscous liquids that vary in volatility and odor, while VX is amber-colored with a high vapor density and odorless. Sarin is universally considered to be the greatest vapor threat of the G-series. VX was formulated with a low volatility to increase the persistence of the toxin in the environment where it is spread. If VX vapors are allowed to accumulate, they are many times more potent and lethal than any of the G-series agents.[2]

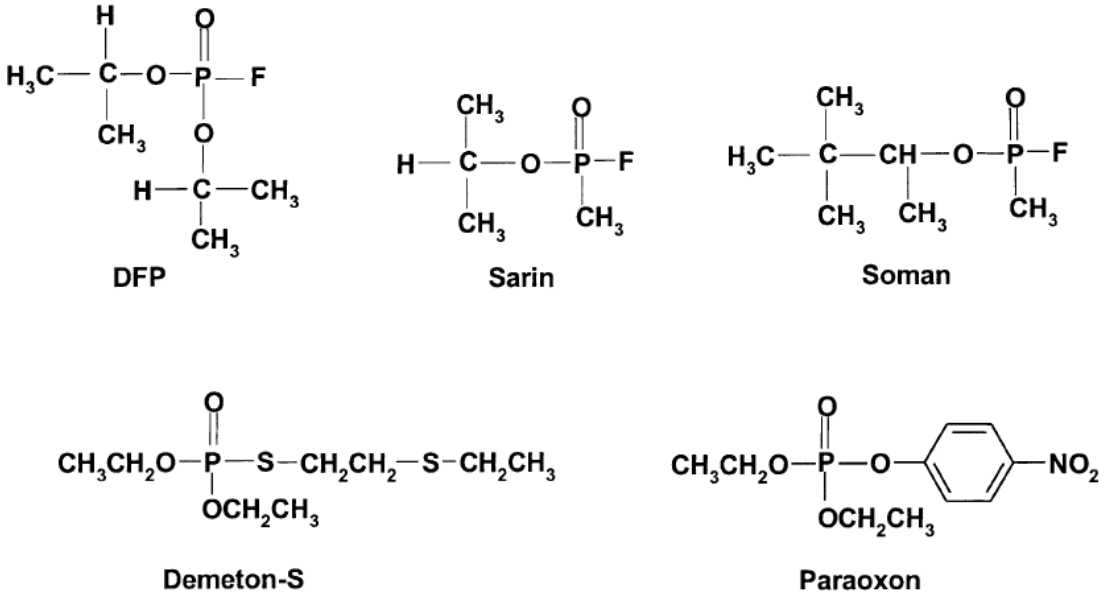

Figure 1: Chemical structures of some organophosphate neurotoxins.[4]

While OP and non-OP neurotoxins differ in many ways, their neurotoxic mechanisms of action are generally the same. Acetylcholine (ACh) is a chemical neurotransmitter crucial to the nervous system, and can be found at neural synapse and neuromuscular junctions. This chemical is released during the firing of synapses, and provides the ON/OFF logic in neurological signaling. Acetylcholinesterase is an enzyme which regulates the amount of acetylcholine through hydrolysis of acetylcholine to choline and acetic acid. Cholinesterases, especially

acetylcholinesterase, are susceptible to irreversible inhibition of their active site by neurotoxic compounds, phenols, and heavy metals. This inhibition of activity through the binding and blocking of the active site by neurotoxins prevents the enzyme from being able to hydrolyze acetylcholine, which will then accumulate in the synapses. The symptoms of neurotoxin exposure depend on how the victim was exposed and the degree of exposure. Usually the symptoms progress through excessive bronchial, salivary, ocular, and intestinal secretions; sweating; miosis; bronchospasm; intestinal hypermotility; bradycardia; muscle fasciculation; twitching; weakness; paralysis; loss of consciousness; convulsions; depression of the central respiratory drive; and death through asphyxiation. Treatment of neurotoxin poisoning has varying success based on the availability of treatment, amount of exposure, and the amount of time between exposure and treatment. The use of pralidoximes and atropine has some success in reactivating AChE (allowing the victim to recover) within a certain period of time and depending on which agent was used.[2] Table 1 shows the LD_{50} for several different OP compounds that have been developed for either agricultural or warfare applications. The discovery and development phosphotriesterase family of enzymes, notably organophosphate hydrolase, organophosphate acid anhydrolase, human paraoxonase, and squid diisopropyl fluorophosphatase, has led to their use in biosensors and decontamination aids.[5, 6]

Table 1: The Toxicity of Selected OP Compounds[7]

OP compounds	LD_{50} dermal (mg/kg)	LD_{50} oral (mg/kg)
Paraoxon	5	1
Parathion	100	42
Demeton-S	10	2
DFP	100	4
Sarin	1.5	0.1
Soman	1	0.1
VX	0.1	0.05

Biosensors

The biosensors field a relatively new multidisciplinary field attracting researchers from many different backgrounds including chemists, biochemists, microbiologists, physicists, and engineers. Biosensors are integrated devices capable of providing quantitative or semi-quantitative analytical information about a system using a biological recognition element which is in direct spatial contact with a transducer.[8] A sensor has three parts, the bio-recognition element, the transducer, and a signal processor (typically a computer). Bio-recognition elements are natural structures or materials which are capable of producing a change in a system when a target is introduced to that system, and can be classified as either kinetic or affinity-based. Common biorecognition elements include antibodies, cells, nucleic acids, and enzymes. Kinetic bio-recognition elements (typically enzymes) chemically convert the target into a compound, or produce some other kind of change in the system (e.g. consumption of reactants) which can be easily recognized by the transducer. Affinity-based bio-recognition elements (such as antibodies) capture the target through some type of binding mechanism, such as antigen-antibody binding, which then is able to be converted to a signal by the transducer. Transducers are elements of the biosensor which measure the change in a system and convert that change to electrical signal. Common transducers rely on electrochemical, optical, or physical changes.[9] Biosensors have been used over the past few decades to detect numerous analytes of significance to biodefense, medicine, and environmental monitoring, such as ricin,[10] botulinum toxins,[11] saxitoxin,[12] staphylococcal enterotoxin B,[13] trichothecene mycotoxins,[14] *Bacillus cereus*,[15] *Bacillus anthracis*,[16] *Campylobacter jejuni*,[17] cholera toxin,[18] *Escherichia coli*,[19] *Listeria monocytogenes*,[20] *Salmonella typhimurium*,[21] *Shigella* spp.,[22] *Staphylococcus aureus*,[23] many viruses,[24, 25] and cancer cells/markers.[26]

Electrochemical Sensors

Electrochemical sensors are a commonly used when an analyte of interest is able to be electrochemically detected either directly or indirectly. An electrochemical cell is formed by the combination of two half-cell reactions involving electrode-electrolyte interactions. The potential of the electrochemical cell can be measured using a voltmeter. A reference electrode can be used as one of the half-cell electrodes, which has a known emf. By using the reference electrode, a unknown value for the other half-cell emf can be determined. Typically a three electrode system is used, containing a working electrode, counter electrode, and reference electrode. There are three types of electrochemical sensors including potentiometry, voltammetry, and impedance. Potentiometery measures the cell potential at zero current. Voltammetry, or amperometry (which is extensively used in this thesis), measures the current based on the chemical reactions that occur when a potential is applied between the electrodes. Finally, impedance involves the use of an alternating current to perturb the cell, which is maintained near steady state and can give information about kinetics and diffusion.[9]

In voltammetry, there are several techniques available including linear-sweep voltammetry, cyclic voltammetry, and chronoamperometry. These techniques involve linearly varying the potential between the working electrode and reference electrode "wired" through a high concentration of an indifferent electrolyte (called the supporting electrolyte) and the electroactive species. The current in the cell is monitored continuously and a voltammogram is recorded with respect to potential. Linear-sweep voltammetry is the most straightforward technique and involves a simple increase in potential from one potential to another uni-directionally, while current is monitored. Cyclic voltammetry is very similar, except that an additional reverse potential sweep is applied (forming a hysteresis) and in some cases several

additional cycles. All electroactive substrates have a standard redox potential, E_0, where the ratio of the activities of the oxidative and reductive forms are in equilibrium at 1:1. Any increase in potential will increase the activity of the oxidative form above that of the reductive, whereas a decrease will increase the activity of the reductive form above that of the oxidative. This leads to a rise in the current of the system above the background current (resulting from residual current from impurities and double layer charging wherein the electrode-solution interface acts as a capacitor). The diffusion of oxidative species to the electrode from the bulk as it is reduced limits the current, and this rate of diffusion decreases leading to a peak in the current. The peak current is directly proportional to the concentration of the oxidized species, and the potential at which the peak occurs is the potential used for chronoamperometry. In cyclic voltammetry, the reverse scan shows a current peak for the reduced species when applied to reversible processes. For irreversible processes, the peaks will be shifted away from each other much more than the standard 0.056V, and in some cases will not be present at all. In chronoamperometry, the potential is held steady and current is monitored as a function of time. The decay of the current occurs due to the collapse of the diffusion layer, which eventually reaches an approximate steady state, thus the current will become independent of time. At this point, with the addition of a flow injection apparatus, small "bullets" or packages of analyte can be measured which form peaks at potentials slightly above the peak potential from LSV or CV (the "overpotential" to account for the difference between the experimental conditions and the theoretical potential determined thermodynamically). This peak height is proportional to concentration, and a calibration curve can be constructed for different peak heights at different concentrations of analyte. A time-independent form of the Cottrell equation (Equation 1) shows the relationship between current and concentration:

$$i = \frac{n \cdot F \cdot A \cdot D^{1/2} \cdot C_{Ox}}{\delta} \quad (1)$$

where i is the peak current, n is number of electrons transferred, F is the Faraday constant, A is the planar area of the electrode, D is the diffusion coefficient for the species, C_{Ox} is the concentration of oxidized species, and δ is a constant related to the thickness of the diffusion layer.[9]

Carbon nanotubes

The properties and merits of carbon nanotubes as novel nanomaterials have been well documented. [27-33] Carbon nanotubes are classified according to the number of concentric graphene cylinders which dictate their structure and properties: Multi-walled (MWNTs), double-walled (DWNTs), and single-walled nanotubes (SWNTs). Multi-walled carbon nanotubes are characterized by several concentric graphene cylinders with the ends of each individually capped with hemispheric fullerenes. Double-walled carbon nanotubes consist of two cylinders while single-walled have a single cylinder. All of these are produced with random distribution of diameters and are held together in bundles by van der Walls forces. Based on their lattice structures, SWNTs can be either armchair, zigzag, or chiral, which determine their electronic properties. Armchair nanotubes are conductive or "metallic" while zigzag and chiral nanotubes are either metallic or semiconducting. Currently there is no way to produce a single type of nanotube; however they generally are produced in a 1:2 ratio of metallic to semiconducting. The room temperature conductivity of a rope of SWNTs ranges from 10,000-30,000 S/cm. They also have a Young's modulus of about 1 TPa, and excellent mechanical properties, which make them ideal scaffolding structures.[33]

Raw carbon nanotubes self-assemble in bundles held together by van der Walls forces, and this causes difficulties in dispersion of the nanotubes in aqueous media, which is necessary

for their application in biological materials. They have no functional groups in their structure, making the use of solvents difficult, which means that chemical modification typically must be used in order to disperse nanotubes.[33] Davis' research group has described several techniques using biomaterials to disperse nanotubes including DNA and lysozyme.[29, 30, 34] Carbon nanotubes have been widely dispersed using the sulfuric/nitric acid treatment, and also using surfactants, water-soluble polymers, and interaction with biological molecules. The technique employed in this thesis utilized the sulfuric/nitric acid treatment which preferentially disrupts the aromatic ring structure at the ends of the nanotubes, and introduces carboxylic acid groups, which can be used to covalently attach biomaterials. However, this acid treatment destroys the electronic structure of the carbon nanotubes, and therefore the electrical properties cannot be fully utilized.[33, 35]

Enzymes/Enzyme Immobilization

Enzymes are proteins which are specialized to catalyze metabolic reactions by dramatically reducing the activation energy necessary for a chemical reaction to occur. In essence, they provide a thermodynamic shortcut for chemical processes. Enzymes are highly specific to their substrates, making them ideal biorecognition elements for biosensors requiring highly selective acquisition of target molecules. Many enzymes carry out their catalytic functions relying solely on their protein structure, while others require non-protein components such as metal ions or organic molecules called cofactors. Because enzymes are proteins, they rely on a stable set of conditions to maintain their structure and therefore activity, and are susceptible to denaturation. Enzymes are highly pH and temperature sensitive, as these conditions affect the secondary and tertiary structure of the protein, and pH can affect the ionization of the enzyme. Generally, enzymes are only active in a limited pH range and have a

particular pH which is considered optimal for activity. The substrate (the "reactant") may also have ionizing groups, which may interact with the enzyme differently at various pH. Increasing temperature will generally increase the rate of catalysis, up until it reaches a temperature where thermally induced denaturation occurs, and competes with the thermodynamic increase in reaction rate.[36]

Enzyme kinetics is concerned with determining the maximum reaction velocity that an enzyme can attain, and is based on several factors including concentration of substrate. At high concentrations of substrate, the rate of reaction does not depend on the concentration, and saturation occurs, wherein every enzyme active site is occupied by substrate. Michaelis and Menten proposed a theory which generally follows the observed phenomena in enzyme kinetics. They assumed that the enzyme (E) and its substrate (S) associate reversibly to form an enzyme-substrate complex (ES), which results in the generation of product (P):

$$E + S \overset{k_1/k_{-1}}{\longleftrightarrow} ES \overset{k_2}{\rightarrow} E + P \tag{2}$$

where k_1, k_{-1}, and k_2 are rate constants for each step of the reaction. These form what is called the Michaelis constant, K_M (described in detail later).[36]

$$K_M = \frac{k_{-1}+k_2}{k_1} \tag{3}$$

The use of enzymes as biofunctional structures has recently been a focus of many research groups. However, there is concern over the longevity, stability, and robustness of structures which are made from fragile and volatile enzymes. Enzymes require specific conditions to maintain their activity, and after time, heating, and exposure to the elements there is a distinct and measureable loss of activity. Therefore research has been focused into making enzymes more stable and robust without compromising their activity. This has been accomplished through several means, either by entrapment in a permeable polymer or by

covalent immobilization/physical adsorption onto a scaffolding material. For mechanical robustness and electrochemical sensing purposes, carbon nanotubes are an ideal material for scaffolding. However, in order for the nanoscale properties of carbon nanotubes to be transferred into micro/macro scale devices, there are a few challenges that must be overcome. Mainly, there are three issues: dispersion, controlling assembly, and efficient loading transfer.[27-31, 33, 37-42]

Organophosphate Hydrolase

In 1996, Rainina et al., from Wild's research group at Texas A&M, described a very special enzyme sequestered and purified from recombinant *E. coli* for the direct detection of organophosphate neurotoxins. This enzyme belongs to the phosphotriesterase family of enzymes, and was the first as such described for use as a recognition element in a biosensor. This enzyme, known as organophosphate hydrolase (OPH), catalytically cleaves P-O, P-F, P-S, and P-CN (preferentially cleaving P-O bonds) bonds of the phosphotriester (organophosphate) and releases two protons, which can be quantitatively correlated to the amount of organophosphate hydrolyzed (through pH measurements). Rainina et al. developed a pH based potentiometry biosensor with a linear detection range for paraoxon of 0.25 – 250 ppm (0.001 – 1.0 mM). [1] Richins et al. developed a similar biocatalyst based on the work pioneered by Wild at TAMU, in which they anchored OPH to the cell wall surface of *E. coli* by forcing the cell to express the proteins on the surface to degrade OP neurotoxins. [43] Wild's group at TAMU genetically modified OPH into several different mutants which showed improved activity towards specific agents such as Soman, Acephate, or VX, adding the possibility to selectively detect and destroy pesticides and chemical warfare agents. [44] Russel et al. developed a poly(ethylene glycol) hydrogel encapsulate seminapthofluorescein (SNAFL)-OPH conjugate as a self-reporting biorecognition element, as SNAFL is a pH-sensitive dye, changing its emission

spectrum at a wavelength of 550 nm in response to pH changes. Using spectrofluorimetry, they could readily detect paraoxon as low as 8×10^{-7}, and the sensor remained stable against denaturation, leaching, and photobleaching when stored in ambient conditions. [44]

Several transduction strategies have been employed with OPH in biosensors including pH electrodes,[1] fluoride ion-sensitive electrodes,[45] pH responsive dyes,[44] pH sensitive field effect transistors (pHFETs),[46, 47] optical techniques,[48-55] and electrochemical techniques.[31, 56, 57] Simonian et al. use pHFETs with OPH immobilized at pHFET gate and an unmodified pHFET gate was used as the reference, and changes in the bulk pH were monitored through measuring the change in the common source voltage. Local pH changes at the modified gate were amplified and voltage was measured and correlated to concentration. [47] Simonian et al. also used Au nanoparticles with fluorophore decoys to exploit changes in fluorescent intensity based on the distance between these two. OPH was immobilized onto the Au NP and the decoy fluorophore was incubated with the NP-enzyme conjugates. When the substrate was introduced to the system, the affinity of the enzyme for substrate caused it to release the decoy, reducing the intensity of fluorescence in proportion to concentration of substrate.[48] Rogers et al. developed a fluorescence based assay to detect a common product among all substrates to OPH, such that they were able to detect any substrate using the same mechanism. They immobilized fluorescein isothicyanate onto the enzyme, which is a pH dependent fluorescent reporter, and monitored the change in pH when exposed to substrate.[55] Simonian's group has demonstrated the enhanced stability and robustness of immobilized OPH on carbon nanotubes and exploitation in building thin films for detecting paraoxon directly using amperometric electrochemical sensors.[7, 31, 56, 57]

Organophosphate Acid Anhydrolase

Organophosphate acid anhydrolase (OPAA) is a prolidase enzyme the encoding genes for which were cloned and sequenced from two species of *Alteromonas*. Similar to OPH, it is capable of hydrolyzing a wide range of organophosphates with P-F, P-O, P-CN, and P-S bonds. [4, 58] It has preferential activity toward P-F bonds and minimal activity for P-O or P-S bonds, and is the enzyme of choice for destroying fluorine-containg organophosphates (e.g. Sarin and Soman). Diisopropylfluorophosphate (DFP) is a phosphonofluoridate neurotoxin which is an ideal analogue for chemical warfare agents due to its similarity to Sarin and Soman in structure but significantly reduced toxicity. [4, 59] Zheng et al. used fluorescence and other spectroscopic techniques to analyze the catalytic hydrolysis of DFP by OPAA, showing its use as a recognition element in biosensors. [59] Simonian et al. used OPAA in a pH based biosensor to discriminately detect DFP in concentrations as low as 20 µM with no response towards P-O and P-S bond containing OP pesticides such as paraoxon and demeton-S. [4]

Acetylcholinesterase

Acetylcholinesterase (AChE) and other cholinesterase enzymes are traditionally used as the biorecognition element in neurotoxin biosensors through inhibition assays based on electrochemical or piezoelectric transduction. The main advantage to this system is its high sensitivity to as low as 10^{-11} M. The most commonly used techniques involve amperometric detection using a synthesized derivative of acetylcholine called acetylthiocholine, and most of the focus involves the incorporation of this enzyme with novel nanomaterials to increase the sensitivity or avoid other problems.[60-62] Below is the reaction scheme for the hydrolysis of ACh by AChE.

$$ACh + H_2O \xrightarrow{AChE} Choline + Acetic\ Acid$$

Acetylthiocholine (ATCh) is used in place of ACh to avoid the need to use choline oxidase and a mediator, since ACh is not electroactive. The product of hydrolysis for ATCh is thiocholine (TCh) and allows for direct amperometric study of AChE, simplifying the system and allowing for rapid determination of enzyme activity. The main disadvantage for AChE inhibition-based sensors is the destruction of enzyme activity, which means the sensor must be discarded after use, or the enzyme must be replaced. Additionally, different neurotoxins inhibit the enzyme to different extents, meaning that calibration of the sensor to an unknown mixed sample could be almost impossible.[63, 64] Thus, Bachmann et al. have used different variants of AChE to detect pesticides using artificial neural networks to discriminate between paraoxon (an organophosphate) and carbofuran (a carbamate). Using four different variants of AChE, they constructed a disposable multi-sensor with the ability to discriminate between binary samples of pesticides through the use of an artificial neural network algorithm for data processing.[63, 64]

Several groups have attempted over the past few decades to genetically engineer AChE to become more sensitive to pesticides at low concentrations and improve the selectivity for the enzyme through increased sensitivity towards specific organophosphates and carbamates.[65] Standard electric eel AChE is not sensitive enough for trace analysis of pesticides; therefore Shulze et al. engineered an AChE enzyme from *Nippostrongylus brasiliensis* "AChE B" through introduction of mutations into the protein sequence. Their modifications lead to an increase in the sensitivity of their enzyme to 10 of 11 pesticides that they tested, and were capable of detecting concentrations of 11 of the 14 most important OPs and carbamates below 10 μg/kg. Their mutant enzymes also exhibited higher temperature stability and storage time as there was no loss in sensitivity of immobilized enzyme on screen printed electrodes after 17 months in storage at room temperature.[66, 67]

Liao et al. developed a liquid crystal biosensor based on enzymatic catalyzed growth of Au nanoparticles. AChE was used to hydrolyze acetylthiocholine, forming thiocholine which reduced $AuCl_4^-$ to Au NPs, avoiding the use of gold nanoseeds. Large Au NPs attenuate the optical signal of the LC biosensor, which disrupts the orientation of the liquid crystals. When hydrolysis of ATCh was mediated by AChE in the presence of an inhibitor or acetylcholine (which competes for hydrolysis with ATCh), catalytic growth of the Au NPs was reduced (less thiocholine), which affected the response from the liquid crystal orientation. They could detect OP neurotoxins to 0.3 nM and ACh to 15 μM.[68]

Other Inhibition-based Enzymes

There are many other enzymes that have been used in inhibition based biosensing systems other than acetylcholinesterase and its variants. Luque de Castro and Herrera discussed in their review the challenges of non-selectivity of inhibition-based enzyme sensors.[69] Patel reviewed the availability of inhibition-based biosensors that are currently available for the detection of a wide range of chemical compounds and food-borne contaminants.[70] Amine also reviewed a selection of biosensors that are based on enzyme inhibition in pollutant and toxic compound determination.[71] While cholinesterases are the most widely used in inhibition-based neurotoxin biosensing, there are many other enzymes that have been used in a similar systems for detection of analytes of interest including: Horse radish peroxidase, tyrosinase, urease, glucose oxidase, invertase, ascorbic acid oxidase, carboxyl esterase, catalase, etc.[72]

Glucose Oxidase

Glucose oxidase is a very well-studied enzyme that has found use in glucose sensors which are used both in clinical and home monitoring of blood glucose concentration for diabetes patients. The first biosensor developed by Clark and Lion in 1962 was based upon this enzyme

and its consumption of oxygen during the oxidation of glucose to gluconolactone.[73] Updike and Hicks used the Clark oxygen electrode and covered it with a polyacrylamide gel membrane containing this enzyme, demonstrating the first "enzyme electrode" for rapid and quantitative monitoring of glucose.[74] The glucose biosensor based on glucose oxidase can be separated into three generations. The first generation of glucose biosensors was based on the oxygen electrode developed by Clark and Lion. Several commercial devices were developed using this concept and are still in use today. There were several problems with this system which included the need for a controlled and constant level of ambient oxygen to produce reliable calibration. Another problem was the fairly high reduction potential needed to reduce oxygen (-0.7 V), which could cause other materials to interfere with the electrode. Guilbault and Lubrano suggested monitoring of the hydrogen peroxide produced as a result of oxidation, however, ascorbic acid could interfere with this reaction at a high potential of 0.65 V.[9, 75] Thus the second generation of biosensors was based on the use of mediators to replace oxygen. The most common mediators used were those based on iron and its complexes, such as ferrocene and ferrocyanide (hexacyanoferrate(III)). Ferrocene is generally the more successful of the iron mediators, and worked by reducing the flavin adenine dinucleotide cofactor in the active site of GOx, which oxidized glucose in the absence of oxygen. This was further reoxidized by the ferrocinium ion, which at proper potential releases electrons as it is reoxidized to ferrocene. These reagents provided a challenge to the development of biosensors, as all of the components were in solution. The work by Cass et al. in 1984 developed a sophisticated approach to immobilizing the enzyme and the ferrocene onto an electrode by evaporating the ferrocene from a toluene solution, and immobilizing the enzyme onto the surface and covered with a membrane.[9, 76] The third generation of glucose biosensors is based on directly couple enzyme electrodes. This is typically

achieved through charge-transfer complexes such as tetrathiafulvalene-tetracyanoquinodimethane (TTF-TCNQ) for direct electron transfer between the electrode and enzyme. Osmium redox sites with flexible polymers have been used by Degani and Heller in a similar fashion, and this work has recently been continued by Calvo et al. in layer-by-layer assembled nanostructures to build biosensors.[9, 77-80]

Multi-Enzyme Strategies

There is a great deal of merit to a system utilizing multiple enzymes for detection of analytes of interest. The versatility for detection of many analytes or complex process it provides could prove useful in systems where more than one type of enzyme may be needed to "cascade" a compound into a detectable analyte. The classic example of this process is the pairing of glucose oxidase with horse radish peroxidase, which eliminates the need for redox mediator in glucose detection. Multi-enzyme platforms could open up the possibility for multiplexed assays of many different analytes. Simonian et al. demonstrated the use of acetylcholinesterase (AChE) with organophosphate hydrolase (OPH) to screen samples for organophosphate neurotoxins and carbamates, in which they discovered that mutual interactions with AChE were not additive, but dependent on the type of chemicals. They were able to separate the effects of the inhibitors by removing the OP compounds with OPH before the samples reached the AChE. Their demonstration showed that it was impossible to have an adequate understanding of an unknown sample of multiple inhibitors with just a single enzyme. They were able to eliminate OP neurotoxins from the samples using OPH and able to detect the true concentration of non-OP neurotoxins with AChE inhibition.[81] Further, they used OPH and organophosphate acid anhydrolase (OPAA) to discriminate between various OP neurotoxins based on their unique activities towards those compounds at various kinetic rates (e.g.

discrimination between P-S and P-O versus P-F bonds).[4] With various other mutant phosphotriesterases showing different kinetic abilities towards different types of bonds, it may be possible to create a multiplex array that "fingerprints" the catalytic response to each of the different OP compounds.[47]

Mantha et al. used carbon nanotubes as a scaffolding support for OPH and DNA to build a layer-by-layer (LbL) assembled OP biosensor. The concept (detailed below) involves electrostatic interactions between oppositely charged species to build nanoscale layers. The increasing number of layers increases the activity due to the presence of more enzyme, and is easily renewed through adsorption of the lost layer.[57] This technique has been used to develop many different biosensors[57, 78, 82-85] and could be employed to construct multi-enzyme structures.

Layer-by-layer Assembly

Layer-by-layer assembly is a nanofabrication technique with has the advantages of being versatile, relatively inexpensive, and easy, while allowing a bottom-up approach to thin film preparation first described by Decher and Hong.[86] As shown in Figure 1, the assembly technique involves repetitive steps of adsorption of layers and a wash step. These layers adsorb onto the surface through electrostatic interactions between charged species, thereby allowing freedom to choose the components of the film, so long as they have a net charge. The relatively high concentration of species in solution will lead to excess adsorption of the species, which first is characterized by charge neutralization and then resaturation will cause charge reversal. Biomaterials, especially proteins which are water-soluble, are well suited for film development using this technique, due to the presence of charged sites at their surface which is dependent on pH. While the assembly process is very simple, the actual mechanism of assembly is not fully

understood. The quality and structure of the films depend heavily on experimental conditions, pH, drying process, washing process, temperature.[87]

Characterization of layer-by-layer assemblies is carried out in many different ways. Surface Plasmon resonance is a commonly used technique for measuring adsorption/desorption of molecules on a surface. This technique has been combined with electrochemistry by Baba et al. so that structural and thickness can be directly measured, while also measuring the electrochemical processes of the film. Surface Plasmon Spectroscopy was used as a technique to characterize the thickness of the ultrathin polymer film to the nanometer scale. Surface Plasmon resonance is a technique that observes the optical changes which occur between the interfaces of dielectric medium (such as water or air) and a thin metal film (usually gold). Surface roughness was measured using the light scattered off the surface of film, which also enhances the Plasmon effect. By connecting an electrode assembly to the instrument, cyclic voltammetry was able to be performed on the assembly, allowing Baba et al. to correlate the optical, electrochemical, and structural properties of the film.[88]

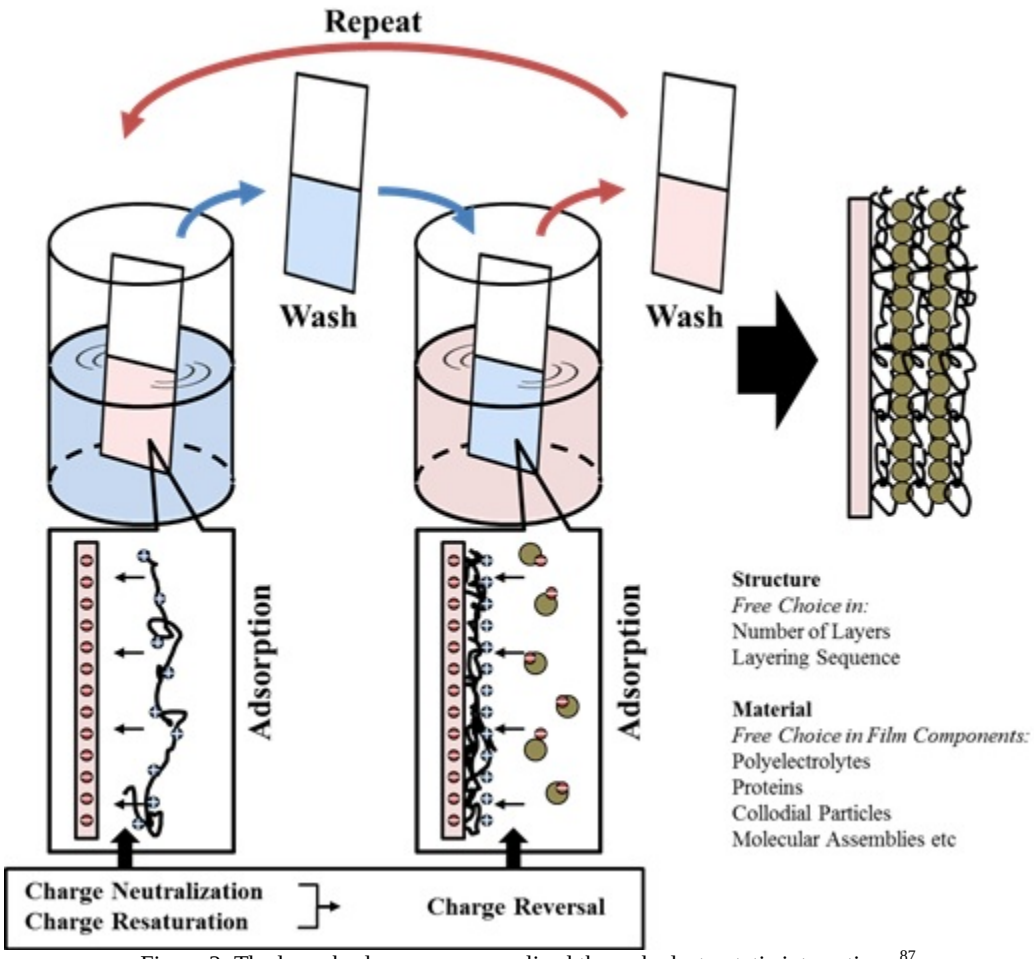

Figure 2: The layer-by-layer process realized through electrostatic interactions.[87]

Wang et al. built layer-by-layer assemblies using a templating techniques to make nanostructured materials with specific properties. The process begins with a template substrate, which has been charged so that the layers can adsorb onto the surface. The layer-by-layer process begins with the different charged polyelectrolytes so that the nanostructure can be tailored to the application. While electrostatic binding is usually the mechanism for layer-by-layer assembly, other mechanisms can be used to similar effect, such as hydrogen bonding, covalent interactions, co-pairing interactions, and hydrophobic interactions. After the desired film thickness, structure, and composition has been fabricated, the substrate is removed so that a free-standing nanostructure is produced. The templates can vary greatly, from planar templates to colloidal, and porous to non-porous.[89]

The diversity of the systems able to be built, demonstrates the versatility of the layer-by-layer assembly process. These systems include but are not limited to: free-standing and nanoporous films, nanotubes, capsules, nanoporous particles, biomimetic structures, and macroporous structures. The properties of these systems are easily controlled through experimental control, material choice, and template choice.

Layer-by-layer assembly has been used significantly in recent years to produce biofunctional catalytic surfaces for biosensor applications. Hodak et al. used glucose oxidase and a modified cationic polymer to build layer-by-layer assembled, reagentless glucose sensors. Glucose oxidase is anionic at neutral pH, while ferrocene modified poly(allylamine) (PAA-Fc) is cationic at neutral pH. By modifying the cationic polymer with ferrocene, this eliminates the need for a carrier buffer with the redox mediator, and will "electrochemically wire" the enzymes to the electrode. The glucose oxidase layers are sandwiched between layers of PAA-Fc and the layered structure is built on a thiol-modified gold surface. Because of the sandwiched structure, the need for mediator in solution or modification of the enzyme is eliminated, making the entire system self-contained. The GOx layers, being electrochemically wired together, act as a cohesive unit, and will enhance the signal, due to the additive effect of the catalytic layers, e.g. more enzyme to oxidize substrate.[77, 78, 82, 83]

Other biomolecules/biopolymers have uses in layered thin films. DNA is a commonly used biopolymer that has been used as an anionic layer in layer-by-layer assemblies. The applications for DNA include DNA sensors, DNA computers, DNA chips, etc. An assembly of DNA and PDDA (poly-(dimethyldiallylammonium chloride)) was formed by Pei et al. on a poly(ethylenimine) (PEI) coated substrate to study the kinetics of adsorption of the two species. Surface Plasmon resonance was used to quantitatively characterize the binding kinetics and the

assembly process of the layers. UV-Vis spectroscopy is also a handy means to qualitatively characterize the adsorption of layers onto a transparent substrate. When combined with flow injection analysis apparatus (FIA) SPR allows for *in situ* real-time analysis of layer adsorption.[90]

Lysozyme is an antimicrobial enzyme found in human tears and chicken egg whites. DNA and Lysozyme have been used to disperse single-walled carbon nanotubes (SWNT). Due to the anionic nature of SWNT-DNA and cationic nature of SWNT-LSZ, they are able to be used in the layer-by-layer process to assemble antimicrobial thin-films. An exposed SWNT-LSZ layer exhibits antimicrobial activity over the long-term, which is advantageous over a controlled release coating, since the coating is not used up over time.[29]

Mantha et al. used multiwalled carbon nanotubes (MWNT) as a scaffold for building a functional pesticide sensor for organophosphates. OPH was covalently immobilized onto the MWNT after functionalizing them with carboxylic acid groups. DNA dispersed MWNT were used as the anionic layers while MWNT-OPH (OPH has a pI 7.6)[91] and MWNT-poly(ethyleneimine) (MWNT-PEI) are used as the cationic layers. After building cushioning layers of MWNT-PEI/MWNT-DNA, MWNT-OPH replaced the PEI layers to provide catalysis of paraoxon to *p*-nitrophenol for electrochemical and optical detection. This sensor was stable, sensitive, and renewable by simply readsorbing the final catalytic layer.[57]

Layer-by-layer is extremely versatile and has the potential to provide multi-enzyme support to biosensing technologies, especially in formats where an analyte may not have a single recognition element, and several recognition events may be needed for a final result. The data presented in this thesis will attempt to convey the possibilities for multianalyte detection and other novel phenomena that layer-by-layer assembly affords its end-users.

Chapter 2: Experimental Procedures

Materials

MWNT, MWNT-COOH, SWNT-COOH prepared by a chemical vapor deposition (CVD) process were purchased from Nanolabs. MWNT prepared by CoMoCat process were purchased from Sigma Aldrich. Organophosphorus hydrolase (OPH) was generously provided by Dr. James Wild and his research group from TAMU. Paraoxon purchased from ChemService,Inc, dissolved in 25 mL DI water and stirred at 4°C for 72 hours, and the final concentration was verified using UV-Vis at 274 nm. 1-Naphthyl-N-methylcarbamate (Carbaryl or Methyl Carbamate), *p*-nitrophenol, acetylcholinesterase (AChE) from electric eel, acetylthiocholine (ATCh), acetylcholine (ACh), glucose oxidase (GOx) from Aspergillus niger, DNA (lyophilized salmon sperm salt), N-hydroxysuccinimide (NHS), sulfo-N-hydroxysuccinimide (sulfo-NHS), N-ethyl-N-(3-dimethylaminopropyl)carbodiimide hydrochloride (EDC), polyethyleneimine (PEI), 3,4-ethylenedioxythiophene (EDOT), sodium dodecyl sulfphate (SDS), lithium perchlorate, poly(styrenesulfonate) (PSS), ferrocene carboxylic acid (FCA), 2-(N-morpholino)ethanesulfonic acid (MES), N-cyclohexyl-2-aminoethanesulfonic acid (CHES), sodium phosphate dibasic, potassium phosphate monobasic, potassium chloride, phosphate buffered saline (PBS), and all other materials were all obtained from Sigma-Aldrich. DI water was obtained from a Millipore Direct-Q 5 Water system (resistivity 18MΩcm^{-2})

Equipment

Electrochemical measurements were obtained using a CHI 660 (CH Instruments, Austin, TX) potentiostat connected to a computer utilizing the chi990b software package. Typical

electrochemical set up consisted of a three-electrode system with a working electrode, counter electrode, and reference electrode. Reference electrode was made of Ag with an insulating layer of AgCl in a saturated KCl solution. Working electrode materials included glassy carbon, carbon ink, and gold. Counter electrode materials included stainless steel, carbon ink, and platinum. Batch mode measurements were made in a homemade 20 mL capacity cell with stopper. The BASi Unicell system was used for flow mode measurements, consisting of a glassy carbon (2mm diameter) working electrode and supporting electrodes all incased in a Teflon flow cell. Screen printed electrodes (from Pine Instruments) were used to perform experiments utilizing disposable technology, and also to test a homemade "universal" flow cell. All flow injection analysis (FIA) measurements were supported by the use of a KD Scientific Legato Series 200 dual syringe pump with a Rheodyne 7125 6-port injection system, with a glass syringe, all secured to an optical bench. A homemade well plate was fabricated to build the layer-by-layer assemblies on the BASi working electrodes. A UV-Vis spectrophotometer (Amersham Biosciences Ultrospec 2100 pro) was used to carry out enzyme kinetic experiments in cuvettes for the OPH enzyme and NT-OPH nanotube/enzyme conjugates. UV-Vis was also utilized to qualitatively determine the layer-by-layer assembly process. Weighing balances (Ohaus Analytical Plus AP250D 0.01mg resolution and Mettler Toledo NewClassic MF MS104S 0.1 mg resolution) were used to measure all sample masses for creating all buffers and solutions. A Branson 1510 bath sonicator was used to disperse all nanotube solutions, and a Sonics Vibra-cell CV33 tip sonicator was used to create both NT-DNA and NT-PEI nanotube/biopolymer conjugates. An Eppendorf 5415R refrigerated centrifuge was used to separate unbound biopolymer/enzyme from nanotube-bound biopolymer/enzyme. A refrigerated platform shaker (Barnstead/Thermodyne RotoMix Type 50800 placed inside a small refrigerator at 4°C) was used to create the nanotube-enzyme

conjugates. A room-temperature platform shaker (New Brunswick Scientific G24 Environmental Incubator Shaker) was used to stir nanotube-crosslinker samples, and during layer-by-layer assembly with the well plate. Vacuum filtration apparatus and 0.2 μm polycarbonate/PTFE filter membranes (Watman) were used to separate nanotubes from unreacted crosslinker, and in the carboxylation procedure. 300 kDa Dialysis membranes (Spectrum Laboratories) were used to separate unbound enzyme from the carbon nanotubes. The Palmsens portable potentiostat with an HP iPAQ pocketPC were used to demonstrate portable sensing. Big Spreeta (Texas Instruments/ICx Nomadics) SPR chips and apparatus connected to a computer with the MultiSPR software package were used to investigate binding interactions between the different layers of nanotube-biopolymer/enzyme conjugates. The Finnpipette II in different volume ranges was used to pipette all solutions. All measurements were performed at room temperature and ambient conditions unless otherwise stated. All enzymes were kept frozen in buffer or lyophilized and stored a freezer until conjugation. All enzyme-nanotube conjugates, enzyme solutions, and buffers were stored at 4°C until use unless otherwise stated. All buffers were prepared in DI water and pH was checked/adjusted using a Cole-Palmer pH Electrode and NaOH/HCl.

Standard Operating Procedures

Verification of Enzyme Activity

Pure OPH (0.55 mg) was diluted in 20 mM CHES containing 50 μM CoCl pH 8.7 to 0.00111 mg/mL. The Reaction Kinetics software package was set up to measure absorbance at 405 nm (the adsorption peak corresponding to p-nitrophenol) for one minute at two second intervals. Nine cuvettes were set up, each containing DI water (amount varied based on the amount of paraoxon) and 100 uL of 200 mM CHES containing 500 μM CoCl pH 8.7. The total

volume of solution after adding paraoxon (PX) and the enzyme to the DI water and CHES was 1 mL. 10 uL of the 0.00111 mg/mL OPH solution (kept refrigerated, and was only out of the refrigerator long enough to obtain the 10 uL) was added to the cuvette, parafilm placed over the top, turned over twice to mix, the bottom tapped twice on the counter, placed into the spectrophotometer and taken as the reference. 1 uL of PX (5.5 mM-10 mM) was then added to cuvette, the parafilm replaced, turned over twice to mix, the bottom tapped twice on the counter, and placed into the spectrophotometer to take the measurements over one minute. This step was performed very quickly (less than 5 seconds from the moment PX is added) to ensure that accurate/precise results were obtained from the instrument. After the measurement, the slope of the plot was taken as the "velocity" of the kinetics. This sequence was repeated for 2, 5, 10, 20, 40, 60, 80, 100 uL of PX. A Michaelis-Menton plot of the data was obtained, and the Origin Software was utilized to calculate k_{cat} and K_M. This procedure was repeated for NT-OPH conjugates, with one minor alteration. The NT-OPH was only diluted to ensure that the kinetic plot was linear, and in most cases was only a 1:10 dilution.

Carboxylation of MWNT, MWNT-COOH, SWNT-COOH

50 mg of carbon nanotubes were suspended into 200 mL 3:1 mixture of H_2SO_4 and HNO_3 and sonicated in the bath sonicator for 6 hours. The black suspension was then added to 800 mL of DI water and filtered through the 0.2 μm polycarbonate or Teflon filter. Polycarbonate is a hydrophilic membrane, but does not have a thick backing, so it is difficult to use. The Teflon filter is hydrophobic, but has a thick backing, which makes it easy to use. Isopropanol was used to "activate" the Teflon filter, so that the acid and water will filter through. Care must be taken not to mix a high concentration of HNO_3 with the IPA, because these compounds will violently react, forming nitrous oxide gas. After fully filtering the diluted acid

through the filter, a black "cake" was removed from the filter, and resuspended in 1 L of DI water, and subsequently filtered through a new membrane. This was repeated until the solution was near neutral pH. The filter with a black grease-like substance was removed from the vacuum apparatus, and placed onto an aluminum foil pan, and dried in a vacuum oven at 80°C overnight. The resulting black, paper-thin material was peeled off the filter membrane and placed into a scintillation vial for storage. The carboxylated carbon nanotubes would disperse easily in aqueous solutions with a small amount (ca 1 min) of sonication. It was observed that the "company-carboxylated" nanotubes (MWNT-COOH/SWNT-COOH) did not have the proper oxidation, as they would not disperse in aqueous media. They were carboxylated a second time using this method. MWNTs in some cases were carboxylated a second time to create more –COOH groups on the ends.

Immobilization of OPH

2 mg of the carboxylated CNT were dispersed in 0.5 mL of DI water using the bath sonicator for 1 hour. The result was an optically homogenous black solution. 0.5 mL of 50 mM MES buffer (pH 4.7) was added to the solution to stabilize the pH during the cross-linker activation step. 0.5 mL of a fresh 320 mM EDC solution and 0.5 mL of a fresh 20 mM sulfo-NHS solution were added to the CNT and MES, and stirred rapidly or shaken quickly (on the room temperature platform shaker) for 30 minutes. The solution was then filtered through a 0.2 µm polycarbonate filter and rinsed with MES buffer to remove excess EDC/NHS and the byproduct urea. The nanotubes were washed off of the filter using 3 mL of 20 mM phosphate buffer (pH 8.3) into a vial. This solution was sonicated for a short time (ca. 1 minute) to redisperse the nanotubes. 0.5 mL of a 1.11 mg/mL solution of OPH was added to the vial, and then placed on the refrigerated platform shaker and shaken at the lowest speed over night at 4°C.

The NT-OPH conjugate solution was then centrifuged at 13,200 RPM at 4°C for 45 minutes, the supernatant was removed and stored at 4°C, and the nanotubes were redispersed in 20 mM CHES with 50 µM CoCl (pH 8.7) for a total of three times to remove unbound protein (Note: when not being actively worked on, the solutions were kept refrigerated at 4°C). The final supernatant was checked for activity towards PX, and if necessary the nanotubes were centrifuged again until no activity in the supernatant remained. The final nanotube conjugate solution was dispersed in 1 mL of CHES and final concentration assumed to be 2 mg/mL.

Preparation of PEI/DNA

2 mg of carboxylated CNT were added to PEI (1 mg/mL) in 5 mL of DI water and sonicated with the tip sonicator (20% amplitude, 1 hr) in an ice bath to disperse the nanotubes. After sonication, the solution was centrifuged at 13,200 RPM for 45 minutes to reduce the amount of unbound polymer. The supernatant was discarded and the resulting black residue was redispersed in DI water with a small amount of sonication (ca. 1 min). Similarly, 0.1 wt% solution of DNA was dissolved in DI water at 35°C with a stir bar for 45 minutes. 0.1 wt% CNT (no carboxylation necessary) were added to the DNA solution and sonicated with the tip sonicator (20% amplitude, 1 hr) in an ice bath. The solution was centrifuged at 13,200 RPM for 45 minutes and the supernatant discarded to reduce the amount of unbound DNA. The black residue was redispersed in DI water with a small amount of sonication (ca. 1 min).

Pretreatment and Preparation of Layer-by-Layer Assemblies

Different substrate materials were used in the preparation of the layer-by-layer assemblies, and the "pre-treatment" for each was different. For glass slides, the slide was placed into piranha solution (3:1 H_2SO_4:H_2O_2) and heated for 15 minutes to hydrophilicize the glass by creating a negatively charged surface. On the Au Spreeta chips, a standard cleaning procedure

was used. The chips were carefully wiped with an ethanol soaked "Kim wipe" and washed with DI water. Then a small amount of piranha solution was applied for 3 minutes to the Au to remove any organic contaminants, and then the chip was washed in with DI water and was sonicated in DI water for 5 minutes. The chip was then plasma cleaned in air (oxygen plasma) for 5 minutes. Glassy carbon electrodes were polished thoroughly with 1 μm, 0.1 μm, and 0.05 μm alumina polish (Beuhler) and rinsed with DI water between each. The electrode was then sonicated in DI water for 15 minutes. Finally the electrode was electrochemically treated with 1 M NaOH for 5 minutes at 1.2V vs Ag/AgCl to produce a negatively charged surface and washed with DI water and dried with high purity nitrogen gas. Carbon ink screen printed electrodes were washed with DI water and treated with the 1 M NaOH for 2 minutes at 1.1V vs. Ag/AgCl to activate the carbon surface and produce negatively charged surface features. The electrode was then washed again with DI water. Excessive time in the NaOH treatment bath would etch away the carbon surface, so the time was reduced to prevent that from occurring.

Layer-by-layer assembly was accomplished by one of three methods. To maintain high concentration of the different solutions, the CNT-biopolymer/enzyme conjugates were drop cast onto the glassy carbon electrodes for a constant period of time (15 minutes, 30 minutes) and then rinsed with DI water, and dried with high purity nitrogen gas before the next layer. On the glass slides and screen-printed/glassy carbon electrodes, the CNT-biopolymer/enzyme conjugate solutions were of sufficient volume to allow the "sensor" to be dipped into the solution for a constant period of time (15 minutes, 30 minutes) and then rinsed with DI water, and then immediately immersed in the next solution (no drying step). For the Au Spreeta chips in SPR, the solutions were pumped at a constant rate (50 μL/min) over the surface of the chip for 15 minutes, or until a stable SPR signal was obtained. Then the next solution was pumped across

the SPR chip. In some cases, water or buffer were passed in between the CNT solutions. For all sensors, a set of "cushion" bilayers consisting of CNT-PEI and CNT-DNA (2 bilayers for a total of 4 layers) was built first. The strong electrostatic interactions between PEI and DNA allow the subsequent enzyme layers to bind to the substrate. Following the support cushion, enzymatic layers were alternatively built onto the support as the charge distribution dictated (i.e. switching between positively and negatively charged constituents).

For the protection of AChE from organophosphates, layer-by-layer assemblies with OPH as the top layer were prepared. For some of the sensors, an additional layer-by-layer assembly was built adjacent to the one built on the electrode, and a high concentration of cushioning layer solutions (CNT-PEI/CNT-DNA) were used to physically adsorb the first layers to the Teflon flow block for the FIA (flow injection analysis) electrodes. This adjacent layer was placed such that the inlet flow would cross the defending layer-by-layer assembly before reaching the detection layer-by-layer assembly. The final layers of both were allowed to dry to maximize the activity enzymatic layers (the thicker the layer, the larger the amount of enzyme, and thus higher activity). These layers were washed directly with DI H_2O to remove unbound CNT-enzyme conjugates.

Pretreatment of FIA Electrodes and Measurements

All FIA electrodes were electrochemically treated by using cyclic voltammetry (CV) to condition the electrode in the working buffer. This pretreatment step reduced the amount of time necessary to reach baseline stability in amperometric detection. A three electrode cell was set up including the Ag/AgCl electrode, counter electrode, and the FIA glassy carbon electrode with the working buffer used as the mobile phase. The electrode potential was cycled between -0.4 V and

1.0 V at a scan rate of 200 mV/s for a total of 40 sweeps (2 sweeps is equivalent to 1 cycle from the low potential to the high potential, then back to the low potential).

During any experiment, a stable baseline was first acquired before any measurements were made. All injections for FIA were preceded with an air-bubble in the sample loop to prevent mixing of the samples, and for a 50 µL loop, a total of at least 100 µL was injected. A consistent timing schedule for injections was kept in order to ensure that the baseline was reached each time after each injection.

Chapter 3: Organophosphate Pesticide Biosensor - OPH Immobilization and Sensor Construction

Immobilization of Enzyme to Carboxylated Nanotubes

The objective in the first part of the research was to recover OPH immobilization on carbon nanotubes and build an organophosphate pesticide biosensor using the layer-by-layer process. Following the work of Mantha et al., multiwalled carbon nanotubes (MWNTs) had to be carboxylated using an acid treatment protocol.[28] The carbon nanotubes were dissolved in a 3:1 Sulfuric Acid to Nitric Acid solution and sonicated for 6 hours, then the acid-MWNT solution was diluted using ultrapure deionized water and filtered through a vacuum filtration apparatus. The nanotubes were re-dispersed in water and filtered several times until neutral pH was reached. The final result was a black grease-like substance on the filter paper, which was dried in a vacuum-oven at 80°C for 12 hours. Carboxylation was deemed successful when the carbon nanotubes would disperse in water with minimal sonication (Figure 3).

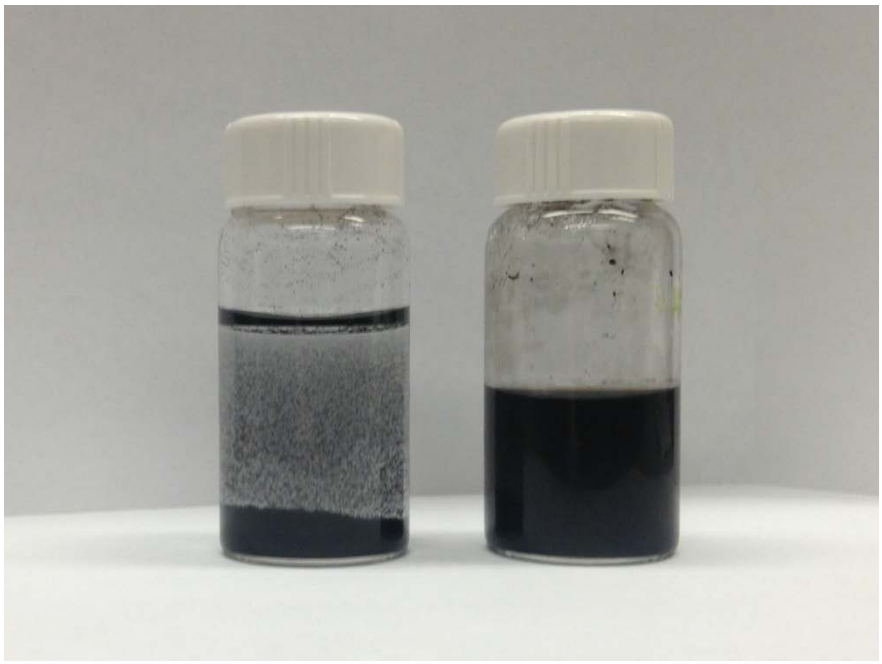

Figure 3: Comparison of Multi-Walled Carbon Nanotubes by visual reference. The (left) vial contains raw nanotubes in water after 5 minutes. The (right) vial contains acid-treated nanotubes in water after 5 months. The difference is clear that the the nanotubes treated with acid are very stable and easily dispersed in aqueous media.

Carbon nanotubes do not easily disperse in aqueous solutions, and chemical modification of the structure with carboxylic acid groups makes them hydrophilic, thereby allowing them to disperse in water. Mantha et al. demonstrated the difference between the raw and modified nanotubes using several characterization techniques including Raman Spectroscopy, Thermogravimetric Analysis, and Fourier Transform Infrared Spectroscopy.[28]

The carboxylated nanotubes (MWNT-COOH) were then dispersed in water using sonication. The carbodiimide chemistry was used to crosslink the carboxylic acid group from the carbon nanotubes to the amine groups on the enzyme organophosphorus hydrolase (OPH) via a two-step process. N-ethyl-N-(3-dimethylaminopropyl)carbodiimide hydrochloride (EDC) and N-hydroxysuccinimide (NHS) were added together with 2-(N-morpholino)ethanesulfonic acid (MES) buffer in differing ratios, concentrations, and pH to the carbon nanotube solution and stirred rapidly for 30 minutes. As seen in Figure 4, the crosslinker forms a stable amine-reactive

ester at the end of the carbon nanotube in the two-step process, as opposed to the unstable o-acylisourea ester.[92]

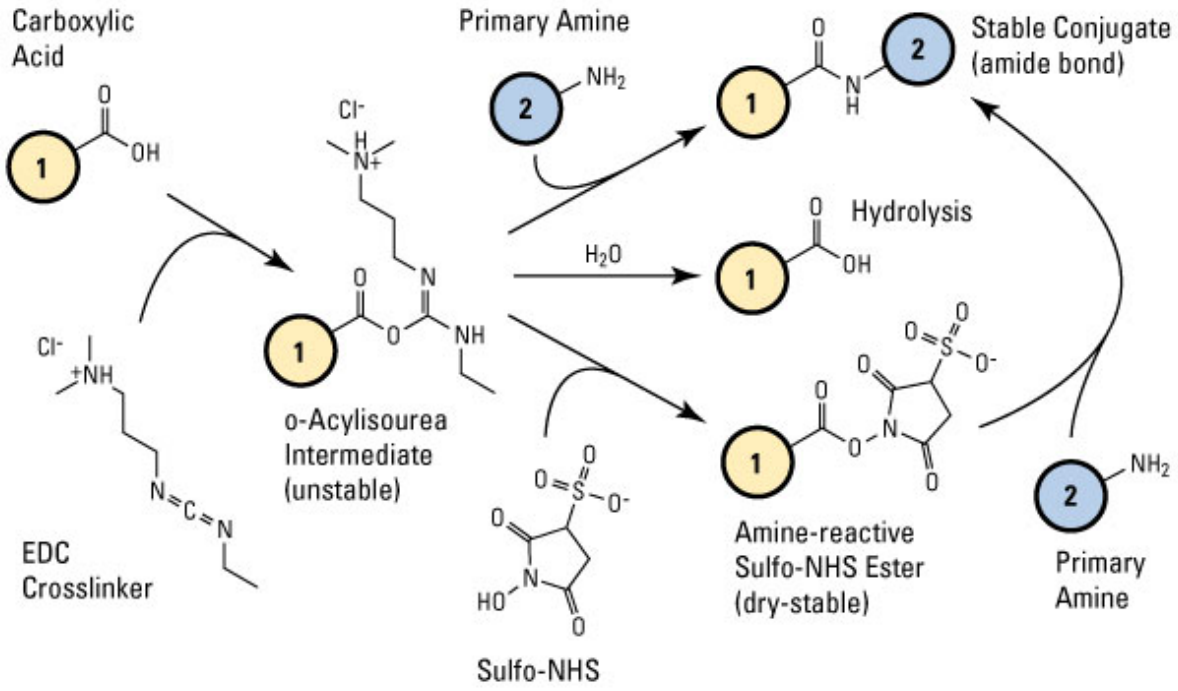

Figure 4: Chemistry of the carbodiimide chemistry via different processes. There are three routes for the reaction to occur: (top) in the presence of a primary amine (such as the enzyme), an amide bond is formed; (middle) if no amine is present then the bond is hydrolyzed back to a carboxylic acid group; (bottom) in the presence of NHS (or sulfo-NHS) a stable amine-reactive NHS ester is formed to replace the unstable o-acylisourea intermediate, which can then be reacted with the primary amine to form an amide bond.[93]

This increases the efficiency of the binding reaction, and allows the excess EDC to be removed by vacuum filtration. The other advantage of the two-step process is that it completely segregates EDC from the protein. While the one-step process (where EDC and the protein are directly reacted together with the carboxylic acid groups) is less complex, it is very inefficient and can lead to the creation of multi-protein complexes. Because proteins have carboxylic acid groups and amine groups they are susceptible to EDC crosslinking. By using the two-step process, the EDC and the protein never come into contact, thus no multi-protein complexes form.[92]

After vacuum filtration to remove excess crosslinker, the MWNT-NHS ester conjugate is recovered and redispersed into buffer (CHES, Phosphate, MES buffer, or a combination of them). The buffers are used to maintain physiological pH of the enzyme during immobilization. OPH is removed from the freezer, and then allowed to thaw in a refrigerator to maintain temperature control. After the enzyme has thawed, it is incubated with the MWNT-NHS ester solution on a platform shaker (slow speed ~30 rpm) for 12 hours at 4°C. The MWNT-OPH solution is then centrifuged at 13200 rpm for 45 minutes at 4°C and the supernatant is removed. This is performed at least three times to remove unbound enzyme from the solution. Finally the MWNT-OPH is concentrated to ~2 mg/mL. To ensure that all unbound enzyme is removed from the solution, enzyme kinetics is performed on the original enzyme, the MWNT-OPH, and the final supernatant (Figure 3 and Table 2).

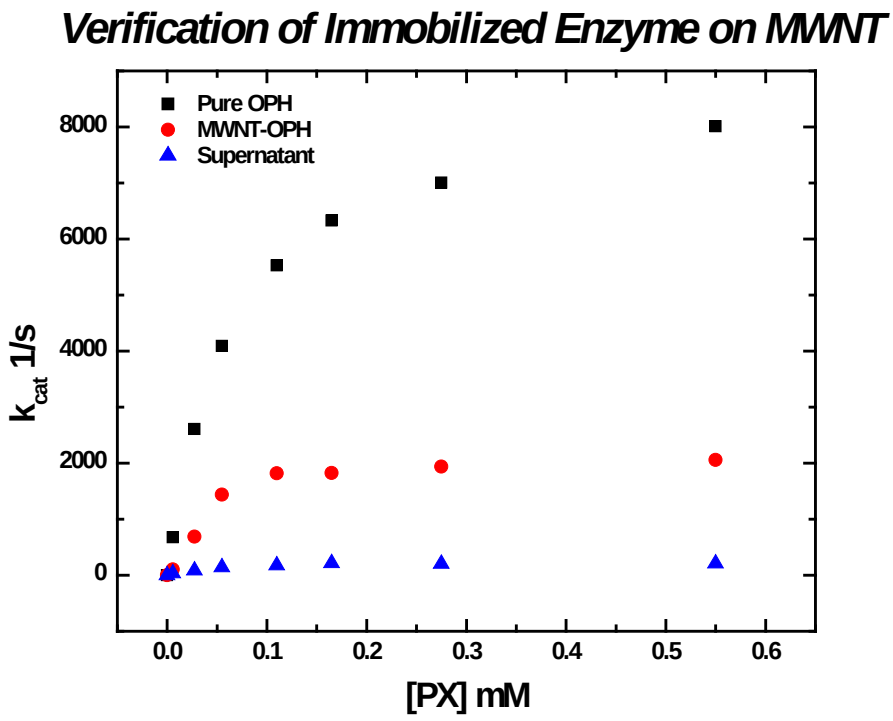

Figure 5: Michaelis Menton plot of free enzyme (Pure OPH), immobilized enzyme (MWNT-OPH), and the supernatant drawn off of the CNT-OPH solution. The increased activity of the CNT-OPH over the supernatant confirms immobilization of OPH onto the MWNT.

Table 2: Activity of OPH and Verification of Immobilization

	V_{max} (kcat·s^{-1})	K_M (mmol)	η_E (M^{-1}·s^{-1})
Pure OPH	8873	0.0658	1.35×10^{8}
MWNT-OPH	2306	0.044	0.52×10^{8}
Supernatant	237.8	0.0395	0.06×10^{8}

Enzyme kinetics is performed by measuring the rate at which a reaction is catalyzed by varying the concentration of substrate (the reactant) and the amount of catalyst (the enzyme). The easiest method to do this is by UV-Visible spectroscopy, wherein the change in absorption of light at a specific wavelength is recorded with respect to time. In this case the product, *p*-nitrophenol absorbs light at 405 nm wavelength. Concentration of product can be related to absorption of light by the Beer-Lambert law (Equation 4):

$$\log\frac{I}{I_0} = A = \varepsilon \cdot C \cdot l \tag{4}$$

where I_0 is the intensity of the incident light, I is the intensity of the transmitted light, A is the absorbance, ε is the extinction coefficient, C is the concentration of the product, and l is the path-length of the light (typically a cuvette at 1 cm).[9]

For enzyme kinetics, the instrument begins with a reference of the sample without the catalyst (enzyme) or the substrate (reactant). From there the catalyst or substrate is added to the cuvette and then the experiment begins by measuring absorbance with respect to time. Typically, the experiment for each concentration requires 1 minute, during which the absorbance is measured every 2 seconds. The data should be linear, and if not, then the amount of catalyst must be reduced and the measurement repeated, such that a linear slope for the change in absorbance over a period of 1 minute can be recorded. The slope of the linear data for each concentration is recorded as:

$$\frac{dA}{dt} = \frac{dA}{\min}$$

where *dA/dt* is the change in absorbance with respect to time. Using the derivative with respect to time of Equation 4, the amount of substrate catalyzed per second is calculated:

$$\frac{dA}{dt} = \varepsilon \cdot \frac{dC}{dt} \cdot l$$

$$V_0 = \frac{dA}{dt} \cdot \frac{1}{\varepsilon} \cdot \frac{1}{l} = \frac{dC}{dt} \tag{5}$$

$$V_0 = \frac{dA \cdot \mathrm{min}^{-1}}{\varepsilon} \cdot \frac{1}{60\mathrm{s}} \cdot 1\mathrm{cm} \cdot \frac{1L}{1000\mathrm{mL}} \cdot \frac{1\times10^6 \mu\mathrm{mol}}{\mathrm{mol}} = \frac{\mu\mathrm{mol}}{\mathrm{s}}$$

For paraoxon, the product is *p*-nitrophenol which has an extinction coefficient of 17000 at 405 nm. The data is plotted as either V_0 or k_{cat} versus concentration of substrate to obtain a Michaelis-Menton plot. The data is fitted to the Michaelis equation[94] (Equation 6) to determine V_{max} and K_m:

$$V_0 = \frac{V_{max} \cdot [S]}{K_M + [S]} \tag{6}$$

where V_{max} is the maximum rate of catalysis capable by the system due to saturation and K_M is the concentration of the substrate at ½ V_{max} and is the inverse of the affinity of the enzyme for substrate.

The turnover number, or k_{cat}, denotes the amount of substrate that can be converted to product per amount of enzyme per second. It is calculated by Equation 7

$$k_{cat} = \frac{V_{max}}{[E_T]} \tag{7}$$

where $[E_T]$ is the total amount of enzyme available in the reaction. The efficiency of the enzyme (η_E) can be calculated by Equation 8

$$\eta_E = \frac{k_{cat}}{K_M} \tag{8}$$

For the purpose of calculating k_{cat}, K_M and efficiency in Table 3, $[E_T]$ for both pure OPH and the MWNT samples was assumed to be the same. For the sake of normalization of the data, all V_0 data was converted to k_{cat} for each concentration of substrate, i.e. dividing the velocity by the concentration of enzyme in the cuvette, modifying Equation 7 as

$$k_{cat} = \frac{V_0}{[E_T]} \tag{9}$$

and subsequently normalizing these values to calculate a rough estimate of the amount of enzyme bound to the carbon nanotubes. This was accomplished by using the k_{cat} values for the pure enzyme in place of the numbers for each MWNT-OPH sample, and back calculating the concentration of enzyme that would be required to obtain those values.

$$[E_T] = \frac{V_0}{k_{cat}} \tag{10}$$

The values of $[E_T]$ were averaged together to form a rough estimate of the amount of enzyme bound, and using a simple % change calculation, the amount of bound enzyme was calculated. The assumption for the absolute amount of pure OPH was based on the concentration of enzyme for each experiment. Initially the same assumption was used for MWNT-OPH, but this was changed to include the absolute amount of OPH that was initially incubated with the activated nanotubes. This change occurred because binding efficiency in some cases was calculated to be over 100%, which is impossible. The change factors that the enzyme pulled to the carbon nanotubes and bound, and that if 100% binding efficiency occurred, meaning all of the enzyme was bound to the carbon nanotubes, then it would all be recovered during the centrifugation steps, and the concentration would change if the nanotubes were dispersed in a different amount of buffer.

The immobilization procedure was optimized to the amount of EDC and pH of the pre-incubation crosslinking step. First the amount of EDC was optimized at a constant concentration

of sulfo-NHS (20 mM) and pH of 6.5 (from Mantha et al.). As seen in Figure 6, as the amount of EDC increases, so does the activity and therefore the amount of OPH bound. However, because both the activity did not reach a maximum and there are several parameters dictating the immobilization, several subsequent experiments were conducted, varying those parameters in order to determine optimal conditions. The ratio between EDC and NHS was investigated as it has been suggested as one of the most important parameters.[41, 42] Figure 7 shows the effect on the ratio of EDC to NHS by varying NHS with respect to a constant concentration of EDC (20 mM) and pH of 6.5. These data suggest that an optimal ratio of 8:1, however, the total effect (overall there was a reduction in activity) is very minimal compared to EDC amount, and therefore another parameter was investigated.

The optimal pH for the carbodiimide chemistry as stated by Hermanson is in the acidic range (~4.5).[92] The pH of MES buffer was varied using NaOH from 4.7 to 6.6, while keeping the EDC concentration constant at 320 mM and NHS at 20 mM. When the pH was acidic, the immobilization efficiency was indeed higher as seen in Figure 8, and the effect was reduced at higher pH. Finally, the pH of the final incubation step was optimized for OPH, and phosphate buffer at a pH of 8.3 performed the best (results not shown). For the following sections in which other enzymes were immobilized, these parameters were used (320 mM EDC, 20 mM NHS in MES buffer at a pH of 4.7; incubate in Phosphate Buffer at a pH of 8.3) and it was assumed to be optimal for these enzymes as well, due to inability to accurately perform enzyme kinetics on these other enzymes. However, as suggested by Lahiri, the final pH of the buffer may be optimal at a pH level of 1 unit below the isoelectric point of the enzyme, but for the purpose of this thesis, that was investigated.[39] In Table 4, a summary of all data can be found with normalization data.

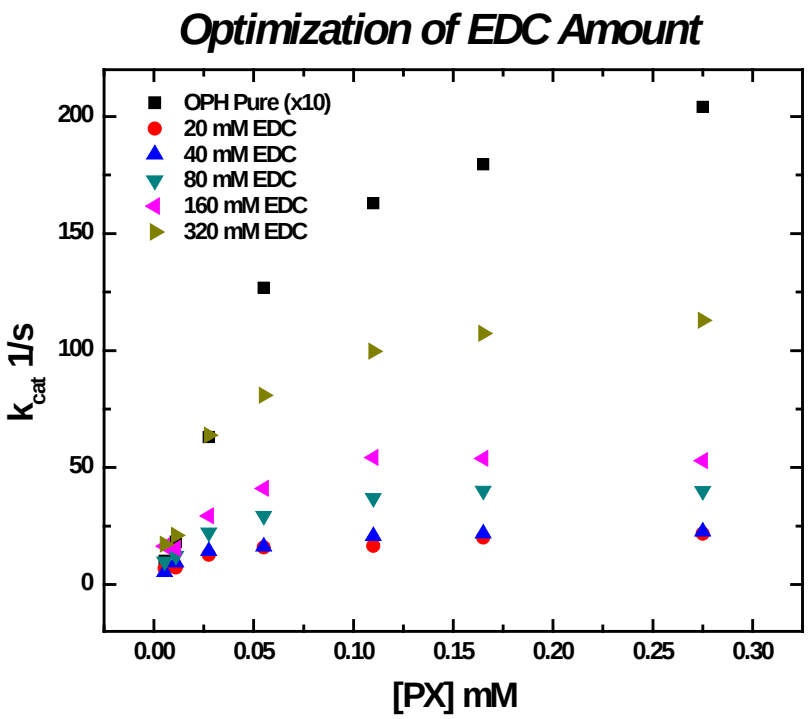

Figure 6: Michaelis-Menton plot showing the effect of concentration of EDC on the binding efficiency of OPH to the MWNT. The Pure OPH data points are reduced 10 fold in order to show all the data. As the concentration increases, the binding efficiency of OPH increases.

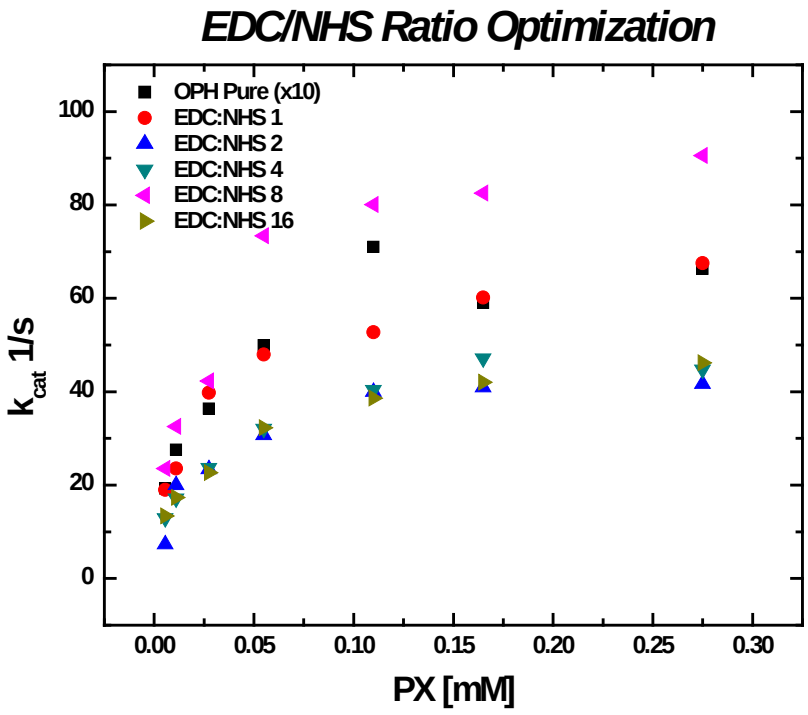

Figure 7: The effect of the ratio between EDC and NHS. Compared to the effect of absolute amount of EDC, there is very little effect, which may be due to the fact that the pH of the crosslinking step was not optimized, or due to the low amount of EDC.

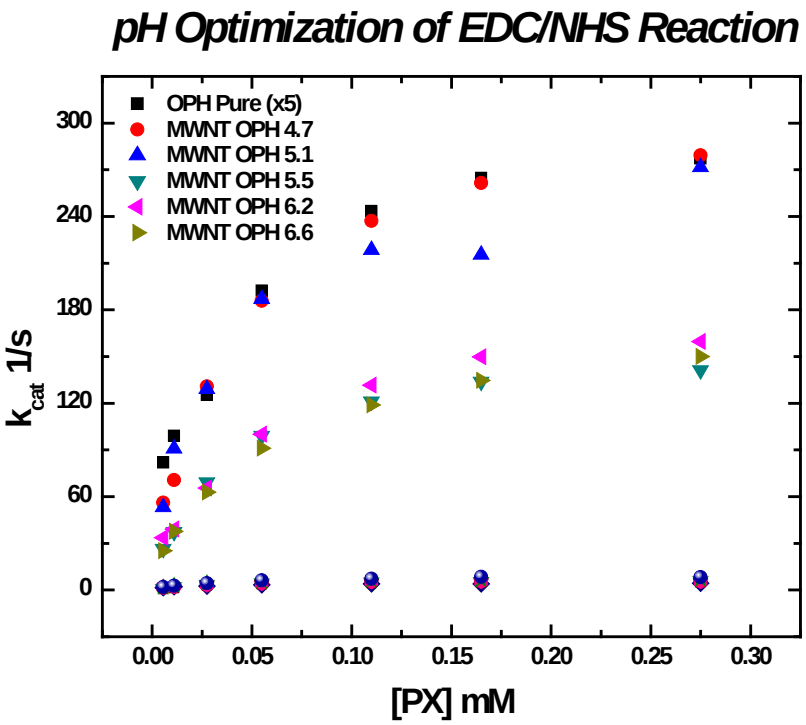

Figure 8: The effect of pH on the efficiency of binding for OPH onto MWNT. At the more acidic pH levels, the efficiency is higher. The data plotted at the bottom represents the supernatants from those samples, and as is shown they are significantly reduced.

Table 3: Enzyme Kinetics Data for Optimization of Pre-Incubation Parameters

EDC Optimization	k_{cat} (s^{-1})	K_M (mmol)	η_E ($M^{-1}sec^{-1}$)
Pure OPH	2655	0.07558	0.351×10^8
20 mM EDC	21.8	0.01932	0.011×10^8
40 mM EDC	23.96	0.01915	0.013×10^8
80 mM EDC	45.16	0.02704	0.017×10^8
160 mM EDC	62.78	0.02950	0.021×10^8
320 mM EDC	129.8	0.03482	0.037×10^8
EDC/NHS Ratio			
Pure OPH	716	0.01965	0.364×10^8
1	67.37	0.01952	0.035×10^8
2	45.5	0.02133	0.021×10^8
4	49.9	0.02451	0.020×10^8
8	97.16	0.02402	0.040×10^8
16	47.73	0.02299	0.021×10^8
pH Optimization			
Pure OPH	1508	0.02747	0.549×10^8
4.7	2228	0.03715	0.600×10^8
5.1	1933	0.02688	0.719×10^8
5.5	1122	0.03434	0.327×10^8
6.2	1305	0.04430	0.295×10^8
6.6	1206	0.04532	0.266×10^8
Supernatant 4.7	4.31	0.01307	0.003×10^8
Supernatant 5.1	6.31	0.02032	0.003×10^8
Supernatant 5.5	5.97	0.01746	0.003×10^8
Supernatant 6.2	7.05	0.01597	0.004×10^8
Supernatant 6.6	9.34	0.02757	0.003×10^8

Table 4: Pre-incubation Crosslinking Optimization

EDC amount	mg OPH	mg OPH bound	% bound	Normalized	Normalized
20 mM	0.78	0.0027	0.35%	28%	100%
40 mM	0.78	0.0028	0.36%	28%	100%
80 mM	0.78	0.0046	0.58%	46%	170%
160 mM	0.78	0.0066	0.84%	66%	240%
320 mM	0.78	0.0099	1.3%	100%	360%
EDC/NHS Ratio					
1	0.78	0.011	1.4%		100%
2	0.78	0.0067	0.86%		64%
4	0.78	0.0073	0.94%		69%
8	0.78	0.044	5.6%		410%
16	0.78	0.0072	0.92%		68%
pH					
4.7	0.78	0.14	18%	180%	
5.1	0.78	0.14	18%	180%	
5.5	0.78	0.073	9.4%	93%	
6.2	0.78	0.079	10.%	100%	
6.6	0.78	0.071	9.2%	91%	

Electrochemical Detection of Paraoxon

Paraoxon, a model organophosphate pesticide, is not an electroactive compound, meaning that when a potential is applied in an electrochemical cell, the chemical has no susceptibility to being changed by the potential. OPH hydrolyzes paraoxon into *p*-nitrophenol, which is electrochemically active, and as shown in the current vs potential graph (cyclic voltammetry) in Figure 9, is oxidized at 0.95V vs Ag/AgCl. This potential is extremely large with respect to other biosensors, and it can cause problems with electrode passivation and when electrochemical modification is required (such as PEDOT).[95, 96] PEDOT was tested at the higher potentials and was found to strip away when coming in contact with *p*-nitrophenol, and deemed unsuitable for electrode treatment in this application.

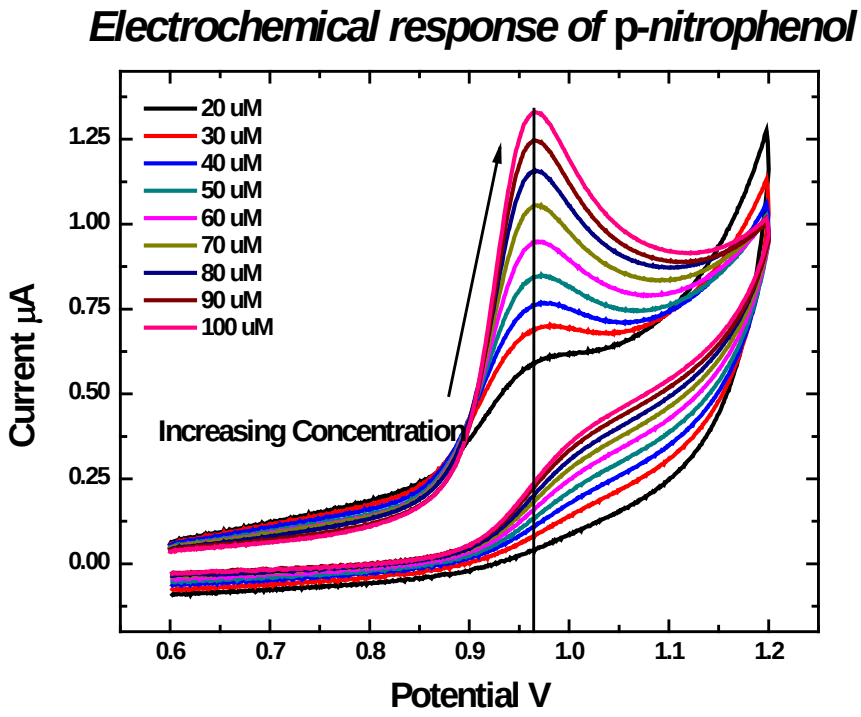

Figure 9: Cyclic voltammetry response for a glassy carbon electrode in PBS buffer with increasing concentrations of *p*-nitrophenol.

Carbon nanotubes as a novel nanomaterial have the promise to reduce the necessary potential to oxidize compounds,[40, 97, 98] but when acid-oxidized, the electronic structure of the

carbon nanotubes is destroyed (through disruption of the intrinsic nanotube sp^2 structure), therefore there is no reduction in required potential.[35] Additionally, there is currently no method for cost-effect production of nanotubes with known and controlled electronic and structural properties.[35] Nonetheless, the carbon nanotubes provide a scaffold for the enzyme and other biomaterials (PEI/DNA) and enhance the stability and mechanical properties of those biomaterials.[31] The layer-by-layer assembly nanofabrication technique provides a powerful tool for building novel sensing structures with versatility, long term stability, and renewability.[28]

Biosensors for detecting paraoxon were developed by electrochemical treatment of glassy carbon working electrodes in NaOH to induce a net negative charge and then alternatively adsorbing MWNT-PEI and MWNT-DNA to build a cushioning layer. The electrostatic interaction between PEI (+40 mV)[99] and DNA (-30 mV)[29] at neutral pH is extremely strong, therefore it is ideal as a precursor scaffolding before the catalytic layers. Two bilayers of MWNT-PEI and MWNT-DNA (as seen in Figure 10) were adsorbed before building the subsequent layers of MWNT-OPH and MWNT-DNA.

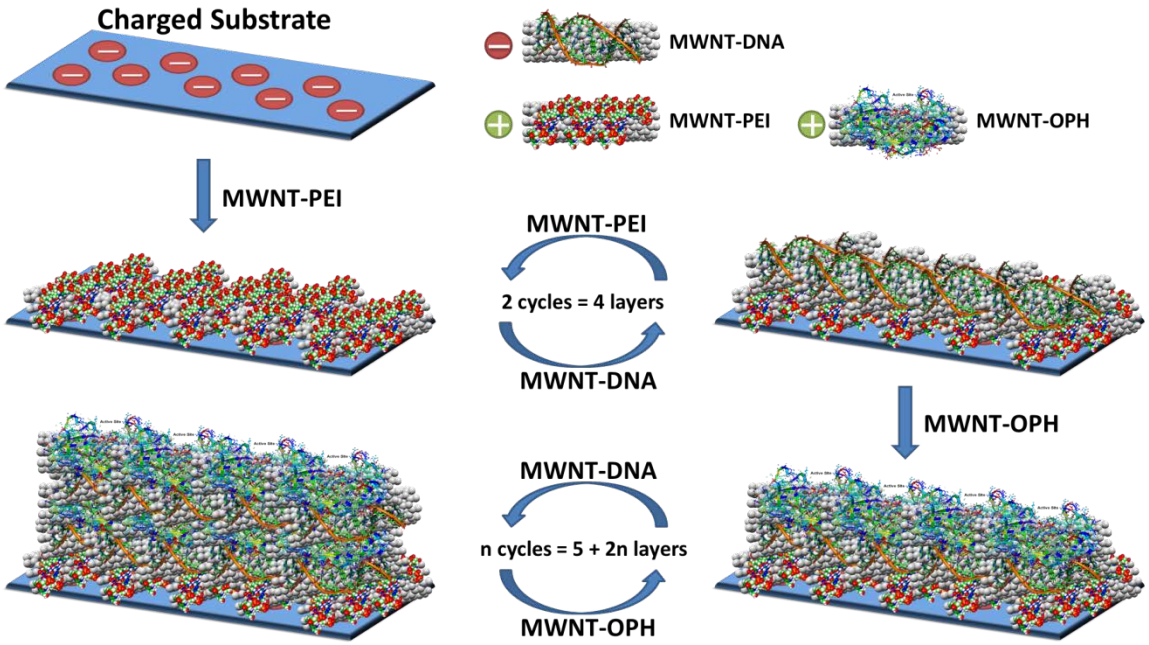

Figure 10: Layer-by-Layer assembly schematic for the OPH/DNA biosensor

The assembly of layers on glass slides demonstrates the attachment of the layers to each other (Figure 11) in UV-Visible spectroscopy. Mantha et al. showed that layers ending in OPH would provide higher activity, than layers ending in DNA, possibly due to the ability of the layer to have access to the bulk solution. Nonetheless, the layers are permeable to substrate, and subsequent research should be devoted to controlling the permeability of the layers through manipulation of thickness and porosity.

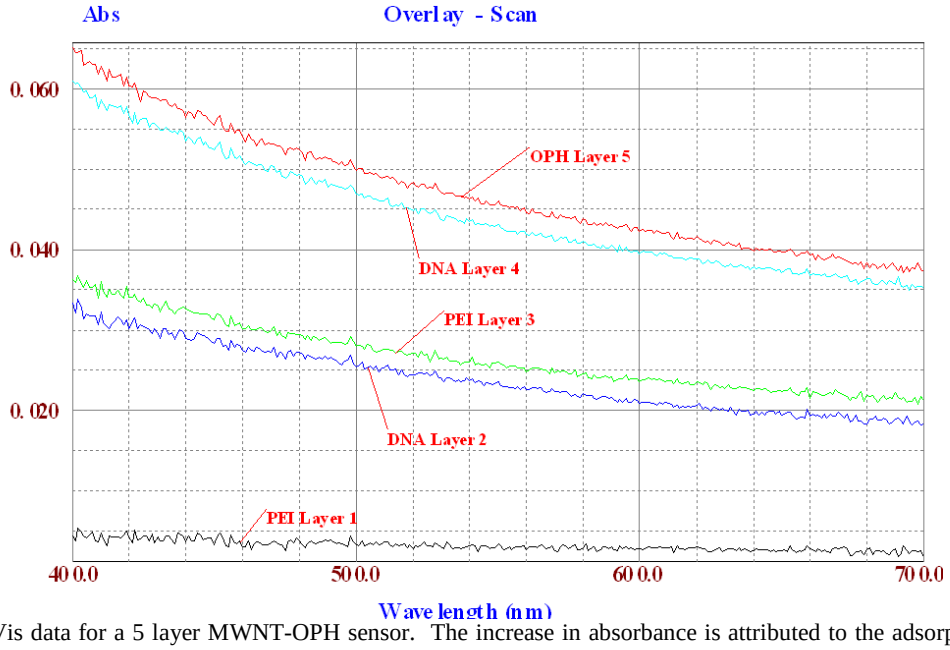

Figure 11: UV-Vis data for a 5 layer MWNT-OPH sensor. The increase in absorbance is attributed to the adsorption of layers onto the glass slide.

Figure 12 and Figure 13 show the UV-Vis spectroscopic and electrochemical responses for *p*-nitrophenol, respectively. As mentioned previously, the concentration and absorbance are directly related by the Beer-Lambert equation (Equation 4). The concentration of the electroactive species in an electrochemical sensor is directly proportional to the concentration of the oxidized species, and is typically calibrated from known concentrations in a buffered electrolyte at a known pH.[9] Figure 14 shows the glass slide verification sensor response to 50 µM PX after 10 minutes of exposure, and as the number of layers increase, so does the response, whereas the sensors ending in MWNT-DNA show lowered response to PX.

In Figure 15, the response of the sensor to paraoxon in the presence of OPH is demonstrated, and is comparable (Figure 16) to that of *p*-nitrophenol. It should be noted that this is for OPH in solution of the batch mode electrochemical cell, so the response will be much higher than for immobilized enzyme. It can be expected that immobilizing the enzyme to a solid support will cause it to lose some degree of freedom, thereby showing a marked decrease in activity. When the solid support material is further immobilized onto an electrode there is even further decrease in activity, as another degree of freedom is removed from the enzyme. Free enzyme can be thought to have three degrees of freedom, in that it is free to have access to substrate in solution and can move in any direction and hold any orientation. Enzyme immobilized onto a free solid support in solution can be thought to have two degrees of freedom, in that it is immobilized onto a support that is free to move. However, the orientation of all the enzymes on the support is dictated by the orientation of the solid support. Finally enzyme immobilized onto a solid support, which is immobilized onto the electrode can be thought to have one degree of freedom, in that it is neither able to move around nor change orientation. The remaining degree of freedom comes from the ability of the substrate to move to access the active site.

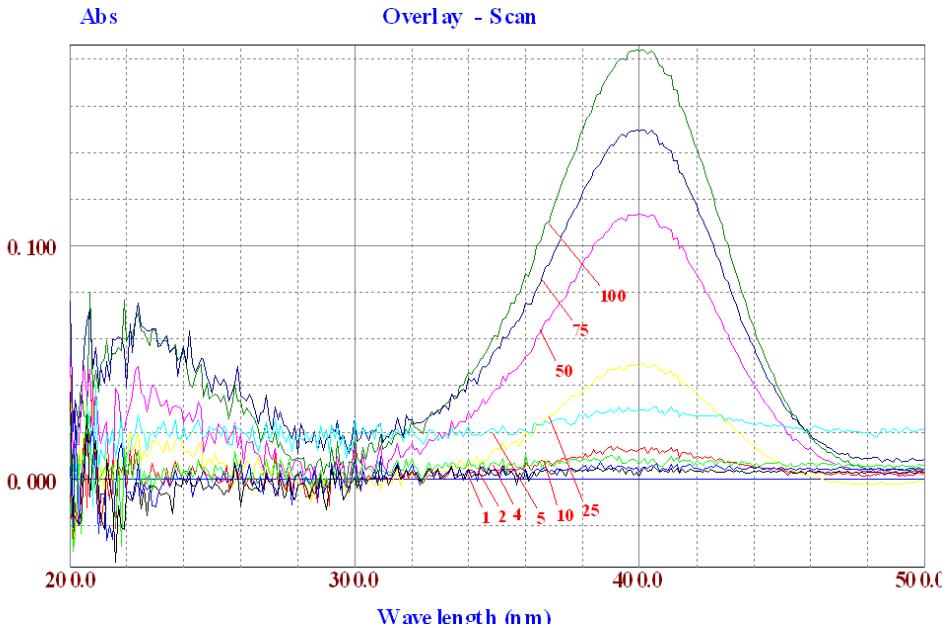

Figure 12: UV-Vis spectra for varying concentrations of *p*-nitrophenol (in µM)

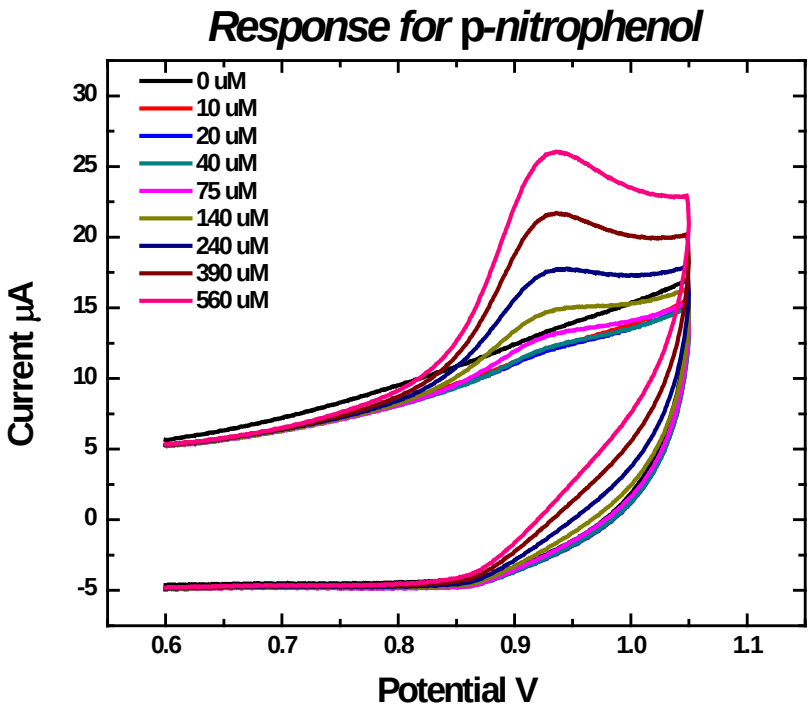

Figure 13: Cylic voltammetry response for *p*-nitrophenol with bare glassy carbon electrode

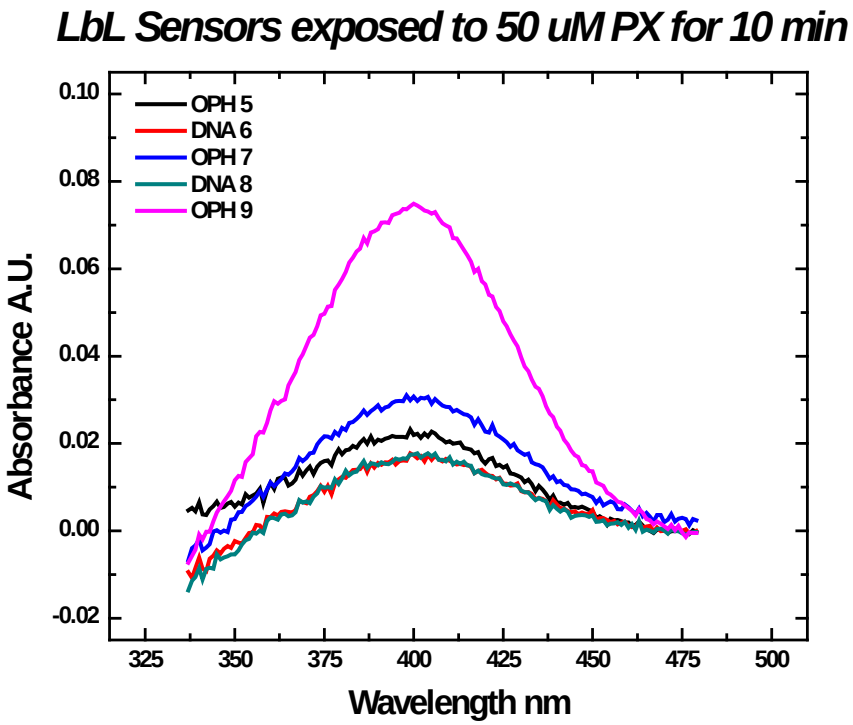

Figure 14: "Verification glass slide sensor" exposed to paraoxon for 10 minutes. The response increases with number of layers, and is decreased for the sensors ending in DNA.

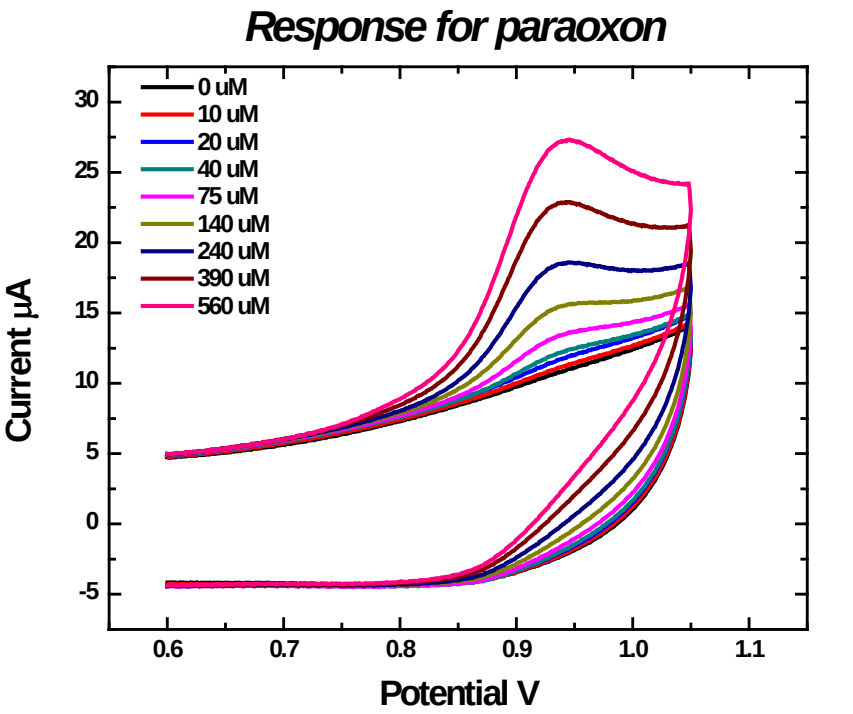

Figure 15: Response of the electrochemical sensor to paraoxon in the presence of OPH, with the enzyme free in solution of the batch mode electrochemical cell.

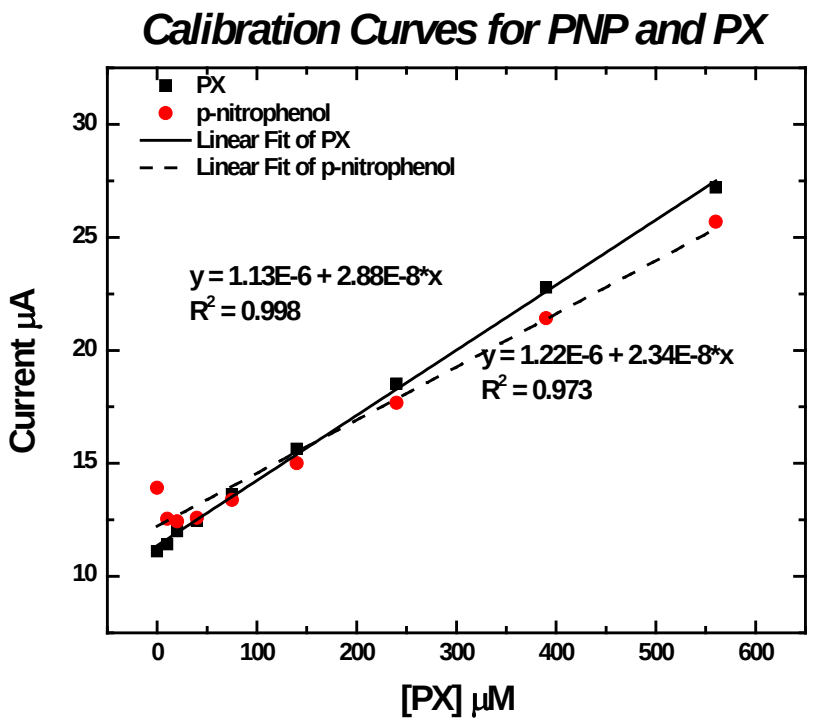

Figure 16: Calibration plots for PX and *p*-nitrophenol (PNP), from the CV plots in the above figures.

Layer-by-layer assembled sensors were built with different numbers of catalysis layers throughout the research. Generally, as the number of layers increased, so did the sensor response to substrate. Figure 17 shows the amperometric current versus time curves for two MWNT-OPH/MWNT-DNA sensors with a total of 5 (1 layer of OPH) or 7 (2 layers of OPH) layers, and Figure 18 shows the calibration curves for these two sensors. These sensors were built using the dipping method, and it should be noted that the last layer was dried onto the sensor, which can be attributed to the large peak heights. The final layers for most sensors were allowed to adsorb overnight under refrigeration (4°C). If there was a cover, the solution would remain overnight, and could be washed off, however if the cover was absent, the solution evaporated leaving a thick layer of MWNT-bioconjugates. The downside to this thick covering of MWNT is that the signal from lower layers is reduced, and generally the enzyme will slowly wash out as buffer flows across the electrodes (the reduction in peak height for subsequent injections of analyte

could be attributed to this). When the catalytic layer is below the top layer, the reduction in peak height is not present, suggesting that the top layer is holding down the lower layers, although the signal from the buried layer is reduced.

Figure 19 shows the response for a 7 layer MWNT-OPH/MWNT-DNA sensor where the last layer was not dried, and the limit of detection for this sensor is 500 nM PX (Figure 20 is the calibration curve). While increasing the number of layers increases signal, it may not be necessary to increase the number of layers in order to save time and materials during the construction process.

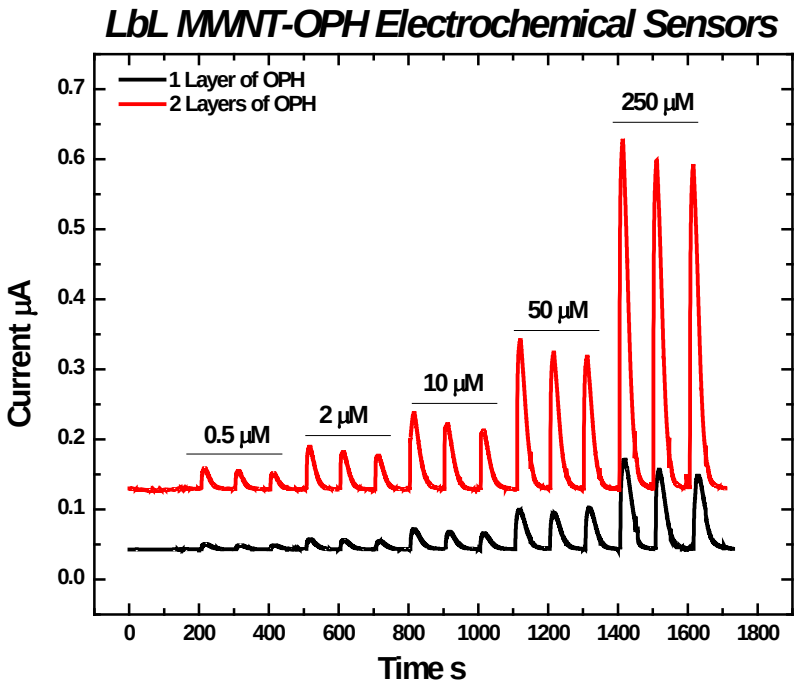

Figure 17: Electrochemical response in amperometry for two sensors with 1 (black) and 2 (red) catalytic layers for different concentrations of PX.

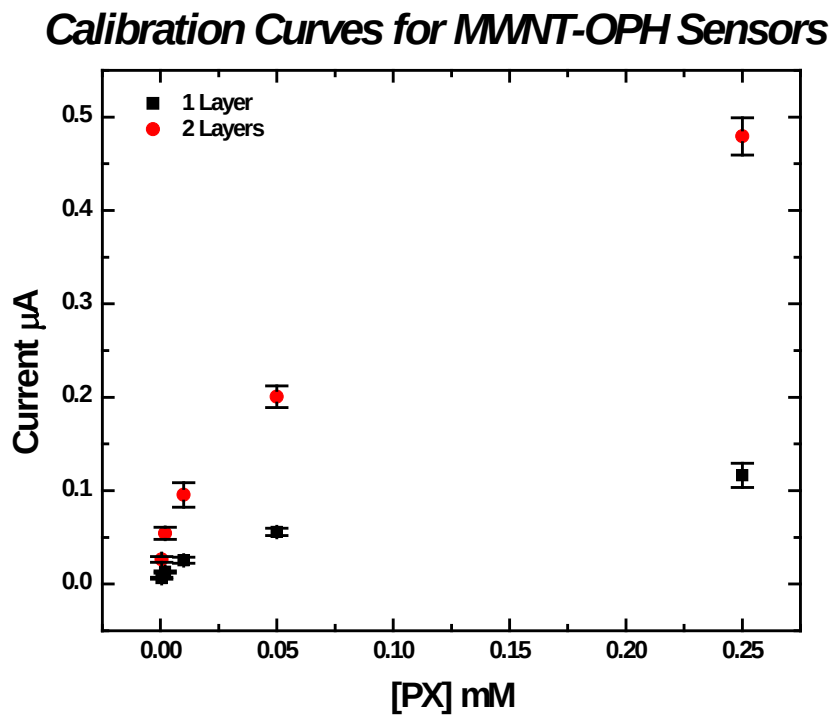

Figure 18: Calibration curves for the two sensors with 1 (black) and 2 (red) catalytic layers for different concentrations of PX. The shape of the calibration curves suggest that the catalytic rate is being limited by the amount of enzyme (too little) or substrate (too much).

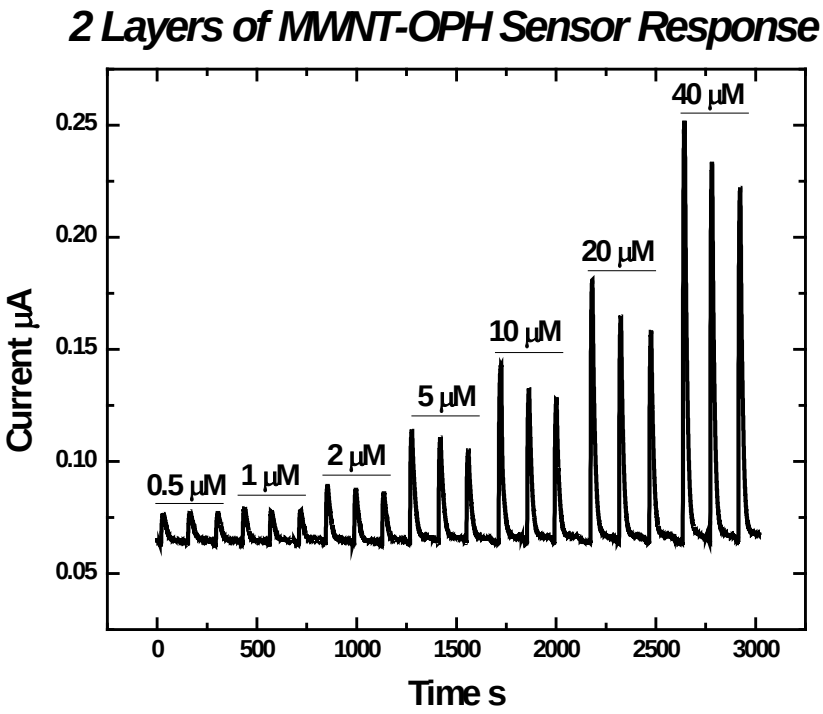

Figure 19: Amperometric response for a sensor with 2 catalytic layers to paraoxon. This sensor did not have the final layer dried. As the concentration increased, the signal for subsequent injections decreased, suggesting either a loss of enzyme activity or fouling of the electrode from *p*-nitrophenol.

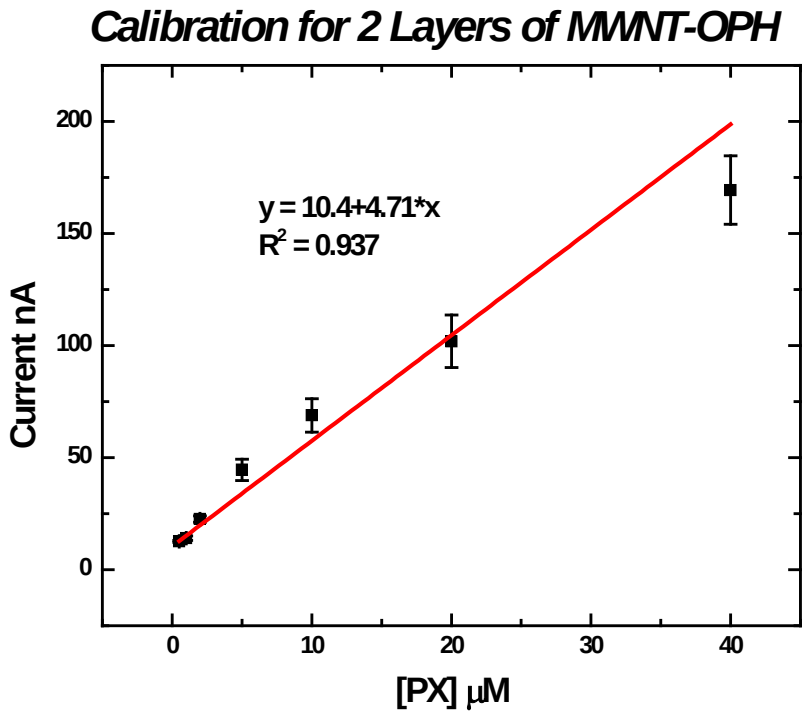

Figure 20: Calibration curve for the MWNT-OPH/MWNT-DNA sensor with two catalytic layers. The limit of detection was calculated to be 156 nM paraoxon.

Conclusions and Future Outlook

This part of the research formed the foundation for the remaining work. Once the carbon nanotubes could be reliably functionalized with OPH, the procedures were then able to be applied to other enzymes (GOx and AChE). The layer-by-layer assembly nanofabrication technique also showed the promise to replace the interlaced MWNT-DNA layers (between catalytic MWNT-OPH layers) with a different enzyme in order to provide multifunctional sensing. Further work in this area, however, could focus on further optimization of the immobilization steps. The data from the experiment testing the effects of the ratio of EDC to NHS were inconclusive. It is apparent that the more EDC is used, the higher the binding efficiency, and that the pH of the buffer for the chemical reactions occurring in the first and second steps of the crosslinking process is a critical parameter. There also needs to be an investigation into how the enzyme is oriented on the nanotubes, and how to control the

orientation of the enzyme during immobilization. Further investigation is necessary to discover why the signal for the amperometric peaks decreases for subsequent peaks of the same concentration.

Chapter 4: Glucose Sensor – Multi-analyte Detection Proof of Concept

Glucose Oxidase Immobilization

The layer-by-layer assembly process allows for complete control over the layer constituents, and therefore has some applicability to multi-analyte detection, wherein different catalytic layers could be interlaced to provide detection of separate compounds. Glucose oxidase is an extremely well-studied redox enzyme and has found use in hundreds of commercial medical devices for glucose monitoring in diabetes patients. The protein has a flavin adenine dinucleotide (FAD) cofactor at its active site, and this cofactor is crucial to the activity of this enzyme. FAD can be stripped away from the active site to render the apo-enzyme, keeping all structural integrity without catalysis. FAD can later be reapplied to the apo-enzyme to restore catalytic ability to the active site. This enzyme catalyzes the oxidation of β-D-glucose to gluconolactone and hydrogen peroxide (Equation 11).

$$\beta\text{-}D\text{-}Glucose + O_2 \xrightarrow{GOx} gluconolactone + H_2O_2 \quad (11)$$

Traditional monitoring of glucose occurs with the use of an oxygen electrode monitoring the depletion of oxygen from the electrolyte. Other methods include the use of electron acceptors or redox mediators such as hexacyanoferrate(III) or ferricinium.[76] Multiple laboratories have described using the layer-by-layer process to develop glucose oxidase (GOx) sensors with redox polymers or organic dyes to molecularly wire the enzyme to the electrode.[78, 83, 100] Still, others have used carbon nanotubes to achieve direct electron transfer between the enzyme and the electrode by using the superior electron transfer properties of the nanotubes to

shuttle electrons from the active site to the electrode.[37, 38, 97, 101] However, because of the chemical modification process that is used to covalently immobilize enzymes to the nanotubes, the electronic structure of the nanotubes is disrupted and direct electron transfer in this case cannot be achieved. Therefore the redox mediator ferrocene monocarboxylic acid was used following the procedures from Cass et al.[76]

The ferrocene redox mediator works in conjunction with deoxygenated buffer as a means for electron transfer to the electrode. When glucose oxidase is deprived of oxygen during catalysis of glucose, the FAD cofactor becomes reduced to $FADH_2$, which then can be oxidized through addition of oxygen to the system or through the ferrocinium ion.[9] Electrochemical detection of glucose occurs through the following reactions (Equation 12a-c):

$$glucose + GOx(FAD) \rightarrow gluconolactone + GOx(FADH_2) + 2H^+ \quad (12a)$$

$$GOx(FADH_2) + 2Fc^+ \rightarrow GOx(FAD) + 2Fc \quad (12b)$$

$$2Fc - 2e^- \rightarrow 2Fc^+ \quad (12c)$$

This reaction scheme allows for the regeneration of the oxidized form of glucose oxidase and the reduced form of the ferrocinium ion, and therefore the catalysis is quasi-reversible, in that the required reactants for catalysis are not depleted from the reaction volume.

Glucose oxidase was covalently attached to acid-oxidized carbon nanotubes in a manner similar to OPH. Glucose was detected in batch mode using cyclic voltammetry at extremely low scan rates (1-5 mV/s) in oxygen depleted 0.5 mM ferrocene carboxylic acid (FcCA) dissolved in phosphate buffered saline (PBS buffer). Figure 21 shows the response of the electrochemical cell to additions of glucose to GOx free in FcCA at a scan rate of 1 mV/s. The change in the shape of the cyclic voltammagram is associated with the chemical reaction described in the above equation.

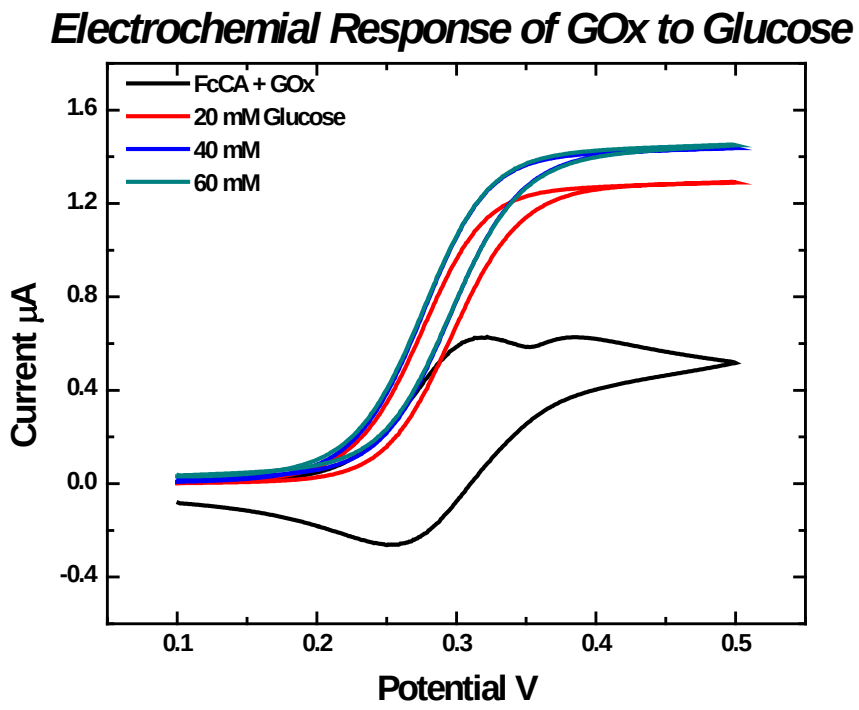

Figure 21: Cyclic Voltammagram showing the response of glucose oxidase to increasing amounts of glucose in deoxygenated ferrocene carboxylic acid.

A similar experiment was performed with glucose oxidase having been attached to carbon nanotubes. Figure 22 shows the CV response of multiwalled-carbon nanotubes immobilized glucose oxidase (MWNT-GOx) free in solution when exposed to increasing amounts of glucose. The signal change is nowhere near as large as with free GOx, however, there is still a change in the shape of the cyclic voltammagram.

Multianalyte Detection

Glucose Oxidase has an acidic isoelectric point, therefore, at neutral pH, the enzyme has a net negative charge. The opposite is true for OPH, which has a net positive charge. Therefore GOx can replace DNA in the layer-by-layer assembled pesticide sensor (Figure 23). Figure 24 shows the response of a 6 layer sensor ending in MWNT-GOx to increasing amounts of glucose. There is a small amount of increase in signal for each injection.

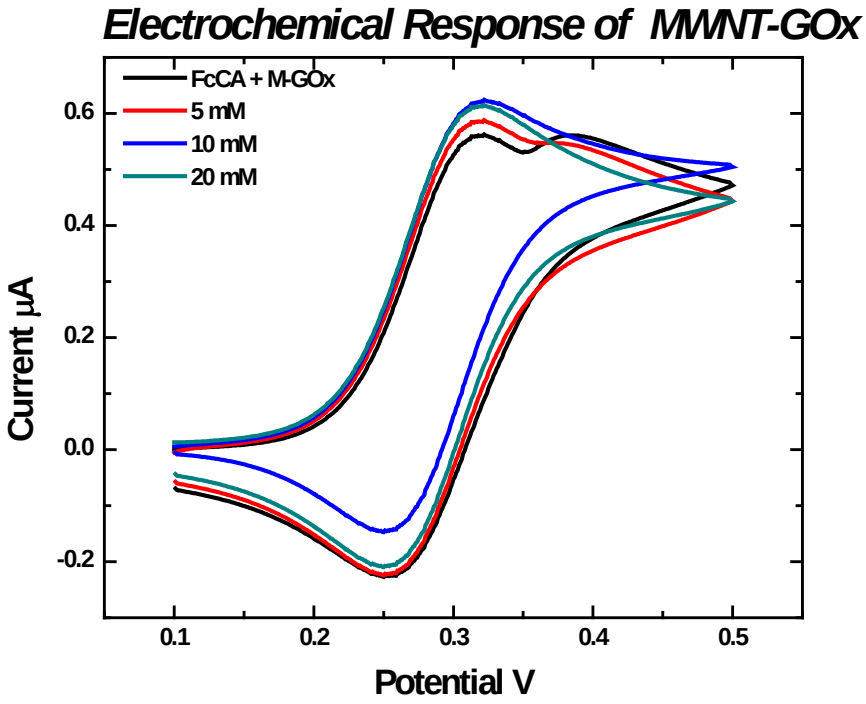

Figure 22: CV response for MWNT-GOx in FcCA to increasing amounts of glucose. The MWNT-GOx was free in solution, and the scan rate was set to 1mV/s.

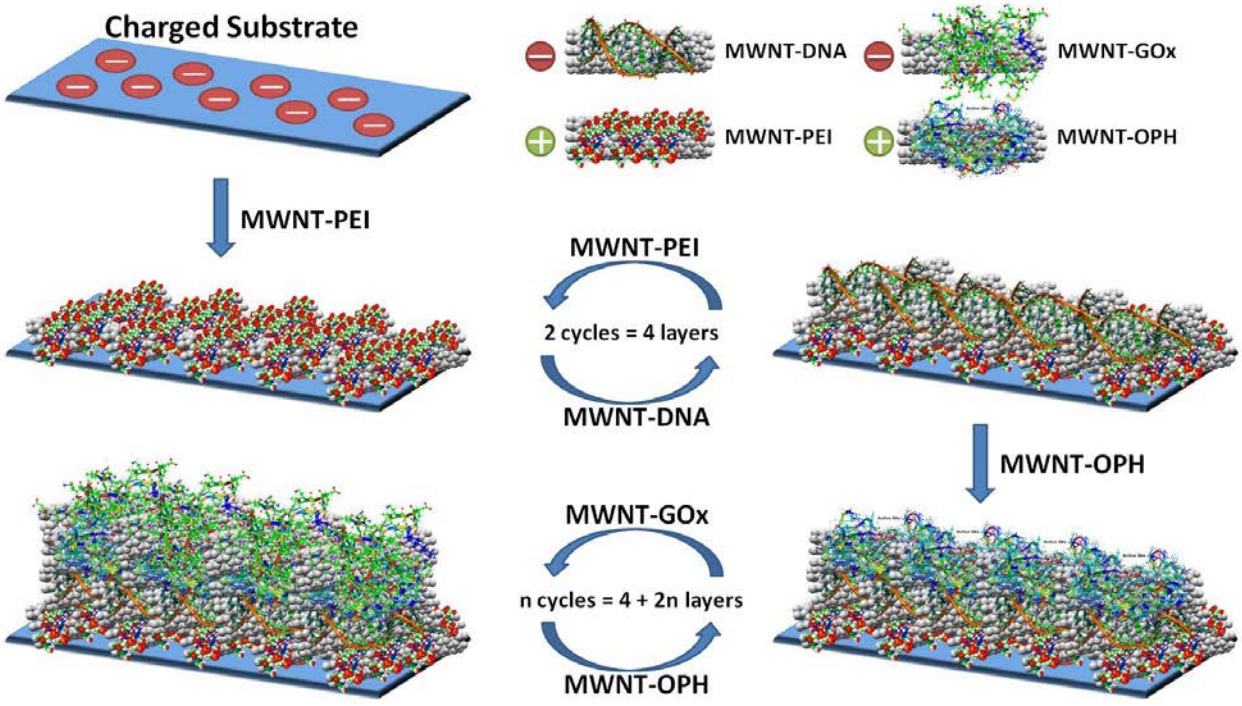

Figure 23: Schematic showing the layer-by-layer assembly of a MWNT-GOx/MWNT-OPH sensor, capable for detection of both glucose and paraoxon.

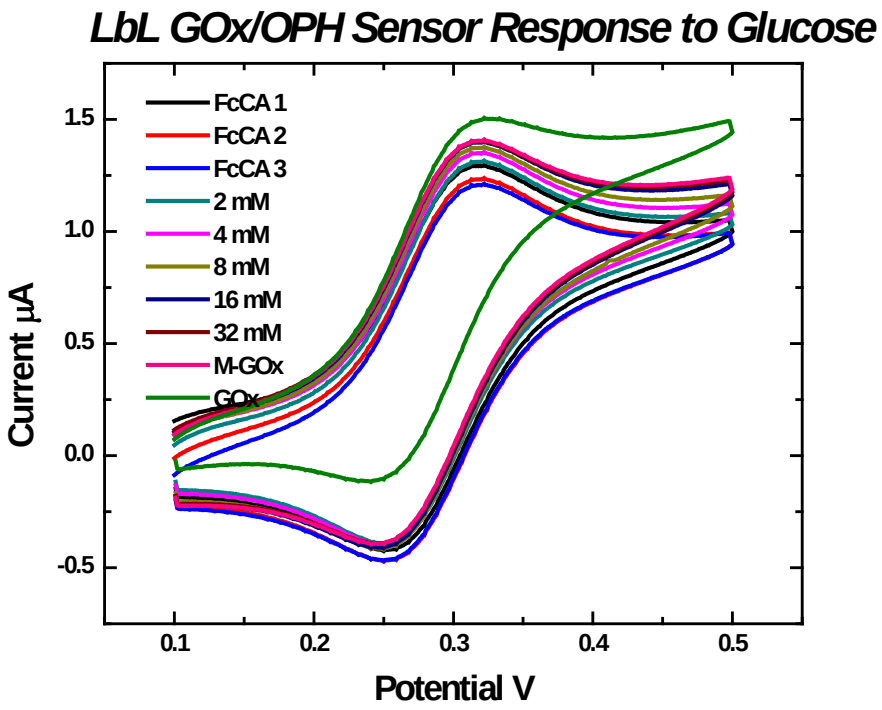

Figure 24: 6 Layer LbL sensor ending in MWNT-GOx. There is a small change in signal with increasing amounts of glucose.

The purpose of this section of the research was to determine if multi-analyte detection on the same solid platform through layer-by-layer assembly is possible. Figure 25 shows the response of GOx free in solution at a fast scan rate (50 mV/s) to glucose, while Figure 26 shows the response to *p*-nitrophenol at the same scan rate, in FcCA. Using a screen-printed electrode as the solid support, an 8 layer (MWNT-GOx as the terminal layer) sensor was constructed. Figure 27 and Figure 28 show the response to increasing amounts of glucose and then paraoxon, followed by free enzyme. The response to glucose is quite diminished compared to paraoxon, probably due to the fast scan rate (the kinetic rate for electron transfer through the redox mediator is very slow, hence the slow scan rate). Further, there appears to be little effect from the enzymes with respect to each other, meaning that any enzyme could be applied in this manner, as long as they operate within the bounds of layer-by-layer assembly. The effect of adsorption time was investigated, as seen in Figure 29. The catalytic layer was buried

underneath a layer of MWNT-GOx, so the substrate had to permeate the top layer to reach the catalytic layer. The increase in adsorption time can be related to an increase in thickness of the layers, which if sufficiently thick, could impede the ability of the substrate to reach the buried layers. Figure 30 shows the flow injection analysis data for an 8 layer MWNT-GOx/MWNT-OPH sensor. The peaks correspond to increasing concentrations of paraoxon. Figure 31 shows the calibration data for that sensor, and compares it to calibration data obtained from a 6 layer MWNT-GOx/MWNT-OPH sensor. As expected, there is a significant increase in catalytic response for the additional layer. Finally, Figure 32 shows the flow injection data for a 7 layer MWNT-OPH/MWNT-GOx sensor, demonstrating the catalytic ability of an OPH terminal multi-analyte sensor. The calibration data is inset in the figure, and the limit of detection was calculated to be 260 nM.

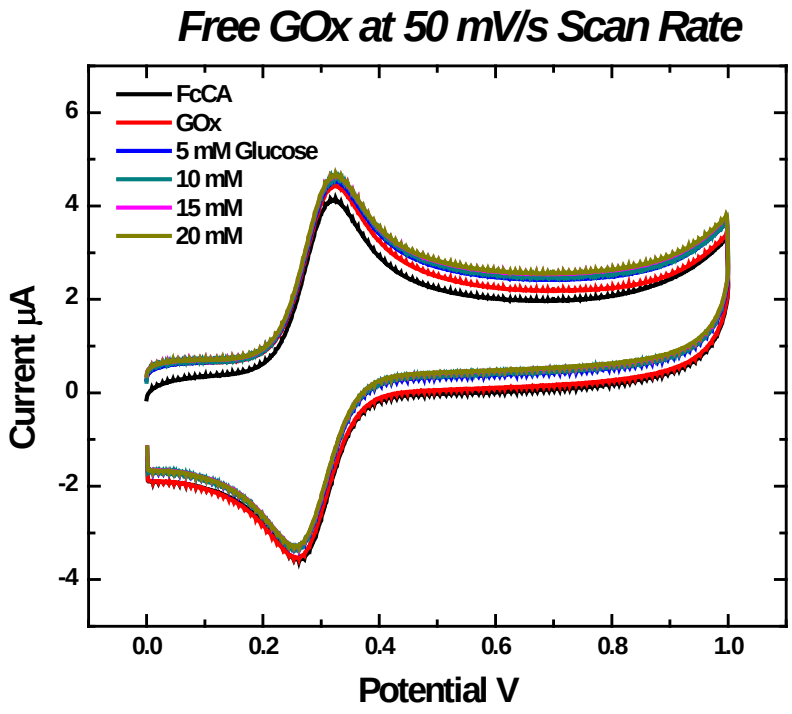

Figure 25: Fast scan rate CV for GOx free in solution. Glucose was added in serial injections to the reaction volume between each scan.

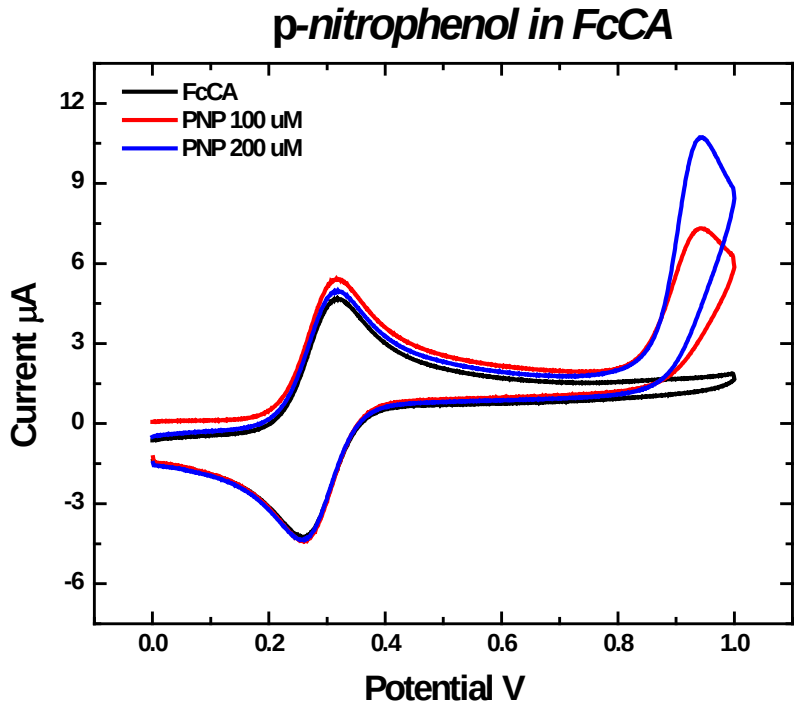

Figure 26: Electrochemical response to *p*-nitrophenol in FcCA. A peak at 0.95V is apparent where expected, and increasing amounts of analyte do not increase the ferrocene peak.

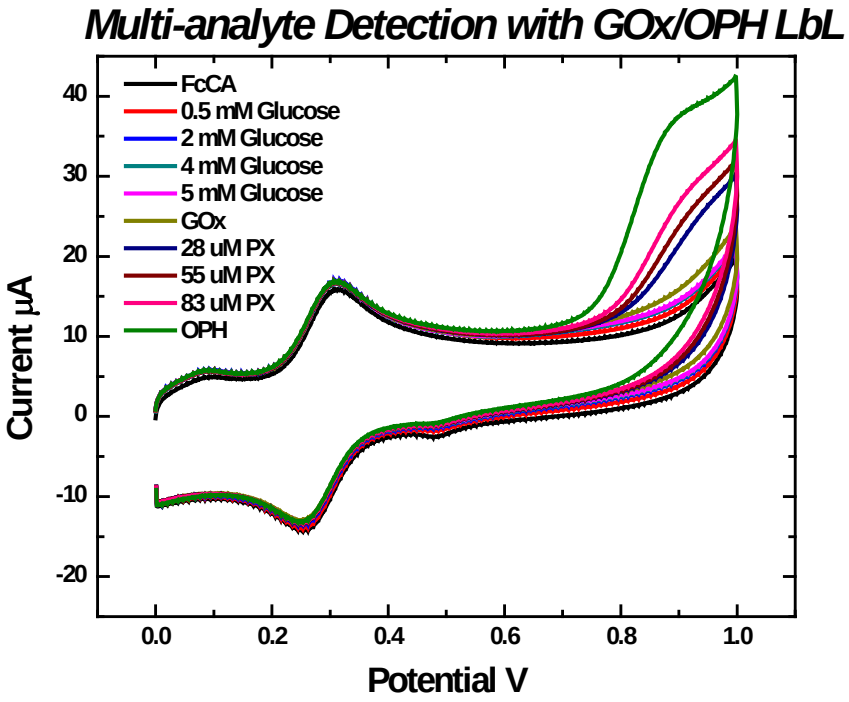

Figure 27: MWNT-GOx/MWNT-OPH sensor response to increasing amounts of glucose and paraoxon. The glucose was added serially first. Paraoxon was added after glucose. A clear increase is shown for paraoxon injections at 0.95V in the above votammaogram.

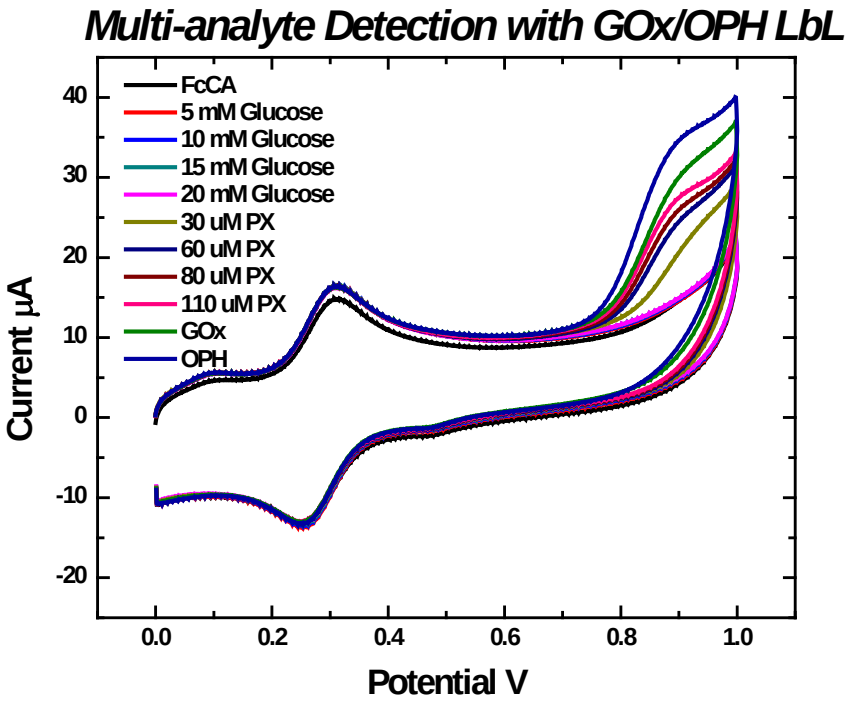

Figure 28: In a similar fashion to Figure 27, glucose and then paraoxon were added to a MWNT-GOx terminal sensor.

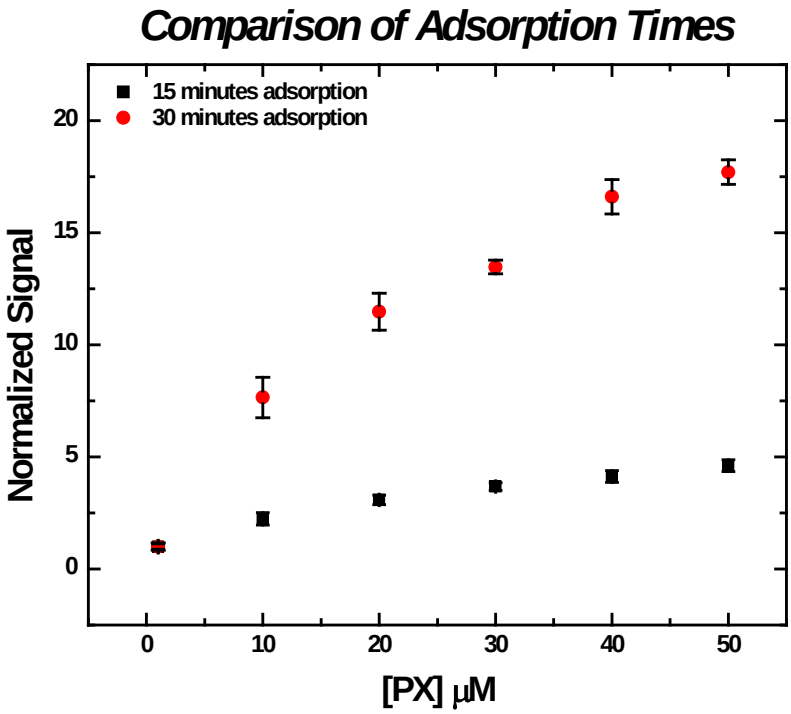

Figure 29: Comparison of adsorption times during layer adsorption. The data points are normalized current signals from paraoxon detection, and the OPH layer was buried underneath a layer of GOx.

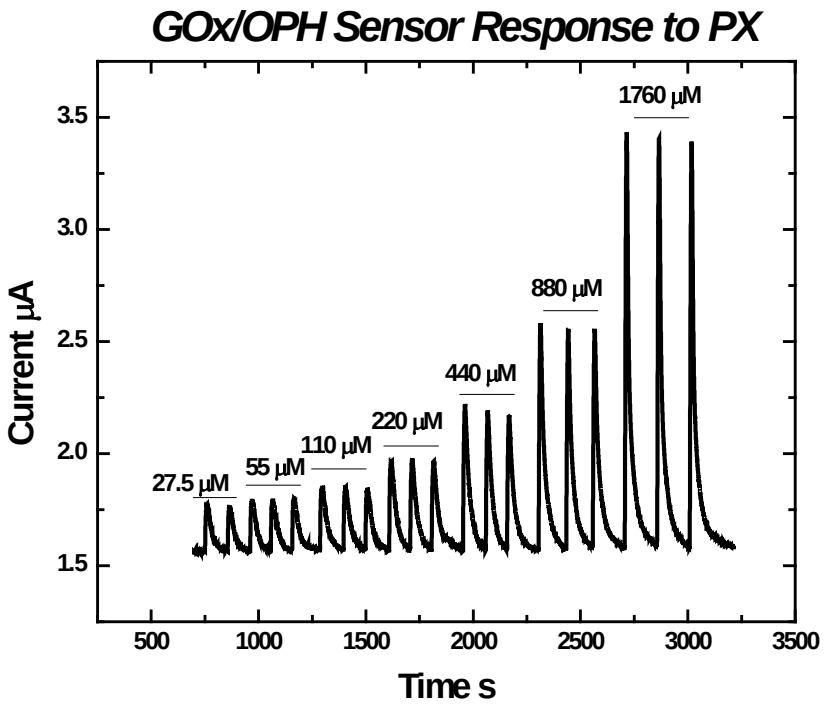

Figure 30: Flow injection analysis of paraoxon on an 8 layer MWNT-GOx terminal sensor. As compared to typical OPH curves, the peaks appear more stable (due to the layer being buried).

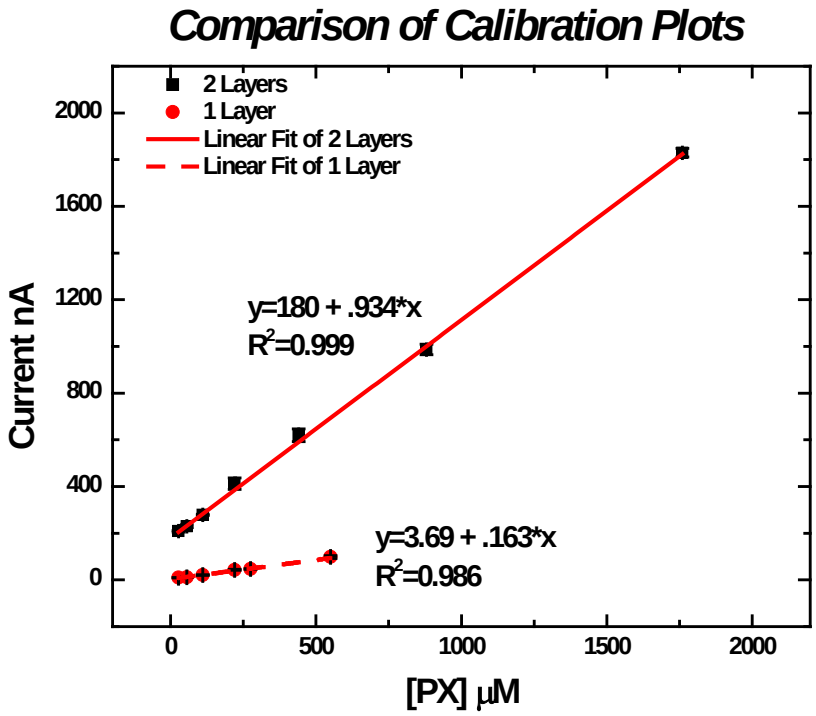

Figure 31: Comparison of the calibration curves for MWNT-GOx terminal sensors with either 1 layer of OPH or 2 layers of OPH. There is significant increase in response with the addition of catalytic layers.

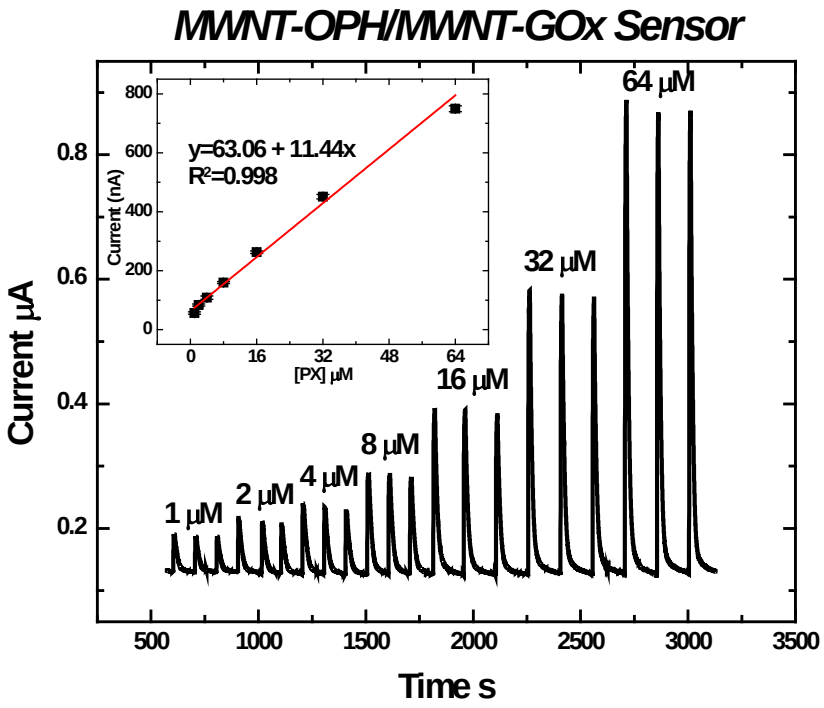

Figure 32: FIA of paraoxon on a 7 layer MWNT-OPH terminal sensor. The calibration curve is shown in the inset, with a limit of detection of 260 nM PX.

Conclusions and Future Outlook

The main challenge in this section was the immobilization of GOx to the carbon nanotubes. This problem was never fully solved; although there is potential to completely fix this problem, from the optimization of the EDC/NHS chemistry from the earlier section in conjunction with the correct pH for the second step of immobilization. Because of the immobilization problem, the ability to detect glucose was very marginal at best. However, the purpose of this experiment was to demonstrate the proof-of concept for multi-analyte detection. A sensor that detects both glucose and pesticides is not very practical, but this section demonstrates the ability of layer-by-layer assembly to accommodate two completely different enzymes with completely different kinetic mechanisms. Therefore this approach could be utilized in a sensor which is capable of detecting two related compounds, and discriminating between them. It could also be used in a "cascade effect" sensor, wherein the product of one

enzyme could be the substrate for another. This novel concept could be useful for the design and realization for biosensor systems to detect many different analytes, especially when a direct "one analyte – one biorecognition element" detection pathway is impossible to accomplish, requiring several recognition events in order to achieve detection. Future work could focus on using the apo-glucose oxidase enzyme (without the cofactor FAD) to study layer penetration, and also optimize the immobilization process for this enzyme onto MWNT.

Chapter 5: Acetylcholinesterase – Dual Enzyme Pesticide Biosensor

Acetylcholinesterase Immobilization

Acetylcholinesterase (AChE) inhibition is the main approach used to detect neurotoxic compounds, and has been well studied over the past few decades.[60-67, 69, 102-108] Nerve agents inhibit the enzyme by irreversibly binding to the active site of AChE, which prevents it from catalyzing the hydrolysis of acetylcholine and its derivatives. A correlation between the loss in activity (inhibition) and the concentration of the nerve agent can be found due to the large number of enzymes present on the surface of the electrode, and that statistically not all of them will be inhibited. While very sensitive (up to 10^{-11} M), this biosensor suffers from limited specificity, since a large number of different compounds such as heavy metals, detergents, etc. are capable of inhibiting AChE. Therefore its use in discriminative detection is very limited. However, its ability to sensitively detect all neurotoxins could be used in conjunction with another enzyme, such as OPH, which can only recognize organophosphate (OP) neurotoxins. Moreover, it is possible to use OPH to screen OP neurotoxins from samples and therefore only non-OP neurotoxins will have an effect on AChE.[109]

Acetylthiocholine (ATCh) is a synthesized derivative of acetylcholine, and is susceptible to hydrolysis by acetylcholine esterase (AChE). The product thiocholine (TCh) is electroactive, which allows direct amperometric study of AChE without using a mediator and choline oxidase (ChOx). This simplifies the electrochemical system and allows for rapid determination of enzyme activity in a reagent-less buffer. It is oxidized above 0.3 V versus Ag/AgCl without the

presence of AChE (Figure 33), however when exposed to AChE, an oxidation peak several orders of magnitude higher than the baseline appears at 0.62 V vs Ag/AgCl on the screen printed carbon ink electrodes (Figure 34). Below is the reaction scheme for the hydrolysis of ATCh by AChE.[105]

$$ATCh + H_2O \xrightarrow{AChE} TCh + Acetic\ Acid \quad (13)$$

In the presence of a neurotoxic compound, AChE activity is lost proportionally to the concentration of the neurotoxin. Figure 35 shows the response in batch mode cyclic voltammetry of 2 units of AChE to different concentrations of ATCh with 15 nM paraoxon in solution with the enzyme, Figure 36 shows the response for the same with 140 nM paraoxon, and Figure 37 with 275 nM paraoxon. Figure 38 shows the calibrations for the various amounts of neurotoxin, and shows a significant decrease in activity at the higher concentrations of neurotoxin. Averaging the % inhibition for each concentration of ATCh, a linear calibration is obtained for AChE inhibition by paraoxon (Figure 39).

AChE was immobilized onto carbon nanotubes in a manner similar to that of OPH, and several concentrations of AChE for the incubation step were investigated. To verify attachment, an experiment in batch mode cyclic voltammetry was performed using soluble nanotube-enzyme conjugates in the presence of substrate. As seen in Figure 40, multi-walled nanotube immobilized acetylcholinesterase (MWNT-AChE) responds in a very similar way to acetylthiocholine as free AChE. Figure 41 confirms ATCh hydrolysis by MWNT-AChE with a negative control (no enzyme). Figure 42 and Figure 43 show the baseline activity and inhibition of MWNT-AChE by carbamate neurotoxin, respectively. From these experiments, it is understood that the MWNT-AChE enzyme behaves in nearly the same way as free AChE.

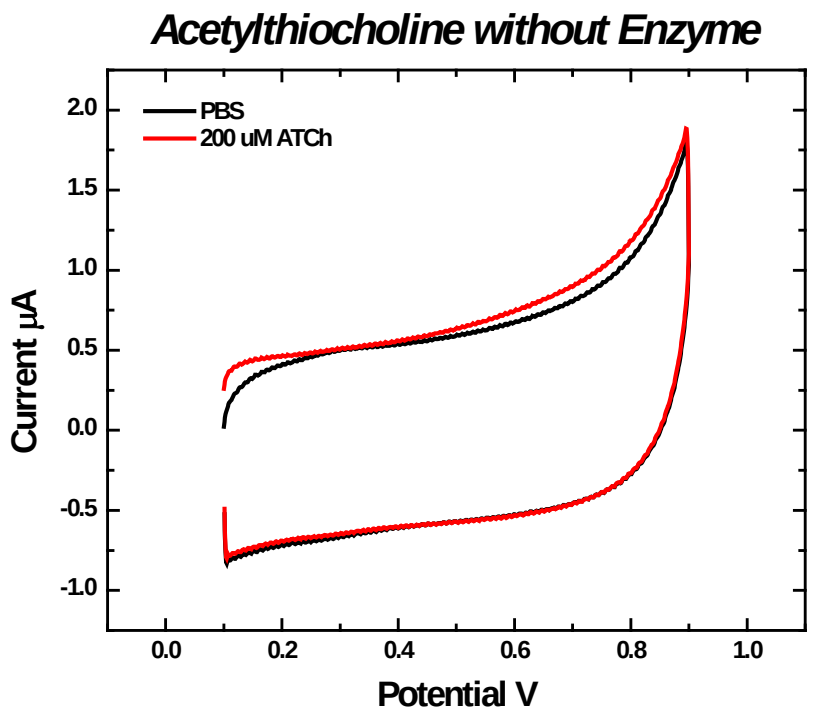

Figure 33: Bare electrode response to acetylthiocholine in buffer. Above 0.3 V, ATCh can be oxidized electrochemically, which means this must be kept in mind when performing any electrochemical experiments will ATCh.

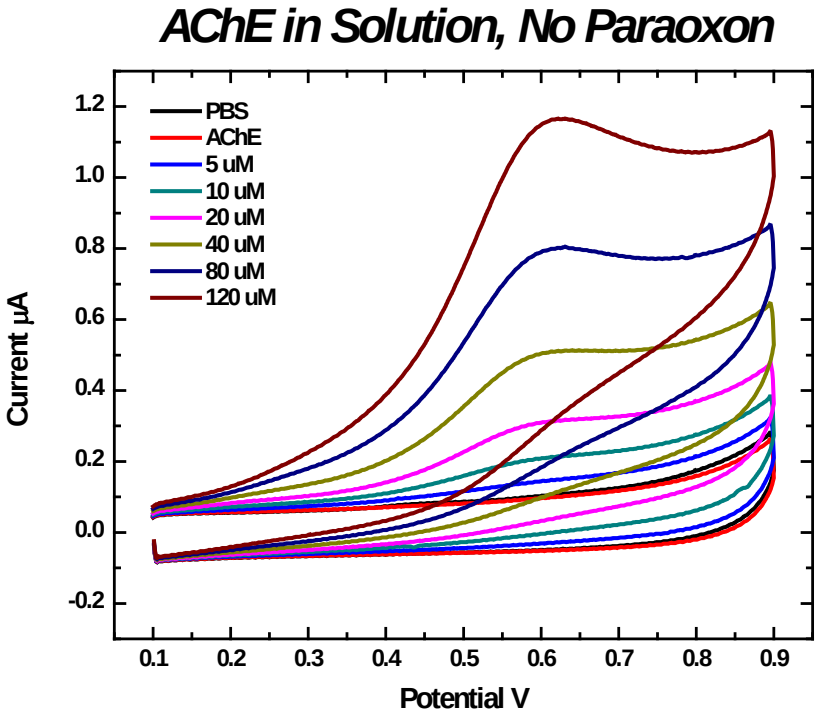

Figure 34: Bare electrode response to acetylthiocholine in buffer in the presence of acetylcholinesterase. An oxidation peak can be seen at 0.62 V, which is attributed to the oxidation of thiocholine, which is the product of hydrolysis of ATCh by AChE.

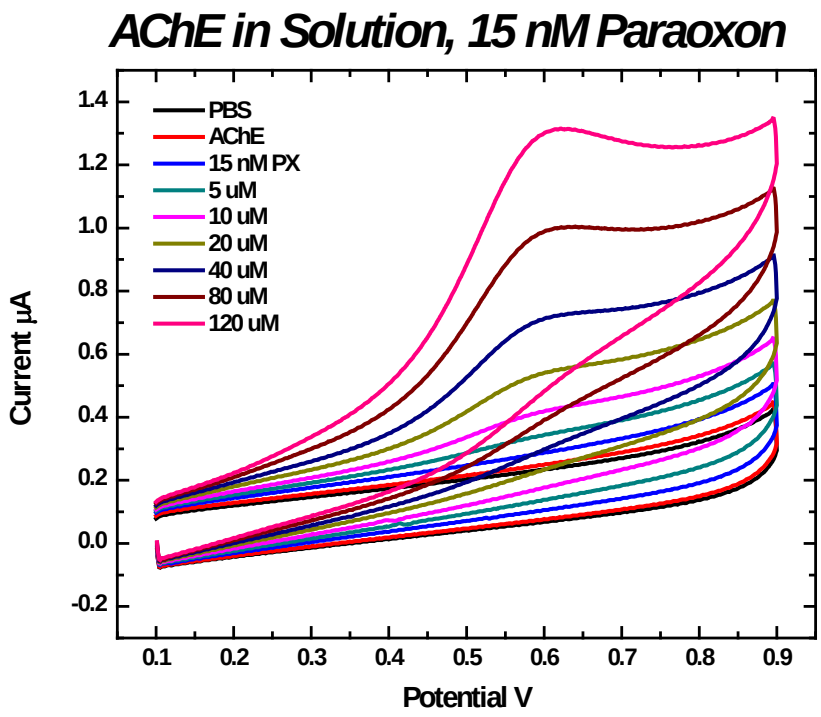

Figure 35: Acetylcholinesterase incubated with 15 nM paraoxon and the signal response to increasing injections of acetylthiocholine.

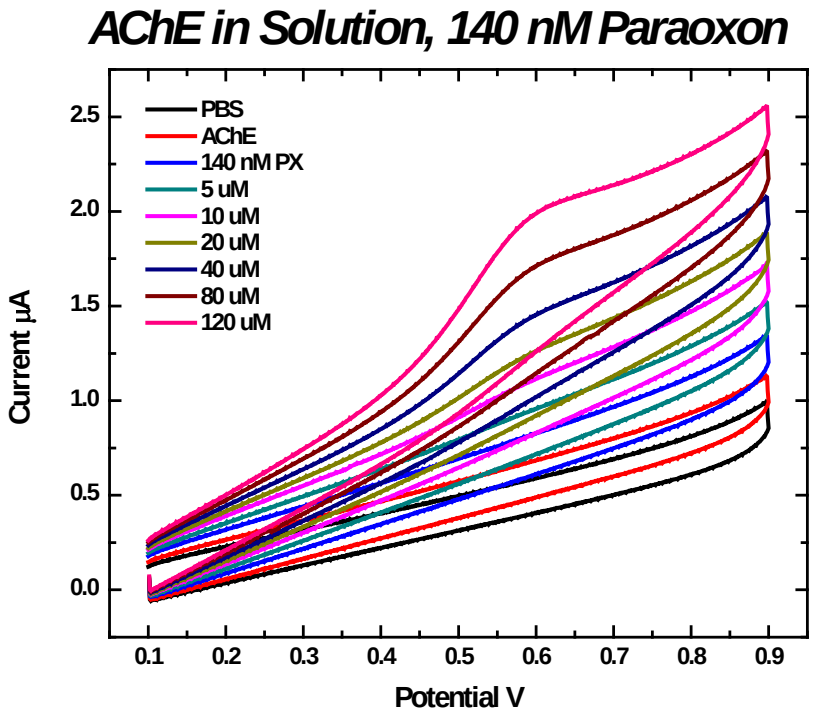

Figure 36: Acetylcholinesterase incubated with 140 nM paraoxon and the signal response to increasing injections of acetylthiocholine.

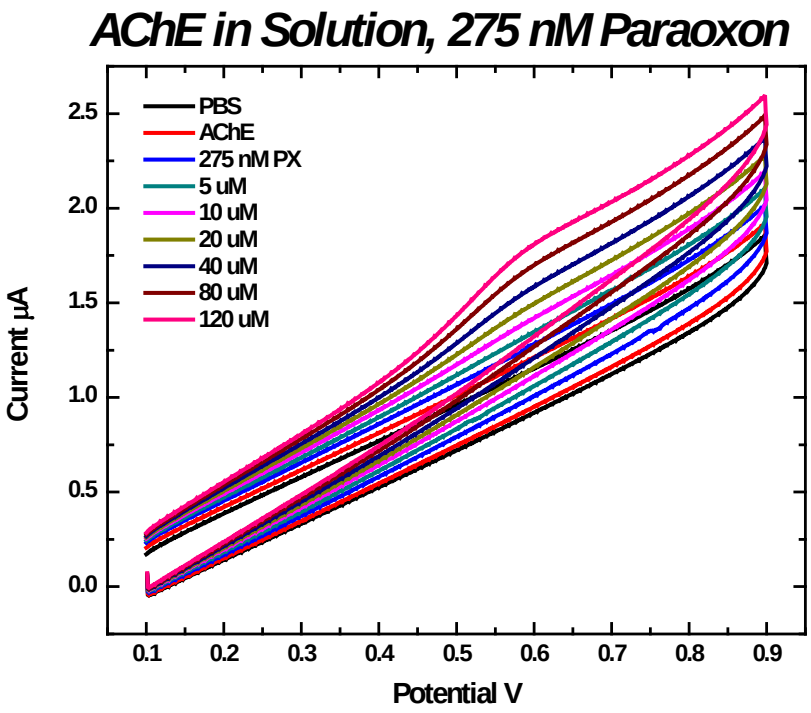

Figure 37: Acetylcholinesterase incubated with 275 nM paraoxon and the signal response to increasing injections of acetylthiocholine.

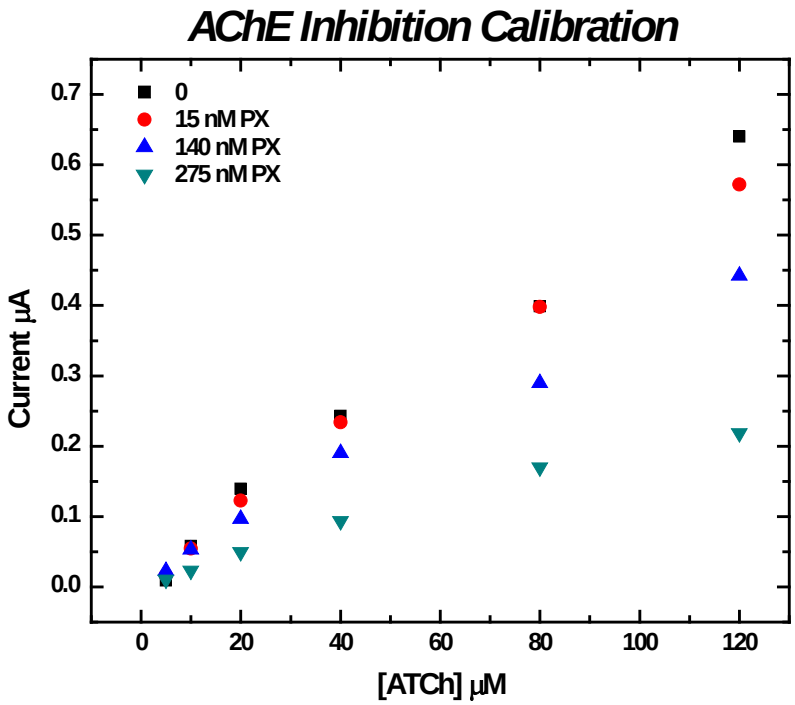

Figure 38: Calibration of cyclic voltammetry experiments for each concentration of paraoxon with respect to concentration of acetylthiocholine. For larger concentrations of paraoxon, there is an increasing amount of loss in activity for each concentration of ATCh.

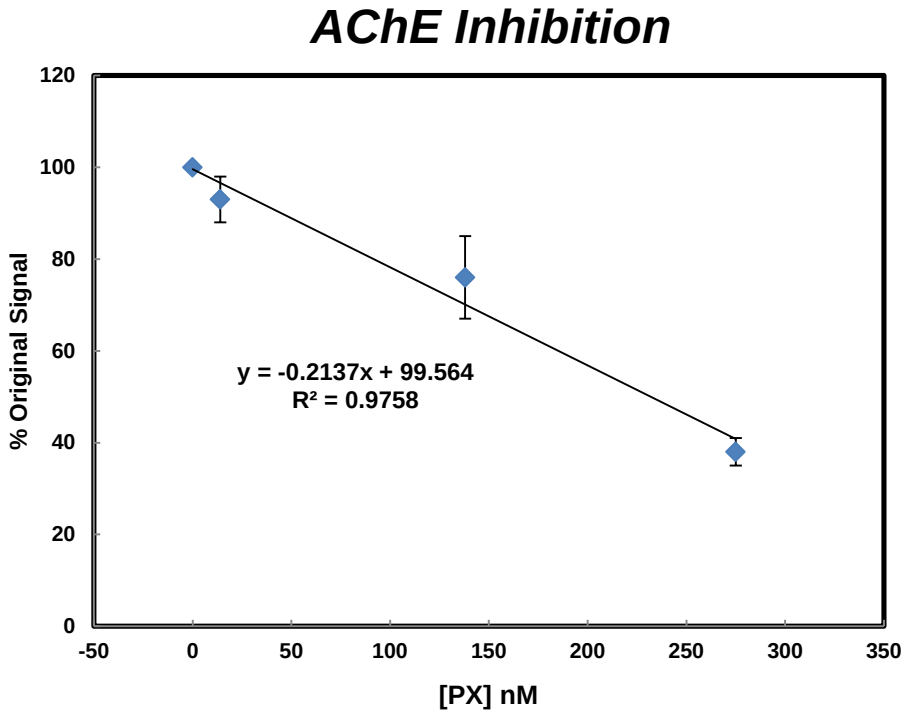

Figure 39: Calibration of the activity of acetylcholinesterase, and as the amount of paraoxon increases, the activity of AChE decreases.

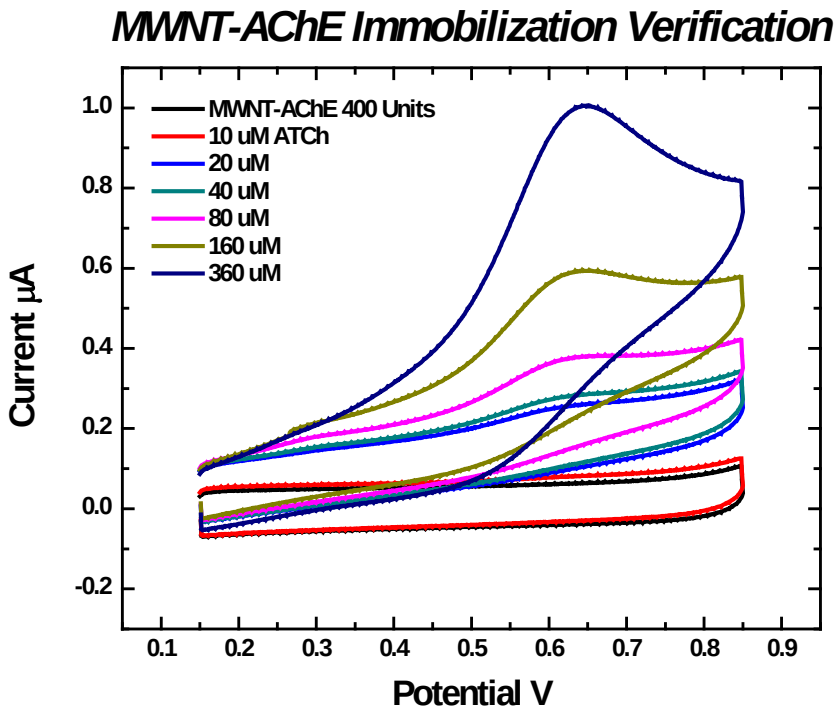

Figure 40: Verification of AChE activity after immobilization of the enzyme onto carbon nanotubes.

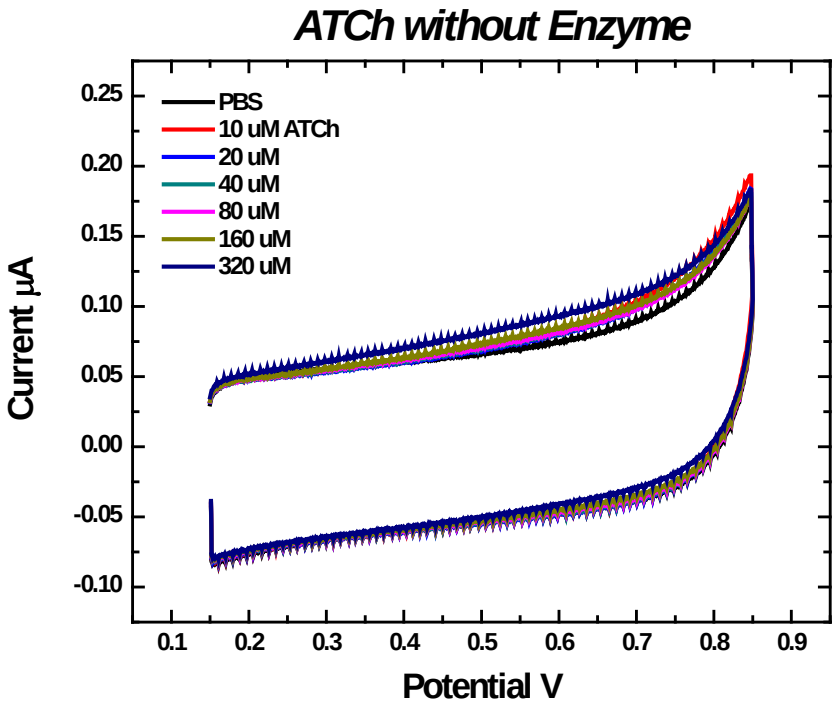

Figure 41: Negative control of ATCh oxidation, demonstrating the significant increase in Figure 38 is only from AChE activity.

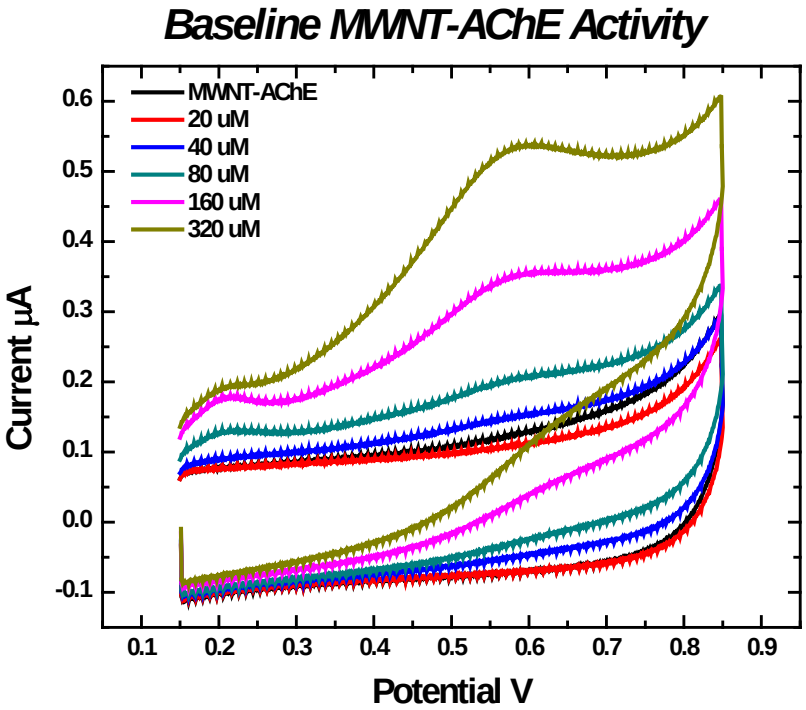

Figure 42: Baseline activity of MWNT-AChE at different concentrations of ATCh, with no neurotoxin present in solution.

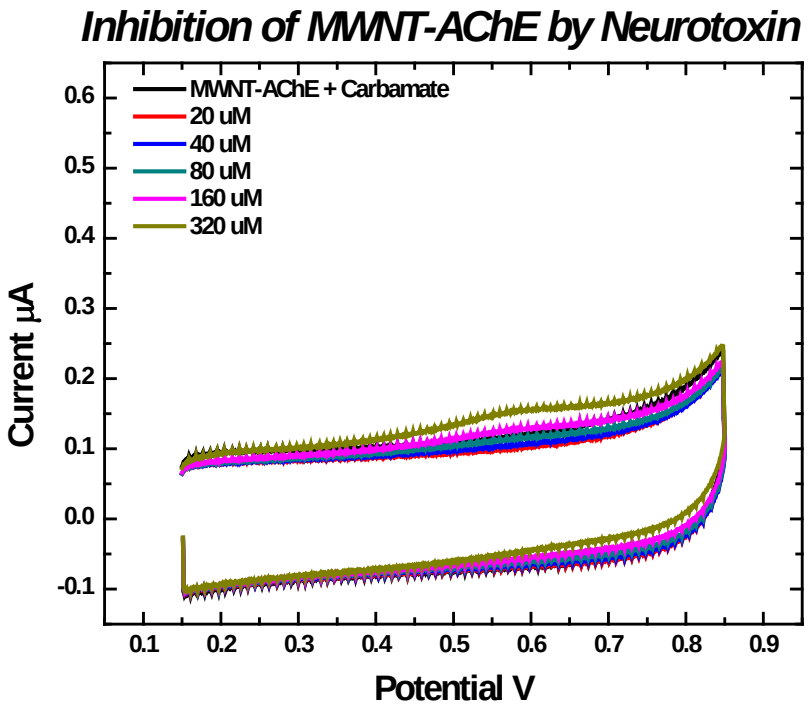

Figure 43: Inhibited activity of MWNT-AChE at different concentrations of ATCh, with methyl carbamate neurotoxin present in solution.

Layer-by-Layer Assembled Pesticide Sensor

Figure 44 is a conceptual figure showing the layer-by-layer assembly of the MWNT-AChE/MWNT-OPH biosensor. Because of the acidic isoelectric point of acetylcholinesterase, at a neutral pH this enzyme has a net negative charge, and can replace the MWNT-DNA or MWNT-GOx as shown in previous sections. Cyclic voltammetry was performed on a 6 layer (MWNT-AChE terminal) sensor in buffer with respect to increasing amounts of ATCh (Figure 45). The oxidation peak for ATCh hydrolysis is reduced slightly to 0.58 V versus Ag/AgCl. Three samples of MWNT-AChE with different concentrations of AChE in the incubation step of immobilization were used to build layer-by-layer assemblies on glassy carbon electrodes and then flow injection analysis was performed in amperometry to measure the response of the sensors to ATCh. Figure 46 shows the response for two of those sensors with 400 and 200 units, and there was very little difference in the two until much higher concentrations. Figure 47 shows

the calibration curves for those enzymes, and their shapes are very similar to those of Michaelis-Menton curves. This could suggest that the amount ATCh is reaching kinetic saturation, in that there is too much substrate to immediately hydrolyze it all.

Figure 48 shows a log-log plot of concentration of ATCh versus current for various numbers of layers of MWNT-AChE, showing a significant increase for each additional catalytic layer. This could possibly be exploited to increase or decrease the sensitivity of the sensor to neurotoxin, controlling the amount of enzyme by controlling the number of layers. OPH and AChE were both used to build a layer-by-layer assembly without the carbon nanotubes, to demonstrate the advantages and disadvantages that MWNT could provide to the system. As seen in Figure 49, the activity of the assembled enzymes for paraoxon is much higher than that for immobilized enzyme. However, the error is much larger because the enzyme will wash away from the electrode without a proper scaffold. When OPH is placed under a layer of AChE, the error is much reduced, because the AChE is protecting it from the bulk flow (although eventually the AChE will completely wash out, leaving the OPH vulnerable).

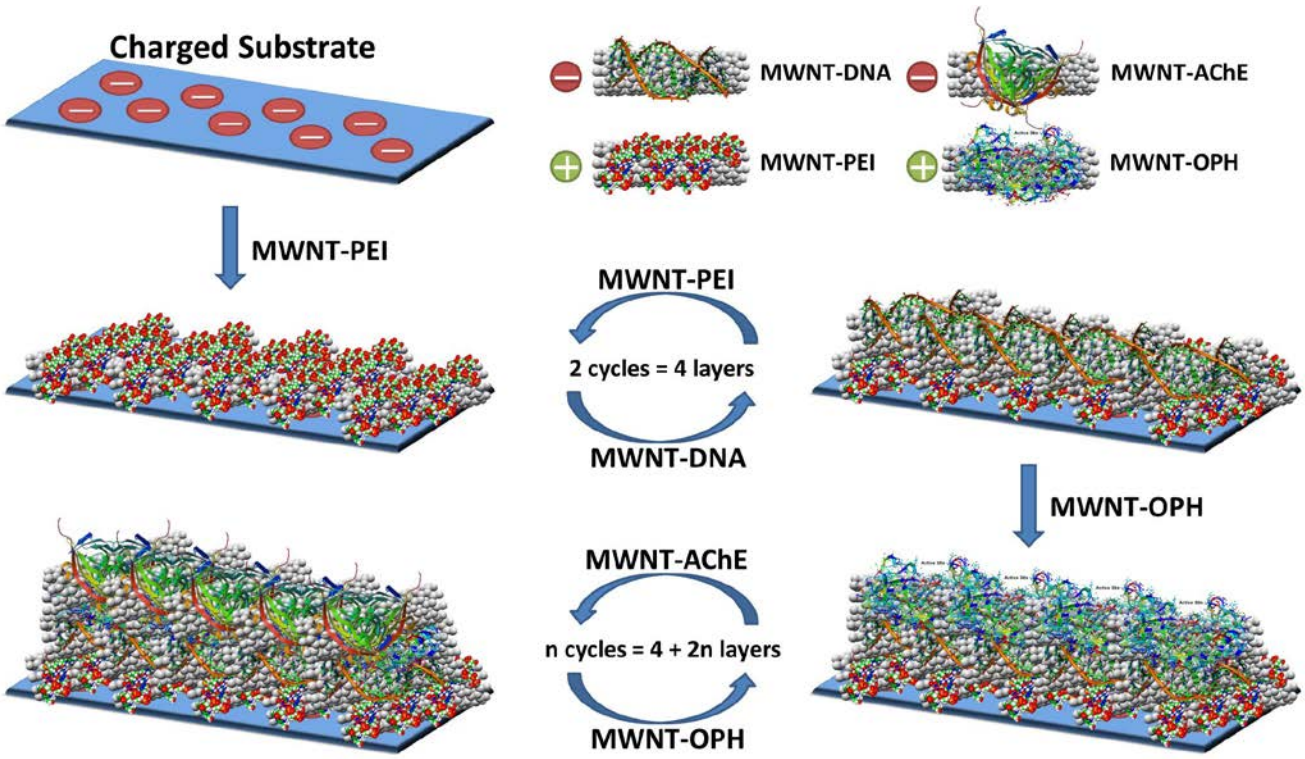

Figure 44: Schematic of the layer-by-layer assembly process of MWNT-AChE and MWNT-OPH, with MWNT-AChE as the anionic layer and MWNT-OPH as the cationic layer.

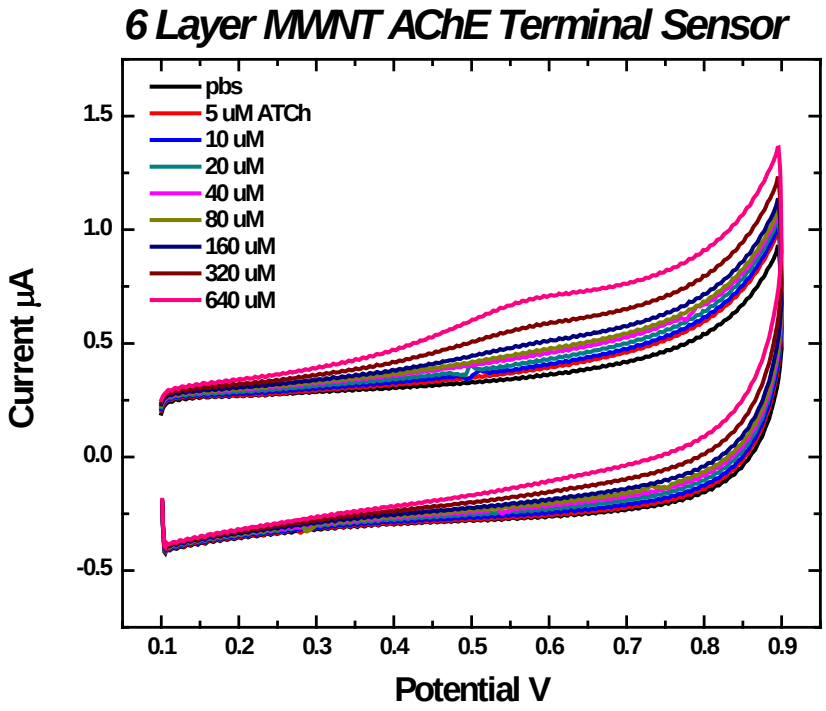

Figure 45: Cyclic voltammagram for a 6 layer MWNT-AChE/MWNT-OPH electrochemical sensor at various concentrations of ATCh.

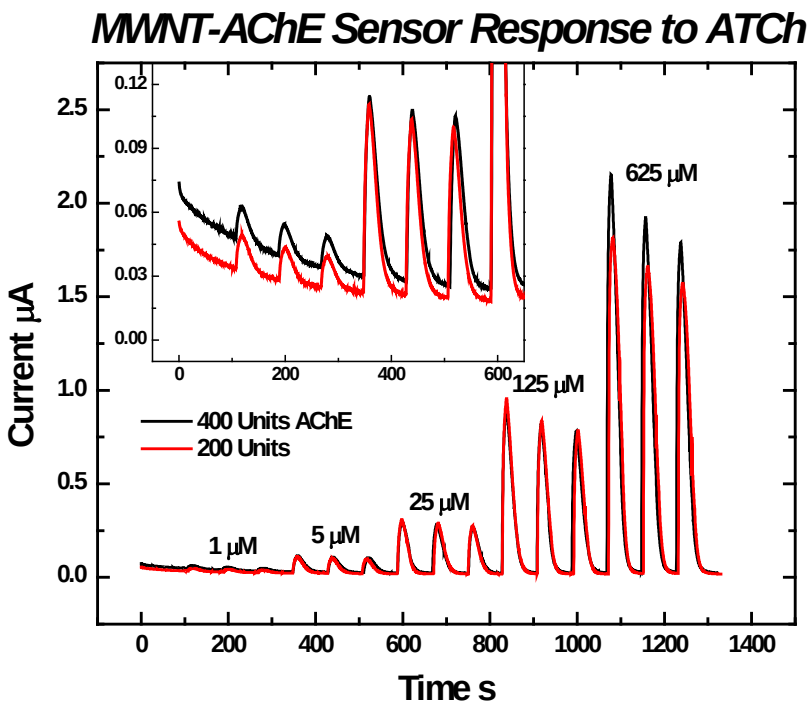

Figure 46: Layer-by-layer assembled sensors using different MWNT-AChE samples differing in amount of enzyme incubated during the second step of immobilization. The first two concentrations of ATCh are inset. The baseline decreases very slightly throughout the experiment due to the dispersion of the diffusion layer at the electrode-electrolyte interface.

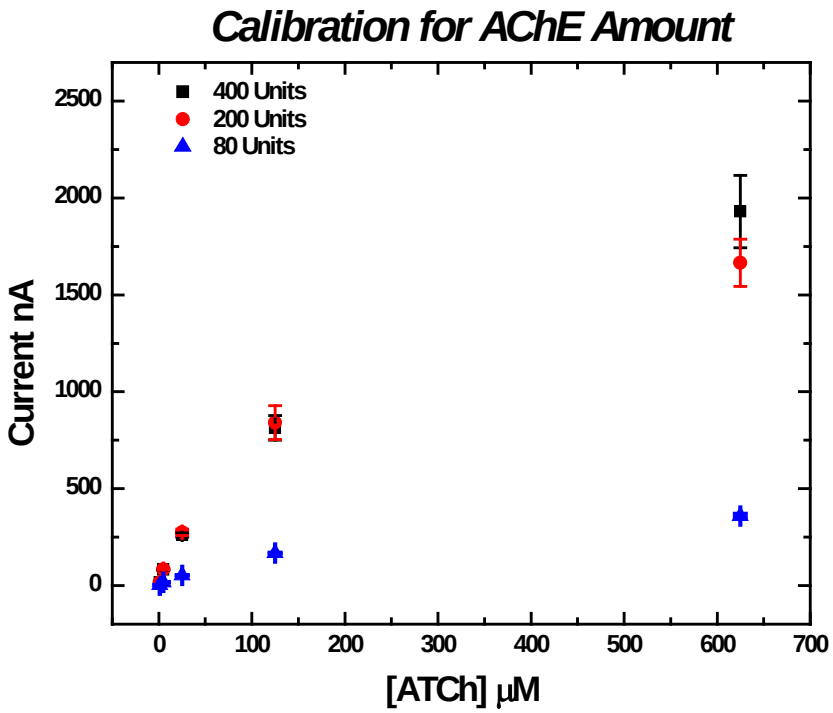

Figure 47: Calibration curves for the three samples of MWNT-AChE with different concentrations of AChE incubated during the second step of immobilization. The curves resemble Michaelis-Menton plots, and could suggest that saturation of substrate is being achieved at higher concentrations.

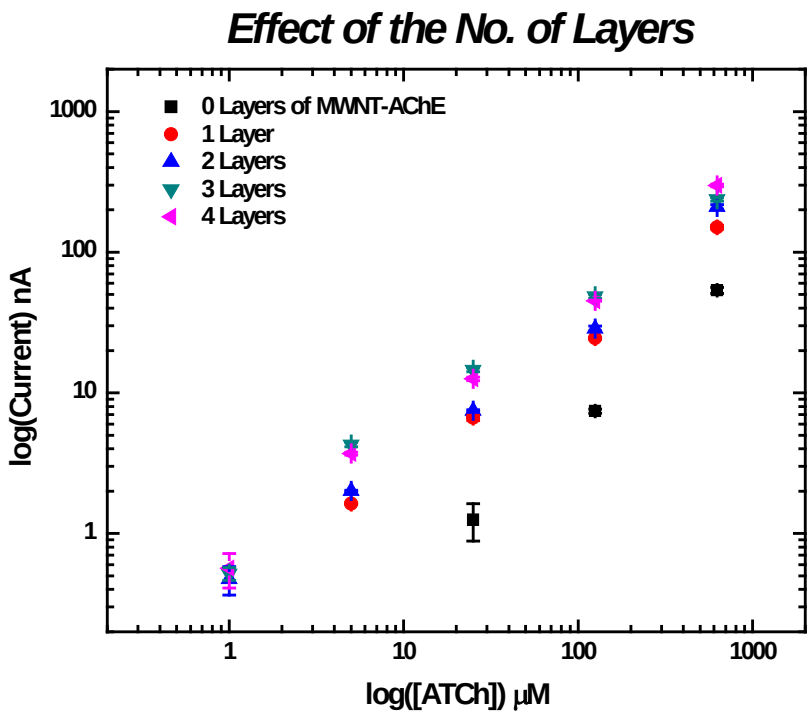

Figure 48: Log-log plot of the calibration curves for different numbers of catalytic layers. The sensitivity of the sensor could be controlled through the manipulation of the number of layers.

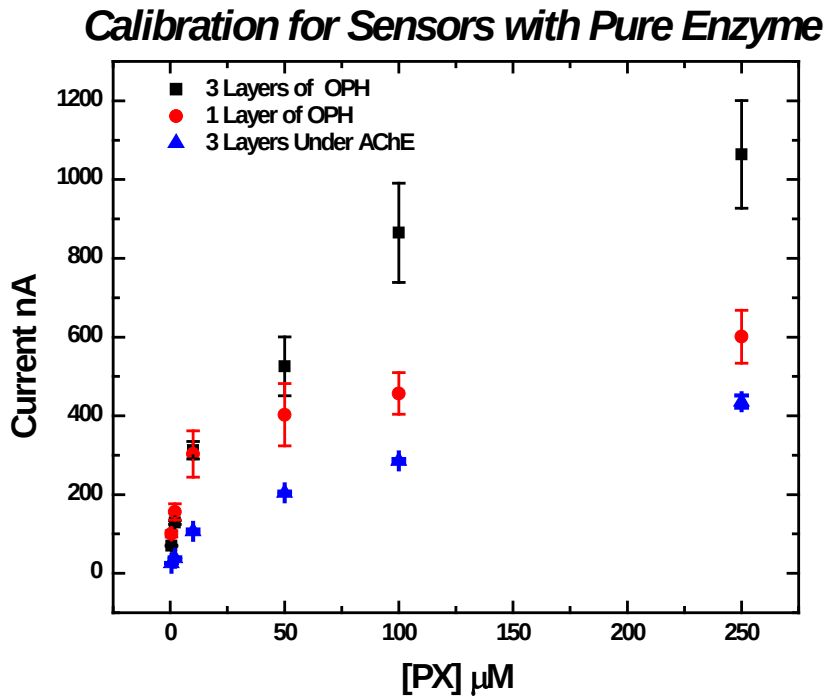

Figure 49: Calibration curves for layer-by-layer assemblies of enzymes without carbon nanotubes, thus no scaffolding to anchor the enzyme to the sensor. The signal for PX injections is higher as one would expect from pure enzyme, but the error is significantly increased from enzyme being washed out. For the layer buried under AChE, the error is reduced, suggesting the AChE is holding the OPH down.

Pralidoximes are capable of restoring activity to AChE after inhibition by neurotoxins, but their effectiveness is much reduced at high concentrations of neurotoxin. Figure 50 shows the baseline activity, inhibition, and the reactivation of the sensor using 1 μM paraoxon to inhibit the enzyme, and then using 20 mM 2-PAM to reactivate it. The high concentration of neurotoxin completely kills all the enzymatic activity, and thus the 2-PAM cannot recover the complete activity of AChE. The reduction in the peak height is attributed to the disassociation of physically adsorbed MWNT-AChE that is not electrostatically bound. This signal eventually stabilizes as shown by the other two traces, and the asymptotic decrease in the peak height.

Discriminative detection between organophosphorus and non-organophosphorus neurotoxins could be realized in a two channel system, with OPH in one channel and AChE in the other. For organophosphorus neurotoxins, both channels would show a change in electrochemistry (the OPH channel would hydrolyze the neurotoxin kinetically, and the AChE would become inhibited by neurotoxin affinity for the active site).

Multianalyte Detection and Protection of AChE

Multianalyte detection was achieved with both MWNT-AChE terminal and MWNT-OPH terminal sensors (Figure 51). Paraoxon was calibrated across both sensors, and ATCh was measured before and after that calibration. For MWNT-AChE terminal sensors, the paraoxon signal was reduced (when compared to the MWNT-OPH sensors) and a change in AChE activity could be seen with the reduction in the ATCh signal. For MWNT-OPH terminal sensors, the paraoxon signal is higher, and there does not seem to be any significant reduction in the signal from AChE. This suggests that OPH could protect AChE from paraoxon, and other organophosphate pesticides. Theoretically, this makes sense in that the kinetic rate for destruction of PX by OPH ($k_{cat} \sim 8900\ s^{-1}$) is extremely high and more efficient than the time it

takes for the neurotoxin to inhibit AChE (typically 15 minutes to reach maximum inhibition).[1, 67] Figure 52 shows the % inhibition of AChE in an OPH terminal sensor that is first exposed to 250 µM paraoxon then to 250 µM methyl carbamate (a non OP pesticide). The AChE activity was measured between both neurotoxins.

Finally, to demonstrate the ability of OPH to protect AChE from OP neurotoxins, two layer-by-layer assemblies were built on a single electrode. One of the LbLs was built right under the inlet channel from the reference electrode and ended with MWNT-OPH, while the other was built over the electrode and ended in MWNT-AChE (Figure 53). The final layers were dried on the electrode to maximize the signal from both enzymes. The baseline activity for MWNT-AChE was measured first, and then buffer was passed over the sensor for 15 minutes at a slow flow rate (200 µL/hr) to simulate the incubation of the enzyme with neurotoxin. ATCh was measured at a flow rate of 10 mL/hr while all inhibition steps were performed at the slow flow rate of 200 µL/hr. The experiment was paused during the inhibition steps to prevent any electrochemical effects at the electrode during incubation. As shown in Figure 54, the inhibition of AChE by PX is greatly reduced at low to high concentrations, and not until the highest concentrations is there any significant loss in activity, when the protection LbL is present. Methyl carbamate is not affected by the OPH, and therefore inhibition is much greater. There was a loss of activity of the AChE for plain buffer for the first injection (and it is taken as the reference for the neurotoxin injections) attributed to the desorption of physically adsorbed MWNT-AChE (non-electrostatic binding), and so the loss in activity for the first two injections of PX are attributed to this effect.

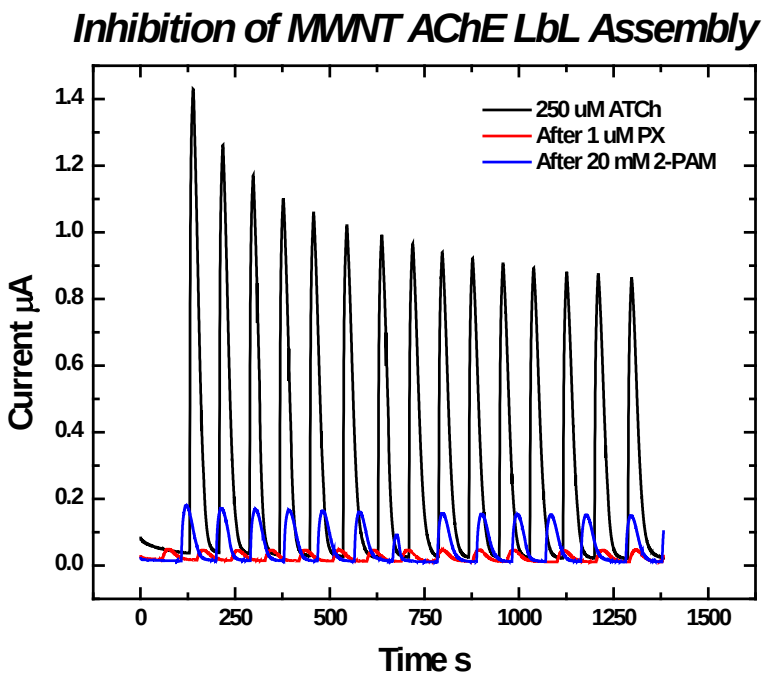

Figure 50: Inhibition and reactivation of AChE by paraoxon and 2-PAM (a pralidoxime), respectively. The decrease in peak height is attributed to desorption of non-electrostatically bound MWNT-AChE, and the signal eventually stabilizes. 2-PAM is limited in its ability to reactivate the enzyme, especially at high concentrations of neurotoxin.

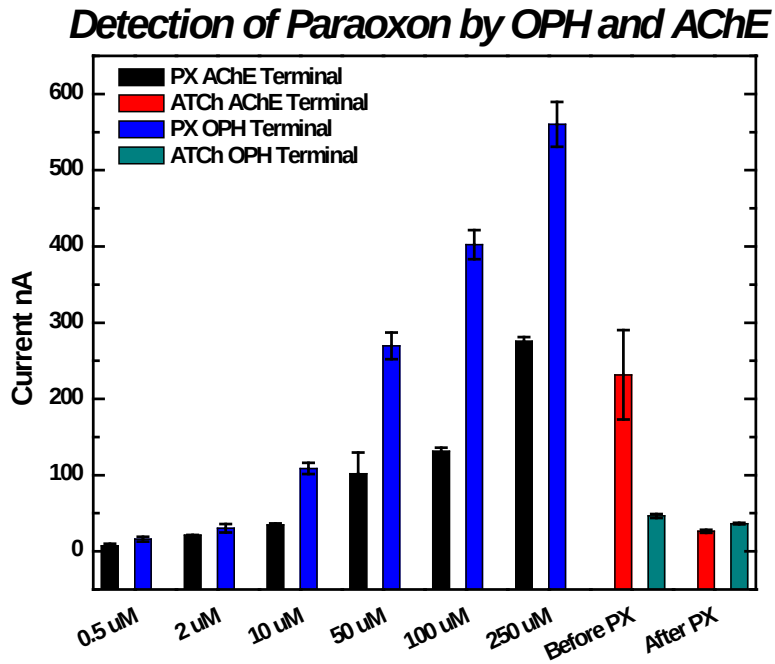

Figure 51: Paraoxon and ATCh responses for sensors with different terminal layers. The AChE terminal sensors showed lower response to paraoxon, while exhibiting higher ATCh signal with inhibition. The OPH terminal sensors showed higher paraoxon response, and significantly reduced inhibition. For each sensor, the initial activity of AChE was measured, then a paraoxon calibration was performed, following that the activity of AChE was measured again. The inhibition in this experiment cannot be attributed to a single concentration of PX as the activity was only measured before and after the calibration for paraoxon.

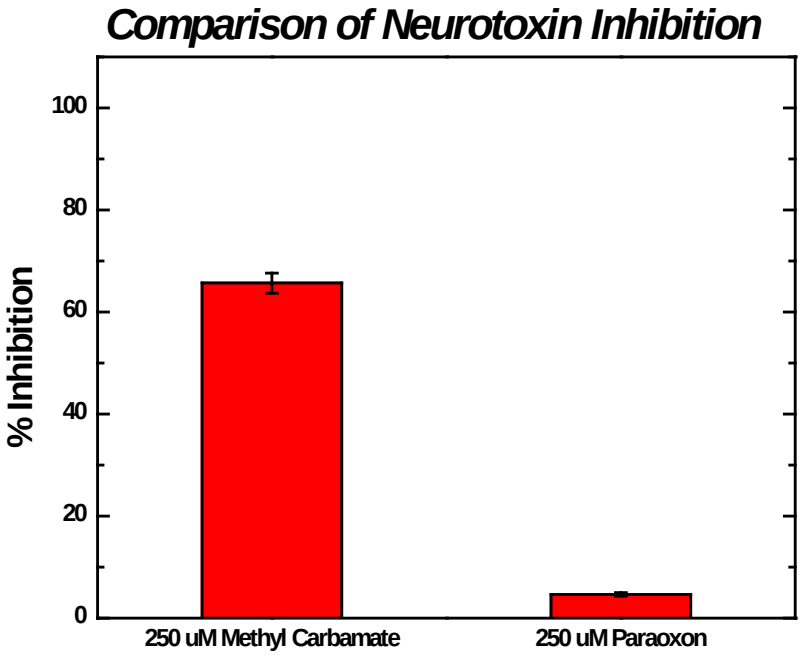

Figure 52: Paraoxon and methyl carbamate were injected onto the same sensor and the activity of AChE before and after paraoxon and then methyl carbamate was checked. The sensor had a layer of MWNT-OPH over the the MWNT-AChE, which (from their respective % inhibition of AChE) was able to protect the AChE from paraoxon.

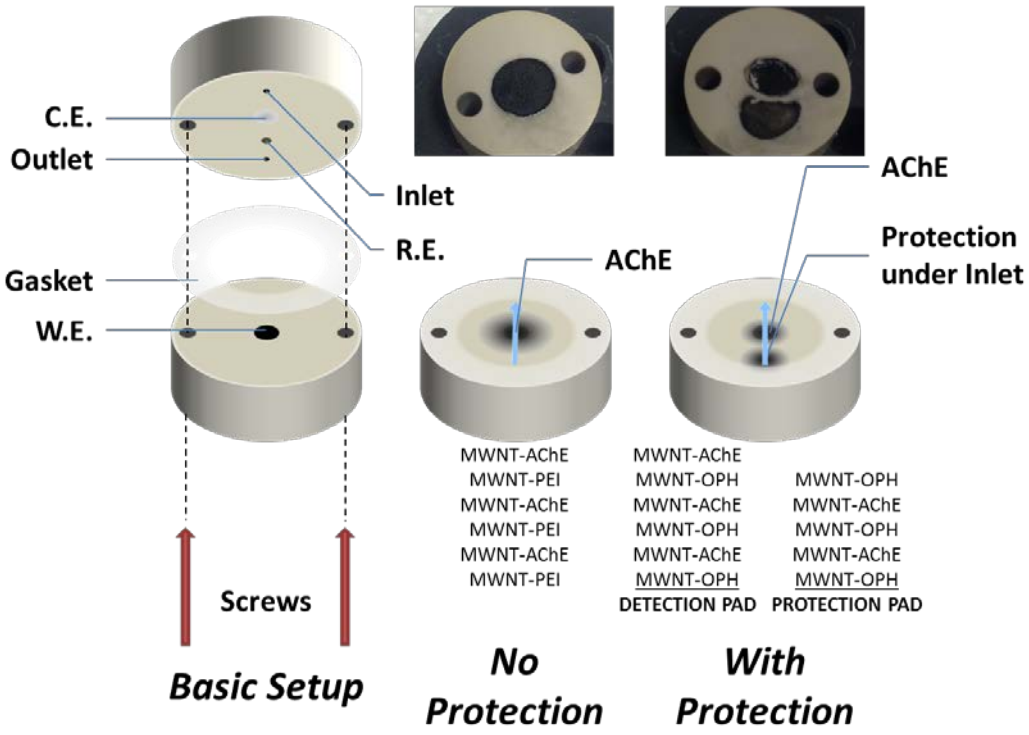

Figure 53: Schematic showing the composition and position of the protection and non-protection sensor layer-by-layer assemblies. The left figure shows the standard glassy carbon FIA set up and how the flow block is assembled. The middle figure shows the non-protection sensor construction. The right figure shows the protection sensor construction. The blue arrow shows the flow direct. The total volume (30 µL) for both sensors was the same (30 µL versus 15/15 µL).

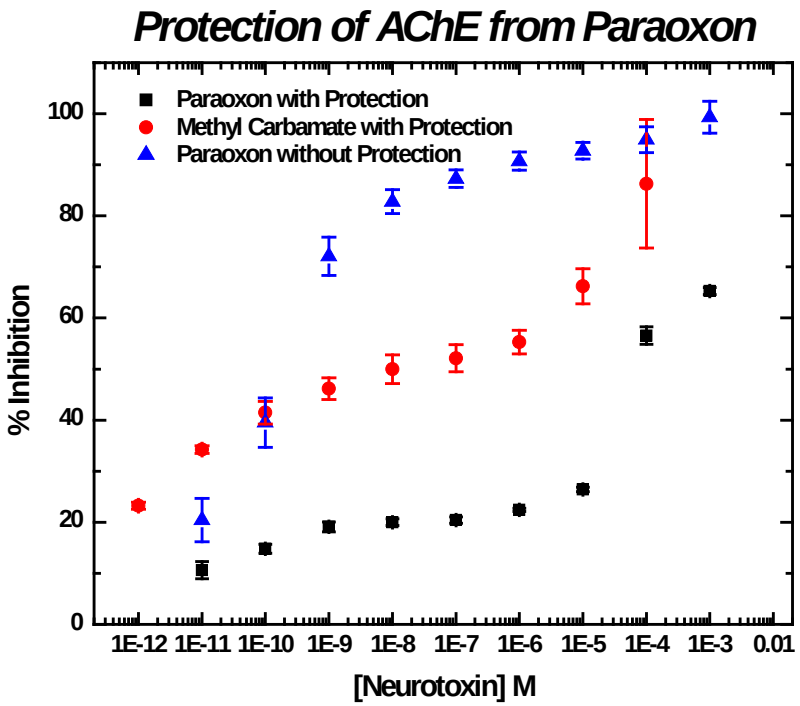

Figure 54: Shows the calibration of % inhibition on a sensor with a protection pad at the inlet (MWNT-OPH terminal LbL assembly) for methyl carbamate and paraoxon. The calibration for no protection is also presented for comparison. One can see that the OPH is preventing the paraoxon from inhibiting OPH at certain concentrations.

Conclusions and Future Outlook

This section provided a glance at the work performed on acetylcholinesterase and organophosphate hydrolase layer-by-layer assemblies for discriminative detection of organophosphorus and non organophosphorus neurotoxins. The layer-by-layer assembly nanofabrication technique is extremely versatile, and allows one to employ multiple biorecognition elements within a single platform. At this point, it may be possible to screen organophosphate neurotoxins from running buffer and prevent them from inhibiting acetylcholinesterase. In a dual channel sensor, discriminate detection could be achieved through determining % inhibition of AChE and comparing it to the OPH channel. If there is signal from the OPH channel, then there is an organophosphate neurotoxin (in this case paraoxon) present. In its current form, this only works for OP neurotoxins that have leaving groups that are electroactive (paraoxon's leaving group is *p*-nitrophenol), and therefore in other systems, pH

may need to be examined. If AChE becomes inhibited and there is no signal from the OPH channel, then there is a non-organophosphate neurotoxin present. Further work would need to be performed to achieve detection and separation of mixed samples. A strong calibration for both paraoxon and carbamates would need to be achieved so that a comparison could be made between the amount of signal from the OPH channel with respect to the % inhibition of AChE channel. This could also be achieved with the protection of AChE from OPs, and complete protection would be needed, so that if a non-OP neurotoxin were to be present, the AChE inhibition can be attributed to only the non-OP neurotoxin.

Chapter 6: Prototype Flow Cell Design and Fabrication

This chapter is dedicated to the late Mr. L.C. Mathison, who provided advice and expertise in developing my engineering drawing skills, and helped provide insight and review for implementing my design and having it professionally manufactured.

Currently there exist many different types of flow cells to allow flow injection analysis (FIA) to be performed on small scale disposable/screen printed electrodes. Prominent examples include BVT and Dropsens (Figure 55), which are commercially available for use only with their supplied electrodes.

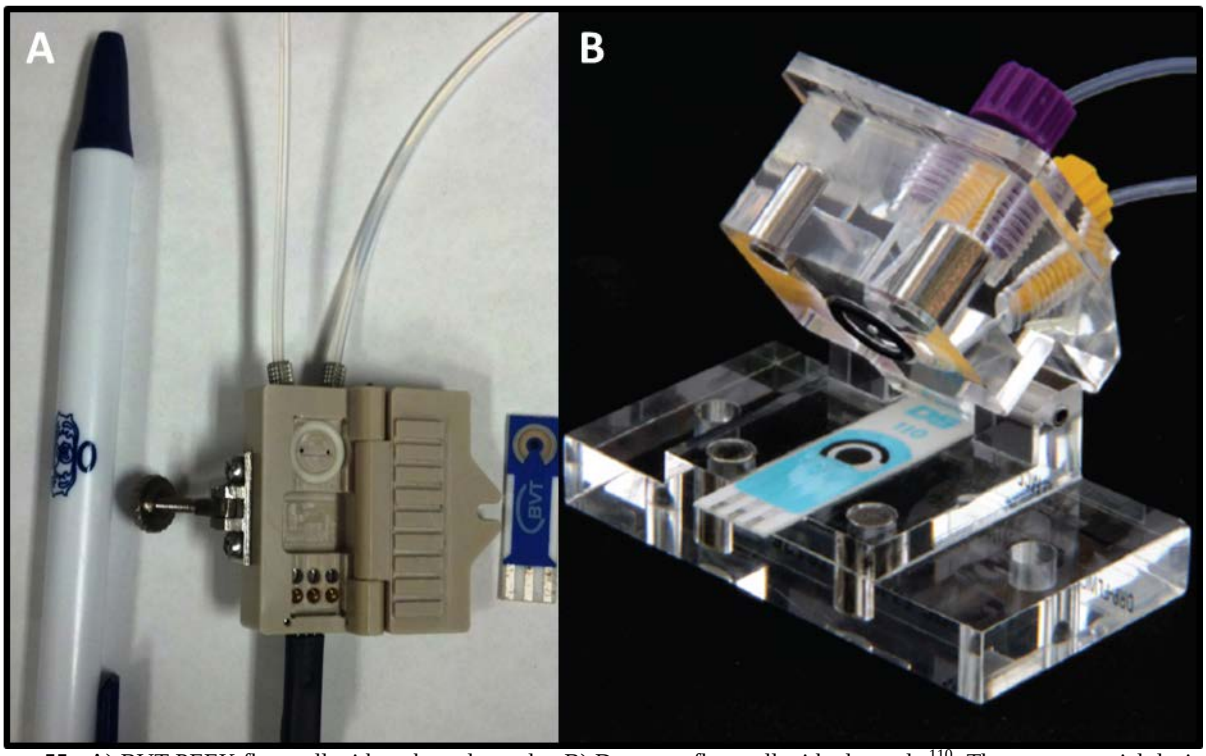

Figure 55: A) BVT PEEK flow cell with carbon electrode. B) Dropsens flow cell with electrode.[110] These commercial devices are readily available, however they are only able to be used with their supplied electrodes, and in the case of (B) the initial investment cost is very high.

The advantage of screen printed electrodes (SPEs) is their manufacturability, cost, and versatility in material choice. BVT (Figure 56A) offers several different types of sensors with different working electrode materials, such as Au-Pt alloy, Au, Pt, Ag, and graphite. For reference electrodes, they allow you to choose between Ag and Ag/AgCl. They also offer pre-modified electrodes with different enzymes such as AChE and GOx. Dropsens (Figure 56B) also offers electrodes with many different modifications and sensor materials. The main drawback of these two electrodes is their W.E. size (BVT W.E. area 0.785 mm^2, Dropsens W.E. area 2 mm^2 to 12.6 mm^2). These technologies have great merit for use, however they are branded, have a high initial cost, and are specific only to their respective electrodes. Pine Instruments (Figure 56C) offers large scale carbon ink working electrodes (area 20 mm^2) that are easily modified with the layer-by-layer process, and provides a good model for a more universal flowcell design.

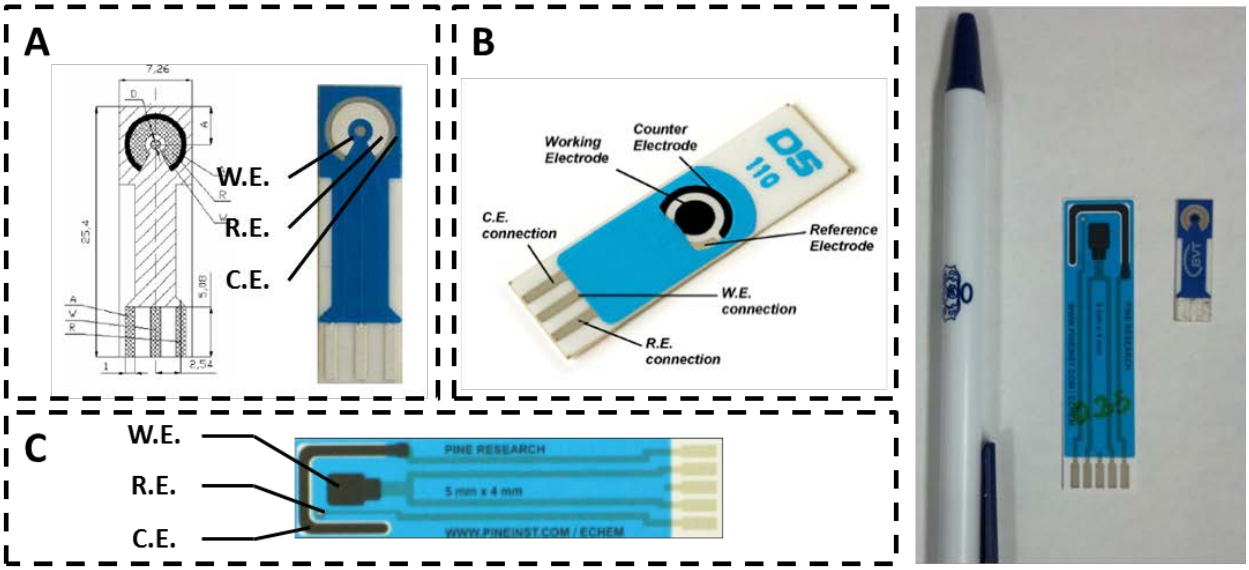

Figure 56: A) BVT,[111] B) Dropsens,[112] and C) Pine Instrumnents screen printed electrodes.[113] Right) Comparison of size between BVT and PI electrodes.

However, no flow cell is currently available for this product, and its layout is rectangular, as opposed to the circular layout of other commercially available products. The challenge was to

design a flow system which allows stable flow across the working and supporting electrodes in this rectangular configuration to enable FIA to be performed on these electrodes. In addition to the engineering challenge presented, this provided an opportunity to facilitate/foment self-teaching and life-long learning, through learning AutoCAD 2012 and some basic machining/milling.

Design #1

The first design (Figure 57) was completed through physical experimentation with machining equipment and involved the use of a single inlet and outlet drilled in through the side with four holes drilled up into the channel of each to allow for linear flow across a rectangular volume. The main problem with this design was the uneven access to each of the 4 channels for the mobile phase (in this case phosphate buffered saline) which meant that an air bubble would form on the working electrode. This air bubble impedes access for the mobile phase/analyte to the working electrode, and thereby reduces signal output for the sensor. From this design, it was apparent that eliminating the air bubble and ensuring that the flow paths are all equal in length would be necessary in order to achieve stable flow.

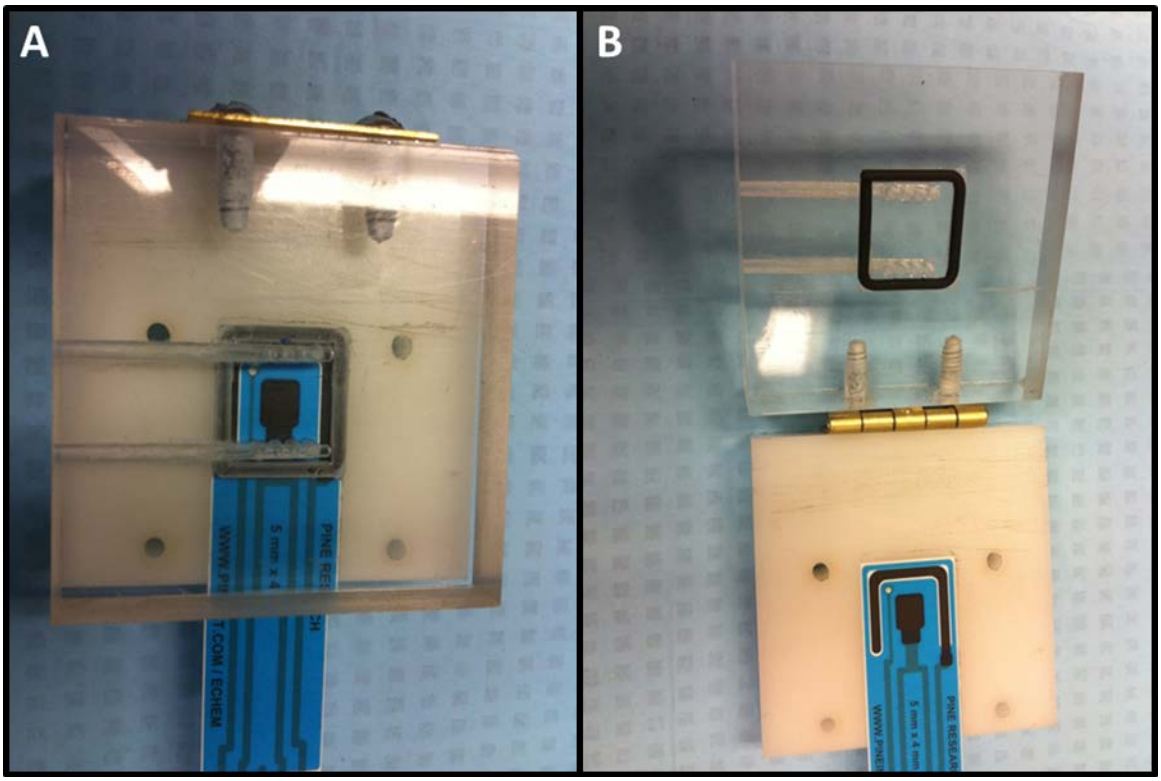

Figure 57: The first SPE flow cell design, which was accomplished by drilling 2 holes in the side to form channels (inlet/outlet) and then drilling up into the channels to make four inlets and outlets over the electrode surface.

Design #2

The second design (Figure 58) was completed using AutoCAD and the design was reviewed by the late Mr. L.C. Mathison, who provided advice and some insight into how a part would be transferred from design on paper to a physical model. This design involved a single inlet with three outlets spaced evenly around the inlet. This design was ultimately rejected due to its complexity in the way it would be manufactured, and a more simple design would be able to be completed.

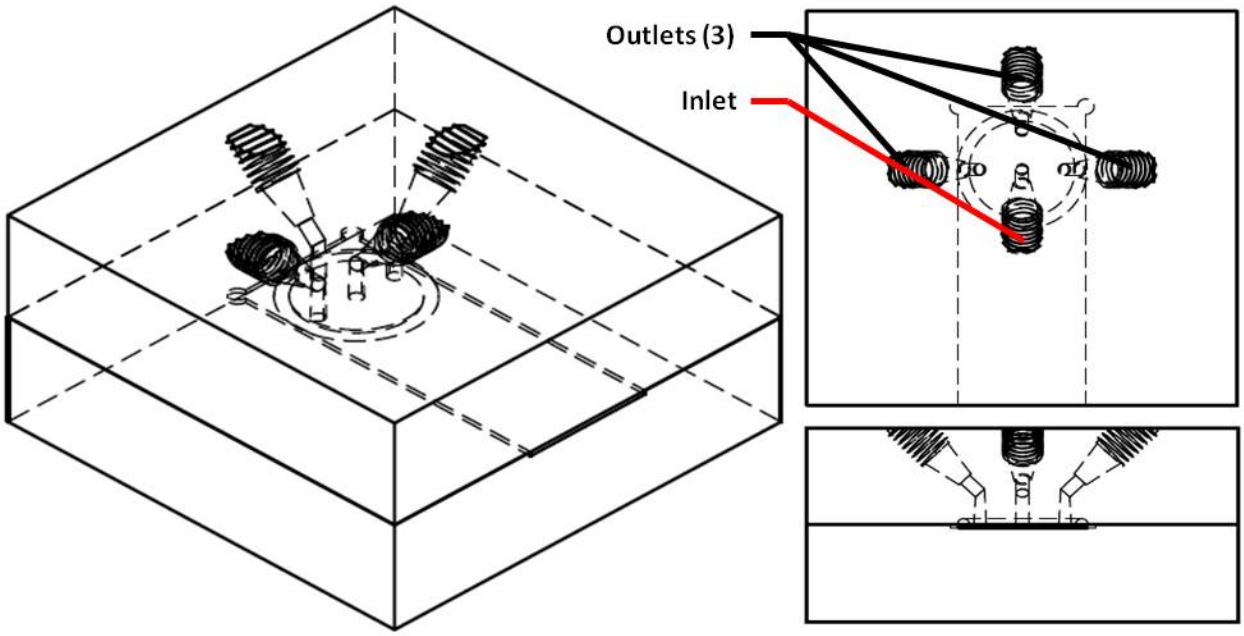

Figure 58: Top, side, and isometric views of a computer designed flow cell with 1 inlet over the center of the working electrode, and three outlets at the edges of the flow volume. The 1/4-28 detail shown was deemed too difficult to accomplish, so this design was rejected for a simpler design.

Design #3

This design (Figure 59) became the basis for the final product, and was designed using AutoCAD. Following the advice from Mr. Mathison, a new type of flow cell design was implemented involving different layers of material with channels and holes machined to allow for flow to and from the electrode. The SPE would have had one inlet on the center of the working electrode, with eight outlets directed radially from the center. This would allow for even flow across the entire surface, and minimize flow effects which might cause air bubbles to accumulate or form. This design has many redundancies, which increase the complexity of the design, and therefore it was rejected in favor of simplifying the design before going to the prototype phase.

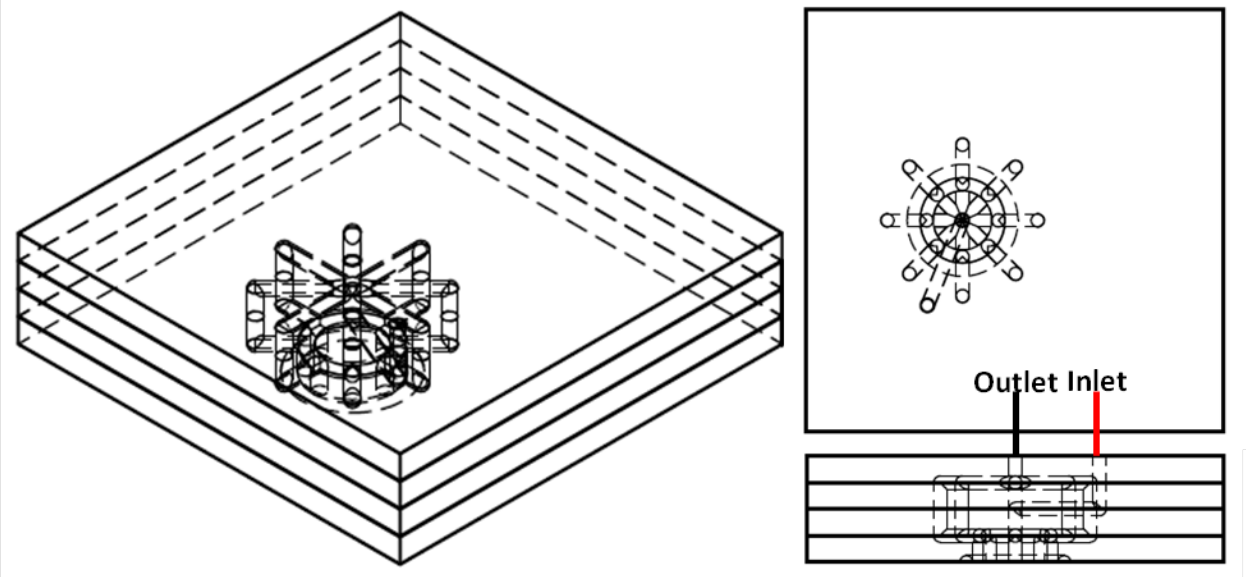

Figure 59: Design #3 involved 4 layers of material with channels machined through and along the faces of each layer. When assembled, this would create a similar effect as Design #2 without the fabrication difficulty. As is apparent from the side view, there are several redundant/unnecessary features in this design. Going forward, those were taken out to save time and material.

Design #4

This is the first of the designs to be built in Autodesk Inventor 2012, and is a simplified and more efficient version of Design #3. This design also incorporated the precise dimensions of the commercial parts after their specifications had been acquired from their respective manufacturers (Thumbscrews (MMC), O-ring (MMC), and the fittings (VICI)). Instead of four layers, this one only needs three, and takes advantage of the design of milling bits, to reduce the need for rounded channels. All of the channels are milled straight down and are square in cross section. The o-ring also has a square cross section to take advantage of the milling bits. This design was sent to a prototyping company and they manufactured the parts out of polycarbonate plates (Figure 60). Polycarbonate was chosen for its transparency, strength, and chemical resistance to aqueous solutions. Unfortunately another problem was created by going to the layer system, as it was necessary to "glue" the layers together in order to create the flow channels for the mobile phase. Acetone chemically reacts with acrylic polymers (such as polycarbonate) and melts/fuses them together. However, this process releases a gas, and does not allow for any

"working time." It became apparent that using acetone to chemically "weld" the layers together left gas bubbles/voids between the layers.

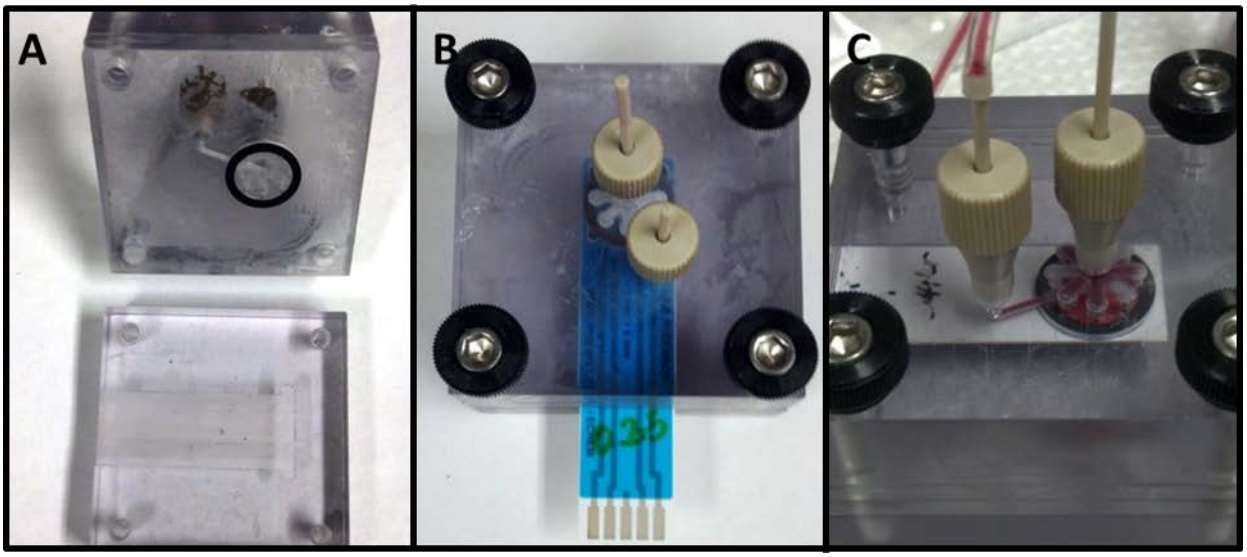

Figure 60: Pictures of Design #4 showing the completed product. The translucence of the polycarbonate comes from the chemical welding process (using acetone to dissolve/glue the polymer together) and was a key problem to be solved with Design #5.

The data for 500 µM ferrocene methanol in 1 M KCl show peak uniformity at low flow rates and is stable at different flow rates ranging from 5 to 120 mL/hr. Figure 61A and Figure 61B compare the current signal profiles for each of the different flow rates as well as the peak height stability over multiple injections.

While these data show good stability and uniform peak profiles, the chemical welding method has some serious drawbacks. In addition to poor optical appearance (the gas bubbles voids makes the flow cell look "cloudy"), the flow cell has some leakage problems, as well as an inadvertent crossing of the inlet and outlet. This is due to erosion from the chemical welding process where the inlet flows between two outlet holes, immediately before the mobile phase reaches the electrode. Therefore, Design #5 was deemed a necessary redesign to correct these minor flaws. To summarize the issues, the chance of cross flow between the inlet and outlets needed to be eliminated and a better "gluing" method needed to be used, in order to maintain optical clarity.

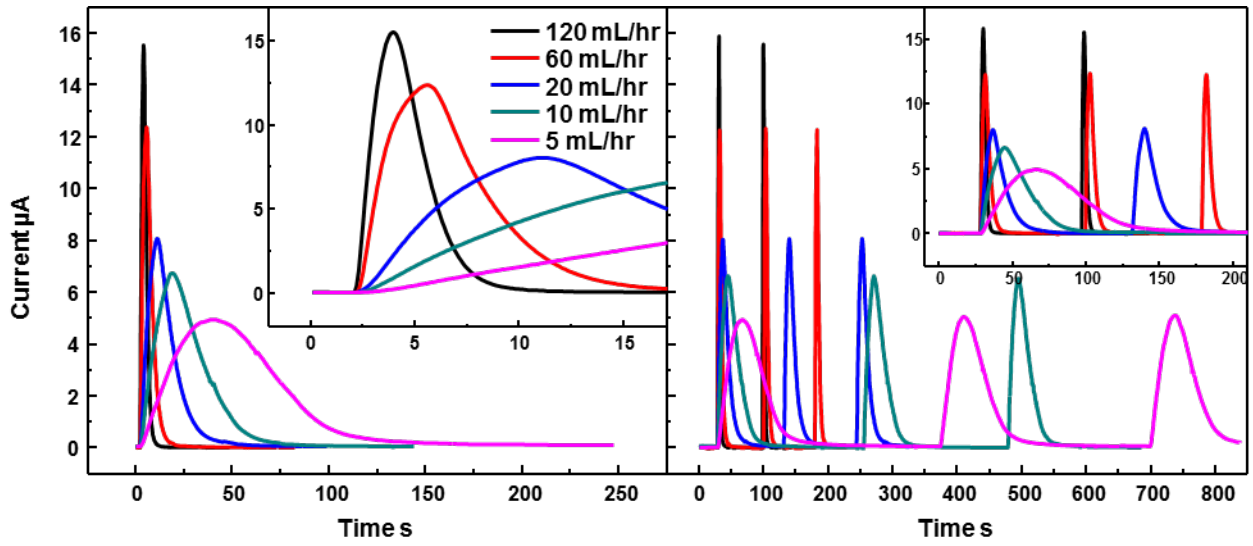

Figure 61: Amperometric data from 500 uM Ferrocene methanol dissolved in 1 M KCl. These data show the responsiveness of the sensor, and ultimately the stability/uniformity of flow in the Design #4 flow cell at different flow rates. The figure on the left compares the peak profile at different flow rates (inset is zoomed on 120 and 60 mL/hr peaks), and the figure on the right compares the peak stability for multiple, sequential injections of the analyte.

Design #5

In order to eliminate the chance for cross flow between the inlet and outlet prior to the mobile phase/analyte reaching the electrode, the outlet channels were reduced in diameter to that of the first (bottom) layer. All chamfering of the outlet holes was also removed, so that there would not be an easy path for wall erosion (in the case of chemically welding) to take place. Several methods of chemical welding and glues were tested with scrap polycarbonate to determine the best one for maintaining optical clarity and sealing the layers together. A gasket was also designed in the event that none of those methods worked. Figure 62A-C are samples of the polymer chemically welded using dichloromethane and different amounts of polycarbonate shavings.

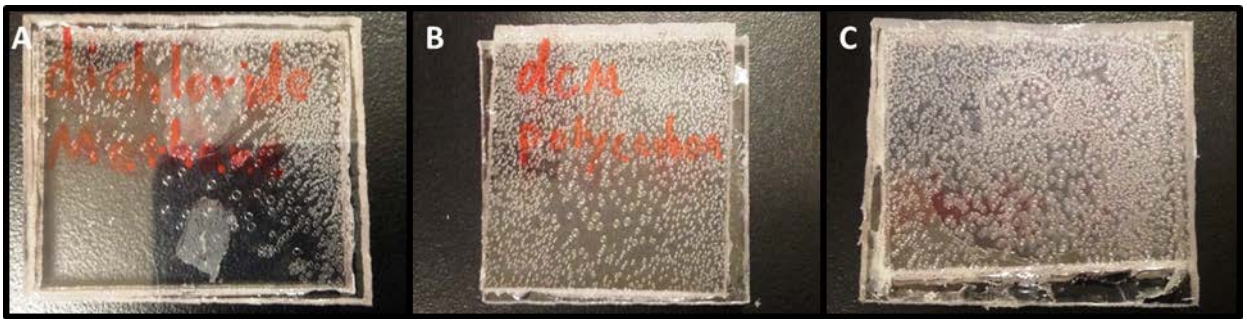

Figure 62: These pictures show the different concentrations of polycarbonate shavings in dichloromethane. A) no shavings B) 500 mg shavings C) 2 g shavings. As the amount of shavings increases, the viscosity (and working time) of the "glue" increases. However, because the chemical reaction releases a gas, the amount of bubbles sandwiched between the two pieces of polymer also increases.

All of these methods produced gas bubbles, although the pure dichloromethane produced the least (it also had no working time). A two-part glue was purchased from ePlastics Inc, which is specifically designed for gluing polycarbonate together. Figure 63 shows the result of gluing two pieces of polycarbonate together, and that few airbubbles are formed, although the polycarbonate becomes translucent.

Using the computational fluid dynamics (Autodesk Simulation CFD 2013) plugin for Inventor, velocity profiles for the BASi Unicell FIA apparatus, Design #1, Design #4, and Design #5 were obtained, to determine flow paths through across the electrodes. Boundary conditions were set for different volume flow rates at the inlet/outlet (both the same) of each design, and a “flow trace” was obtained for each design (Figure 64, see also appendix). Volume flow rate had little effect (10, 15, 20 mL/hr) on the results, and only affected the magnitude of the velocity. Figure 65 shows the layers before the new glue was applied, and Figure 66 shows the final product.

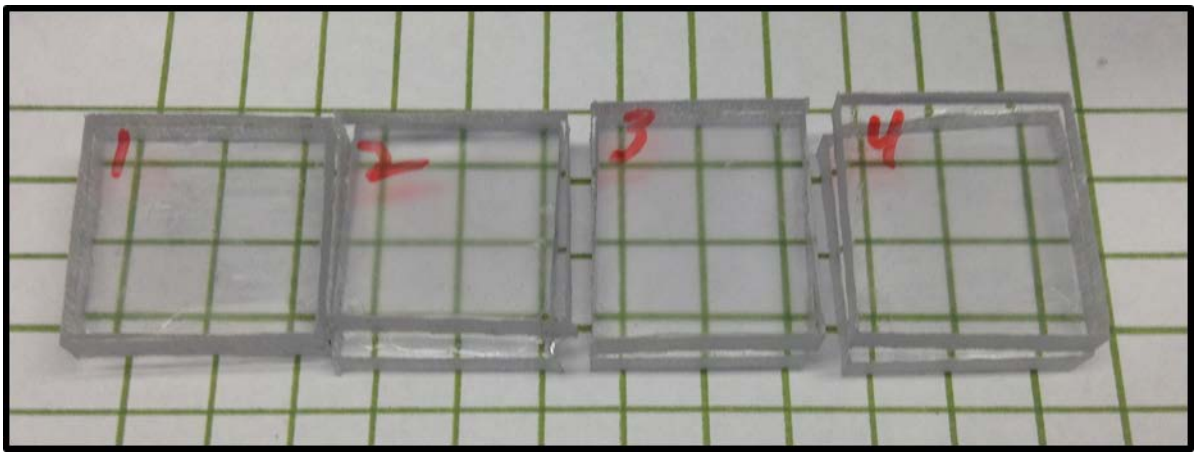

Figure 63: Polycarbonate glue samples after 48 hours of drying time.

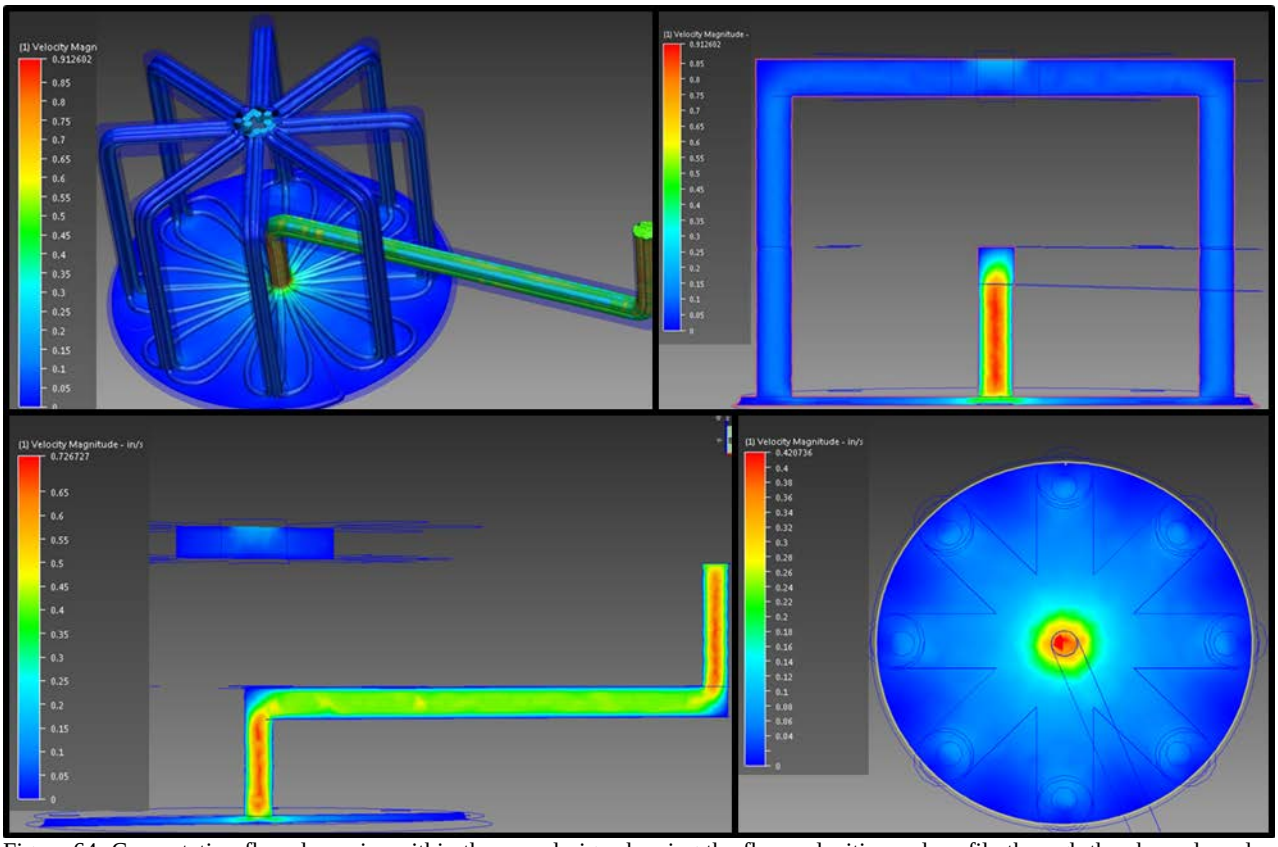

Figure 64: Computation flow dynamics within the new design showing the flow velocities and profile through the channels and across the electrode.

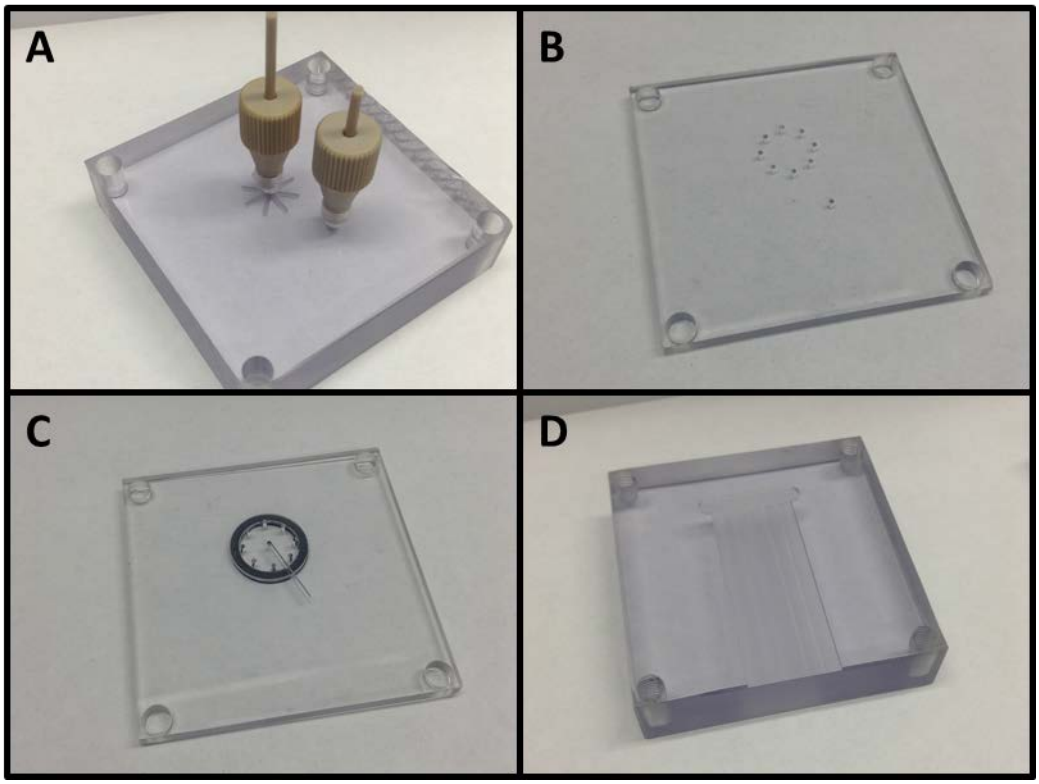

Figure 65: Photographs of each of the layers. (**A**) The top layer holding the fittings to interface with the tygon tubing. (**B**) The middle layer which separates the inlet and outlet channels. (**C**) The bottom layer which forms the interface between the flowcell and the electrode. (**D**) The bottom piece which the electrode sits in and to which the upper piece (all three layers) screws into.

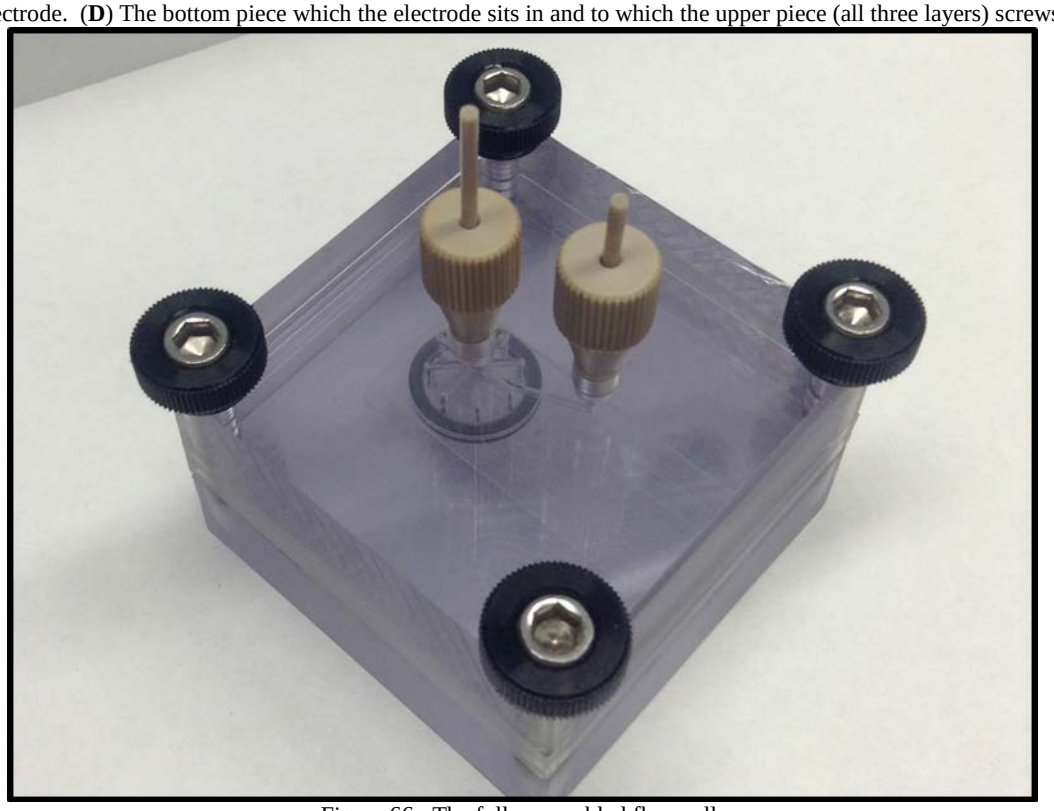
Figure 66: The fully assembled flow cell.

Conclusions and Future Outlook

A flow cell was designed and successfully constructed for use with various different types of screen printed electrodes. The final product had excellent transparency and fluidics. This product could be more easily fabricated using a 3D printer, which would eliminate the need for gluing the layers together, and there are transparent 3D printer materials available. However, the polycarbonate is not a good material to use with organic chemicals such as acetone and phenols. Therefore a material like polyethyletherketone (PEEK) might be better suited for applications requiring the use of highly concentrated organic materials. Furthermore the bottom piece could be modified to allow different types of screen printed electrodes to be used with little change in design.

Overall Conclusions and Suggestions for Future Work

This thesis discusses the use of layer-by-layer assembly to build electrochemical sensors which are able to detect two analytes simultaneously using two different enzymes. This work forms the basis for the implementation of a sensing device capable of detection and discrimination of many different neurotoxic compounds. Acetylcholinesterase provides sensitive (10^{-11} M) detection of all neurotoxins, as well as some phenolic compounds and heavy metals, while organophosphate hydrolase directly detects only organophosphate neurotoxins (preferentially hydrolyzing P-O bonds). The combination of these two enzymes has been achieved such that discriminate detection of organophosphate and non-organophosphate compounds is possible with this system. A consequence of this combination may have yielded a system that is capable of protecting acetylcholinesterase from organophosphorus compounds, meaning a sensor that is only susceptible to non-organophosphates may be realized with further work and implementation.

This work has also demonstrated the versatility of the layer-by-layer assembly technique and feasibility of building sensors capable to detect multiple analytes on a single platform. Two completely different enzymes (organophosphate hydrolase and glucose oxidase) were combined to build a sensor which could detect neurotoxins, with little influence from the glucose oxidase. Although the glucose detection part of the sensor was never fully developed, this provides evidence that any combination of enzymes is possible within the bounds of the layer-by-layer assembly rules (must be charged and alternatively adsorbed). Future work could focus on using the apo-glucose oxidase (GOx without the FAD cofactor) to study the penetration of the layers

by building a sensor with inactive layers and burying the active layer to see how far substrate can penetrate into the sensor. Optimization and validation of glucose immobilization also has yet to be realized in this work (although this has been achieved many times by many other laboratories and research facilities).

Zeta potential experiments could be performed to determine the best pH for layer-by-layer assembly of the film components. This would provide a general idea of the charge characteristics for each enzyme/biomaterial and allow one to ensure the strongest interaction between layers, reducing the chance for desorption. The reason for the subsequent peak reduction phenomenon should be investigated. There is evidence that it could be layer desorption, but it could also be the result of fouling or contamination of the film. Strict manipulation and control of the enzyme immobilization and layer adsorption in the layer-by-layer assemblies will be necessary to achieving a strong and reliable calibration for OP and non-OP neurotoxin detection. Investigation of the layer properties at different adsorption pH and concentrations of layer constituent materials could lead to an optimal final result for these calibrations. It will be important to know how well the substrates will be able to penetrate into the lower layers when there are different layer properties (closed layers versus open layers). Finally, control over the sensitivity of the AChE inhibition mechanism could be realized through using various amounts of AChE layers. A large amount of enzyme could adversely affect the sensitivity of the sensor when the lower concentrations of neurotoxin are unable to produce any significant inhibition result.

This work is only the initial part of a neurotoxin sensor as many other enzymes could be incorporated into the film to provide discriminate detection (OPAA for fluorine-containing OPs, tyrosinase for phenols, etc.) among many different compounds. The multi-enzyme/multi-analyte

biosensor principle can be also applied to many other systems which may require several recognition events before a final result is achieved.

References

1. E. Rainina, E. Efremenco, S. Varfolomeyev, A. Simonian and J. Wild, *Biosensors and Bioelectronics*, 1996, **11**, 991-1000.

2. A. Watson, D. Opresko, R. Young, V. Hauschild, J. King and K. Bakshi, *Handbook of Toxicology of Chemical Warfare Agents", Ed. by RC Gupta.—Oxford: Elsevier*, 2009, 43-67.

3. UN, *Convention on the Prohibition of the Development, Production, Stockpiling and Use of Chemical Weapons and on their Destruction*, treaties.un.org/Pages/ViewDetails.aspx?src=TREATY&mtdsg_no=XXVI-3&chapter=26&lang=en, Accessed March, 2013.

4. A. Simonian, J. Grimsley, A. Flounders, J. Schoeniger, T.-C. Cheng, J. DeFrank and J. Wild, *Analytica chimica acta*, 2001, **442**, 15-23.

5. M.-M. Blum, C. M. Timperley, G. R. Williams, H. Thiermann and F. Worek, *Biochemistry*, 2008, **47**, 5216-5224.

6. S. D. Kirby, J. R. Norris, J. Richard Smith, B. J. Bahnson and D. M. Cerasoli, *Chemico-biological interactions*, 2012.

7. J. Kirsch, V. A. Davis and A. L. Simonian, Sensors, 2012 IEEE, 2012.

8. D. R. Thévenot, K. Toth, R. A. Durst and G. S. Wilson, *Biosensors and Bioelectronics*, 2001, **16**, 121-131.

9. B. R. Eggins, *Chemical sensors and biosensors*, Wiley, 2008.

10. H. Uzawa, K. Ohga, Y. Shinozaki, I. Ohsawa, T. Nagatsuka, Y. Seto and Y. Nishida, *Biosensors and Bioelectronics*, 2008, **24**, 923-927.

11. G. Ferracci, S. Marconi, C. Mazuet, E. Jover, M.-P. Blanchard, M. Seagar, M. Popoff and C. Lévêque, *Analytical biochemistry*, 2011, **410**, 281-288.

12. K. Campbell, S. A. Haughey, H. v. d. Top, H. v. Egmond, N. Vilariño, L. M. Botana and C. T. Elliott, *Analytical chemistry*, 2010, **82**, 2977-2988.

13. M. Labib, M. Hedström, M. Amin and B. Mattiasson, *Analytical and Bioanalytical Chemistry*, 2009, **393**, 1539-1544.

14. J. P. Meneely, F. Ricci, H. P. van Egmond and C. T. Elliott, *TrAC Trends in Analytical Chemistry*, 2011, **30**, 192-203.

15. S. Pal and E. C. Alocilja, *Biosensors and Bioelectronics*, 2010, **26**, 1624-1630.

16. T. B. Tims and D. V. Lim, *Journal of microbiological methods*, 2004, **59**, 127-130.

17. T. J. Gnanaprakasa, O. A. Oyarzabal, E. V. Olsen, V. A. Pedrosa and A. L. Simonian, *Sensors and Actuators B: Chemical*, 2011, **156**, 304-311.

18. M. M. Ngundi, C. R. Taitt and F. S. Ligler, *Biosensors and Bioelectronics*, 2006, **22**, 124-130.

19. N. V. Kulagina, K. M. Shaffer, G. P. Anderson, F. S. Ligler and C. R. Taitt, *Analytica chimica acta*, 2006, **575**, 9-15.

20. S.-H. Ohk and A. K. Bhunia, *Food microbiology*, 2012.

21. S. Li, Y. Li, H. Chen, S. Horikawa, W. Shen, A. Simonian and B. A. Chin, *Biosensors and Bioelectronics*, 2010, **26**, 1313-1319.

22. K. E. Sapsford, A. Rasooly, C. R. Taitt and F. S. Ligler, *Analytical chemistry*, 2004, **76**, 433-440.

23. A. Subramanian, J. Irudayaraj and T. Ryan, *Sensors and Actuators B: Chemical*, 2006, **114**, 192-198.

24. A. Gupta, D. Akin and R. Bashir, *Applied Physics Letters*, 2004, **84**, 1976-1978.

25. A. A. Yanik, M. Huang, O. Kamohara, A. Artar, T. W. Geisbert, J. H. Connor and H. Altug, *Nano letters*, 2010, **10**, 4962-4969.

26. Y. Li, H. Lee and R. Corn, *Analytical chemistry*, 2007, **79**, 1082-1088.

27. Y. Gao and I. Kyratzis, *Bioconjugate chemistry*, 2008, **19**, 1945-1950.

28. S. Mantha, V. A. Pedrosa, E. V. Olsen, V. A. Davis and A. L. Simonian, *Langmuir*, 2010.

29. D. Nepal, S. Balasubramanian, A. L. Simonian and V. A. Davis, *Nano letters*, 2008, **8**, 1896-1901.

30. V. A. Pedrosa, T. Gnanaprakasa, S. Balasubramanian, E. V. Olsen, V. A. Davis and A. L. Simonian, *Electrochemistry Communications*, 2009, **11**, 1401-1404.

31. V. A. Pedrosa, S. Paliwal, S. Balasubramanian, D. Nepal, V. Davis, J. Wild, E. Ramanculov and A. Simonian, *Colloids and Surfaces B: Biointerfaces*, 2010, **77**, 69-74.

32. Z. Wang, M. D. Shirley, S. T. Meikle, R. L. D. Whitby and S. V. Mikhalovsky, *Carbon*, 2009, **47**, 73-79.

33. C. S. S. R. Kumar, *Biofunctionalization of Nanomaterials, by Challa SSR Kumar (Editor), pp. 377. ISBN 3-527-31381-8. Wiley-VCH, November 2005.*, 2005, **1**.

34. D. W. Horn, K. Tracy, C. J. Easley and V. A. Davis, *The Journal of Physical Chemistry C*, 2012, **116**, 10341-10348.

35. S. Banerjee, T. Hemraj-Benny and S. S. Wong, *Advanced Materials*, 2005, **17**, 17-29.

36. R. H. Garret and C. M. Grisham, *Forth Worth*, 1995.

37. C. Cai and J. Chen, *Analytical biochemistry*, 2004, **332**, 75-83.

38. A. Guiseppi-Elie, C. Lei and R. H. Baughman, *Nanotechnology*, 2002, **13**, 559.

39. J. Lahiri, L. Isaacs, J. Tien and G. M. Whitesides, *Analytical chemistry*, 1999, **71**, 777-790.

40. Y. Lin, F. Lu, Y. Tu and Z. Ren, *Nano letters*, 2004, **4**, 191-195.

41. D. Sehgal and I. K. Vijay, *Analytical biochemistry*, 1994, **218**, 87-91.

42. B. L. Tee and G. Kaletunç, *Biotechnology progress*, 2009, **25**, 436-445.

43. R. D. Richins, I. Kaneva, A. Mulchandani and W. Chen, *Nature biotechnology*, 1997, **15**, 984-987.

44. R. J. Russell, M. V. Pishko, A. L. Simonian and J. R. Wild, *Analytical chemistry*, 1999, **71**, 4909-4912.

45. A. Simonian, B. DiSioudi and J. Wild, *Analytica chimica acta*, 1999, **389**, 189-196.

46. A. Flounders, A. Singh, J. Volponi, S. Carichner, K. Wally, A. Simonian, J. Wild and J. Schoeniger, *Biosensors and Bioelectronics*, 1999, **14**, 715-722.

47. A. Simonian, A. Flounders and J. Wild, *Electroanalysis*, 2004, **16**, 1896-1906.

48. A. Simonian, T. Good, S.-S. Wang and J. Wild, *Analytica chimica acta*, 2005, **534**, 69-77.

49. L. Viveros, S. Paliwal, D. McCrae, J. Wild and A. Simonian, *Sensors and Actuators B: Chemical*, 2006, **115**, 150-157.

50. M. Zourob, A. Simonian, J. Wild, S. Mohr, X. Fan, I. Abdulhalim and N. Goddard, *Analyst*, 2006, **132**, 114-120.

51. S. Paliwal, M. Wales, T. Good, J. Grimsley, J. Wild and A. Simonian, *Analytica chimica acta*, 2007, **596**, 9-15.

52. M. Ramanathan and A. L. Simonian, *Biosensors and Bioelectronics*, 2007, **22**, 3001-3007.

53. A. Mulchandani, S. Pan and W. Chen, *Biotechnology progress*, 2008, **15**, 130-134.

54. X. Ji, J. Zheng, J. Xu, V. K. Rastogi, T.-C. Cheng, J. J. DeFrank and R. M. Leblanc, *The Journal of Physical Chemistry B*, 2005, **109**, 3793-3799.

55. K. R. Rogers, Y. Wang, A. Mulchandani, P. Mulchandani and W. Chen, *Biotechnology progress*, 2008, **15**, 517-521.

56. J. Kirsch and A. Simonian, ECS PRiME Honolulu 222, 2012.

57. S. Mantha, V. A. Pedrosa, E. V. Olsen, V. A. Davis and A. L. Simonian, *Langmuir*, 2010, **26**, 19114-19119.

58. S. V. Mello, M. Mabrouki, X. Cao, R. M. Leblanc, T.-C. Cheng and J. J. DeFrank, *Biomacromolecules*, 2003, **4**, 968-973.

59. J. Zheng, C. A. Constantine, L. Zhao, V. K. Rastogi, T.-C. Cheng, J. J. DeFrank and R. M. Leblanc, *Biomacromolecules*, 2005, **6**, 1555-1560.

60. D. Du, X. Ye, J. Cai, J. Liu and A. Zhang, *Biosensors and Bioelectronics*, 2010, **25**, 2503-2508.

61. A. N. Ivanov, R. R. Younusov, G. A. Evtugyn, F. Arduini, D. Moscone and G. Palleschi, *Talanta*, 2011, **85**, 216-221.

62. X. Sun and X. Wang, *Biosensors and Bioelectronics*, 2010, **25**, 2611-2614.

63. T. T. Bachmann and R. D. Schmid, *Analytica chimica acta*, 1999, **401**, 95-103.

64. T. T. Bachmann, B. Leca, F. Vilatte, J.-L. Marty, D. Fournier and R. D. Schmid, *Biosensors and Bioelectronics*, 2000, **15**, 193-201.

65. H. Schulze, S. Vorlová, F. Villatte, T. T. Bachmann and R. D. Schmid, *Biosensors and Bioelectronics*, 2003, **18**, 201-209.

66. H. Schulze, S. B. Muench, F. Villatte, R. D. Schmid and T. T. Bachmann, *Analytical chemistry*, 2005, **77**, 5823-5830.

67. Y. Zhang, S. B. Muench, H. Schulze, R. Perz, B. Yang, R. D. Schmid and T. T. Bachmann, *Journal of agricultural and food chemistry*, 2005, **53**, 5110-5115.

68. S. Liao, Y. Qiao, W. Han, Z. Xie, Z. Wu, G. Shen and R. Yu, *Analytical chemistry*, 2011, **84**, 45-49.

69. M. D. Luque de Castro and M. C. Herrera, *Biosensors and Bioelectronics*, 2003, **18**, 279-294.

70. P. D. Patel, *TrAC Trends in Analytical Chemistry*, 2002, **21**, 96-115.

71. A. Amine, H. Mohammadi, I. Bourais and G. Palleschi, *Biosensors & Bioelectronics*, 2006, **21**, 1405.

72. F. Arduini, University of Rome, 2008.

73. L. C. Clark and C. Lyons, *Annals of the New York Academy of Sciences*, 1962, **102**, 29-45.

74. S. J. Updike and G. P. Hicks, *Nature*, 1967, **214**, 986-988.

75. G. G. Guilbault and G. J. Lubrano, *Analytica chimica acta*, 1973, **64**, 439-455.

76. A. E. G. Cass, G. Davis, G. D. Francis, H. A. O. Hill, W. J. Aston, I. J. Higgins, E. V. Plotkin, L. D. L. Scott and A. P. F. Turner, *Analytical chemistry*, 1984, **56**, 667-671.

77. E. J. Calvo, R. Etchenique, C. Danilowicz and L. Diaz, *Analytical chemistry*, 1996, **68**, 4186-4193.

78. E. J. Calvo, R. Etchenique, L. Pietrasanta, A. Wolosiuk and C. Danilowicz, *Analytical chemistry*, 2001, **73**, 1161-1168.

79. Y. Degani and A. Heller, *Journal of Physical Chemistry*, 1987, **91**, 1285-1289.

80. J. Wang, *Chemical reviews*, 2008, **108**, 814.

81. A. Simonian, E. Efremenko and J. Wild, *Analytica chimica acta*, 2001, **444**, 179-186.

82. E. S. Forzani, V. M. SolÃ-s and E. J. Calvo, *Analytical chemistry*, 2000, **72**, 5300-5307.

83. J. Hodak, R. Etchenique, E. J. Calvo, K. Singhal and P. N. Bartlett, *Langmuir*, 1997, **13**, 2708-2716.

84. M. D. Shirsat, C. O. Too and G. G. Wallace, *Electroanalysis*, 2008, **20**, 150-156.

85. W. Zhao, J. J. Xu and H. Y. Chen, *Electroanalysis*, 2006, **18**, 1737-1748.

86. G. Decher and J. D. Hong, Makromolekulare Chemie. Macromolecular Symposia, 1991.

87. K. Ariga, J. P. Hill and Q. Ji, *Physical Chemistry Chemical Physics*, 2007, **9**, 2319-2340.

88. A. Baba, M.-K. Park, R. C. Advincula and W. Knoll, *Langmuir*, 2002, **18**, 4648-4652.

89. Y. Wang, A. S. Angelatos and F. Caruso, *Chemistry of Materials*, 2007, **20**, 848-858.

90. R. Pei, X. Cui, X. Yang and E. Wang, *Biomacromolecules*, 2001, **2**, 463-468.

91. X. Cao, S. V. Mello, G. Sui, M. Mabrouki, R. M. Leblanc, V. K. Rostogi, T.-C. Cheng and J. J. DeFrank, *Langmuir*, 2002, **18**, 7616-7622.

92. G. T. Hermanson, *Bioconjugate Techniques*, 2nd edn., Academic Press, Inc., 2008.

93. ThermoScientific, *Chemistry of Crosslinking: Carbodiimide Crosslinker Chemistry*, http://www.piercenet.com/browse.cfm?fldID=F3305493-0FBC-93DA-2720-4412D198A9C9, Accessed April, 2013.

94. L. Menten and M. I. Michaelis, *Biochem Z*, 1913, **49**, 333-369.

95. X. Yang, J. Kirsch, E. V. Olsen, J. W. Fergus and A. L. Simonian, *Sensors and Actuators B: Chemical*, 2012.

96. X. Yang, A. Zitova, J. Kirsch, J. W. Fergus, R. A. Overfelt and A. L. Simonian, *Sensors and Actuators B: Chemical*, 2012, **161**, 564-569.

97. Y. Liu, M. Wang, F. Zhao, Z. Xu and S. Dong, *Biosensors and Bioelectronics*, 2005, **21**, 984-988.

98. T. O. Tran, E. G. Lammert, J. Chen, S. A. Merchant, D. B. Brunski, J. C. Keay, M. B. Johnson, D. T. Glatzhofer and D. W. Schmidtke, *Langmuir*, 2011, **27**, 6201-6210.

99. L. Jiang and L. Gao, *Carbon*, 2003, **41**, 2923-2929.

100. W. Zhao, J. J. Xu, C. G. Shi and H. Y. Chen, *Langmuir*, 2005, **21**, 9630-9634.

101. T. W. Tsai, G. Heckert, L. F. Neves, Y. Tan, D. Y. Kao, R. G. Harrison, D. E. Resasco and D. W. Schmidtke, *Analytical chemistry*, 2009, **81**, 7917-7925.

102. K. Lai, N. J. Stolowich and J. R. Wild, *Archives of biochemistry and biophysics*, 1995, **318**, 59-64.

103. S. Rodriguez-Mozaz, M. J. Alda, M. P. Marco and D. Barcelo, *Talanta*, 2005, **65**, 291-297.

104. S. Rodriguez-Mozaz, M. J. Lopez de Alda and D. Barcelo, *Analytical and bioanalytical chemistry*, 2006, **386**, 1025-1041.

105. P. C. Pandey, S. Upadhyay, H. C. Pathak, C. M. D. Pandey and I. Tiwari, *Sensors and Actuators B: Chemical*, 2000, **62**, 109-116.

106. V. Dounin, A. J. Veloso, H. Schulze, T. T. Bachmann and K. Kerman, *Analytica chimica acta*, 2010, **669**, 63-67.

107. C. B. Roepcke, S. B. Muench, H. Schulze, T. Bachmann, R. D. Schmid and B. Hauer, *Journal of agricultural and food chemistry*, 2010, **58**, 8748-8756.

108. F. Villatte, H. Schulze, R. Schmid and T. Bachmann, *Analytical and Bioanalytical Chemistry*, 2002, **372**, 322-326.

109. A. Simonian, E. Rainina and J. Wild, *Analytical letters*, 1997, **30**, 2453-2468.

110. Dropsens, *Flow Cell Data Sheet*, http://dropsens.com/en/pdfs_productos/new_brochures/flwcl-flwcltef-flwclpeek.pdf, Accessed March, 2013.

111. BVT-Technologies, *Electrode Datasheet*, http://www.bvt.cz/_ftp/Senzory/AC1.pdf, Accessed March, 2013.

112. Dropsens, *Screen-printed Electrode*, http://dropsens.com/en/screen_printed_electrodes_pag.html, Accessed March, 2013.

113. Pine-Instruments, *Screen Printed Electrodes (Carbon)*, http://www.pineinst.com/echem/viewproduct.asp?ID=46564, Accessed March, 2013.

Appendix

The following CFD data is for the 20 mL/hr boundary conditions set. All data was acquired in the Autodesk Simulation Computation Fluid Dynamics 2013 plug-in for Autodesk Inventor 2013. The final schematics for the flowcell are shown following the CFD data. Finally photographs of the experiment set up of most apparatus are shown.

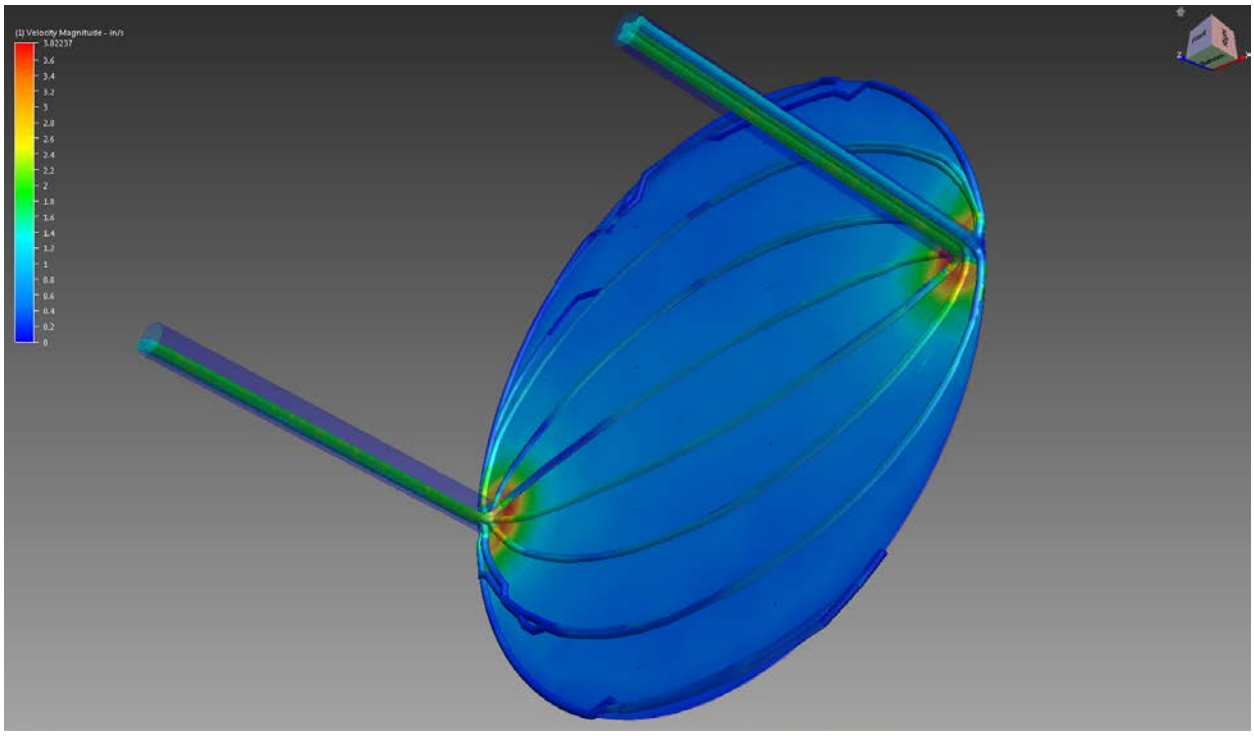

BASi Flow Injection Analysis Electrode with flow trace

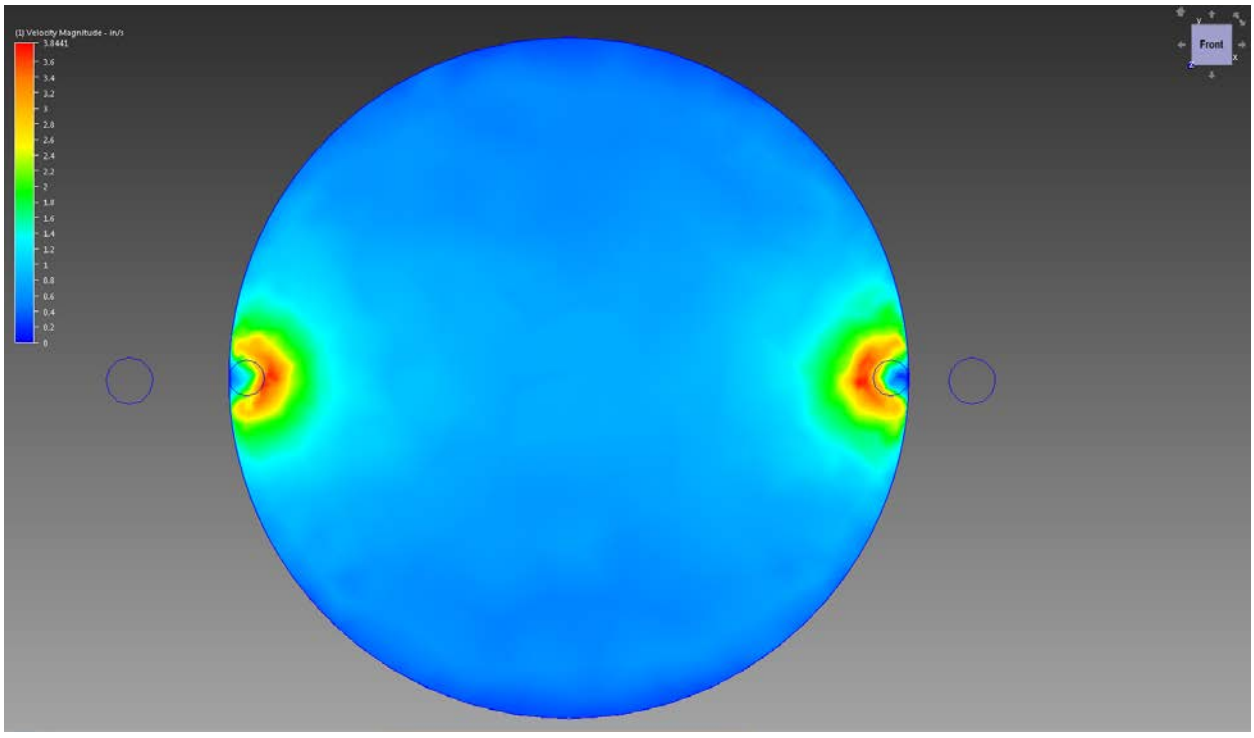

BASi Flow Injection Analysis Electrode electrode-liquid interface

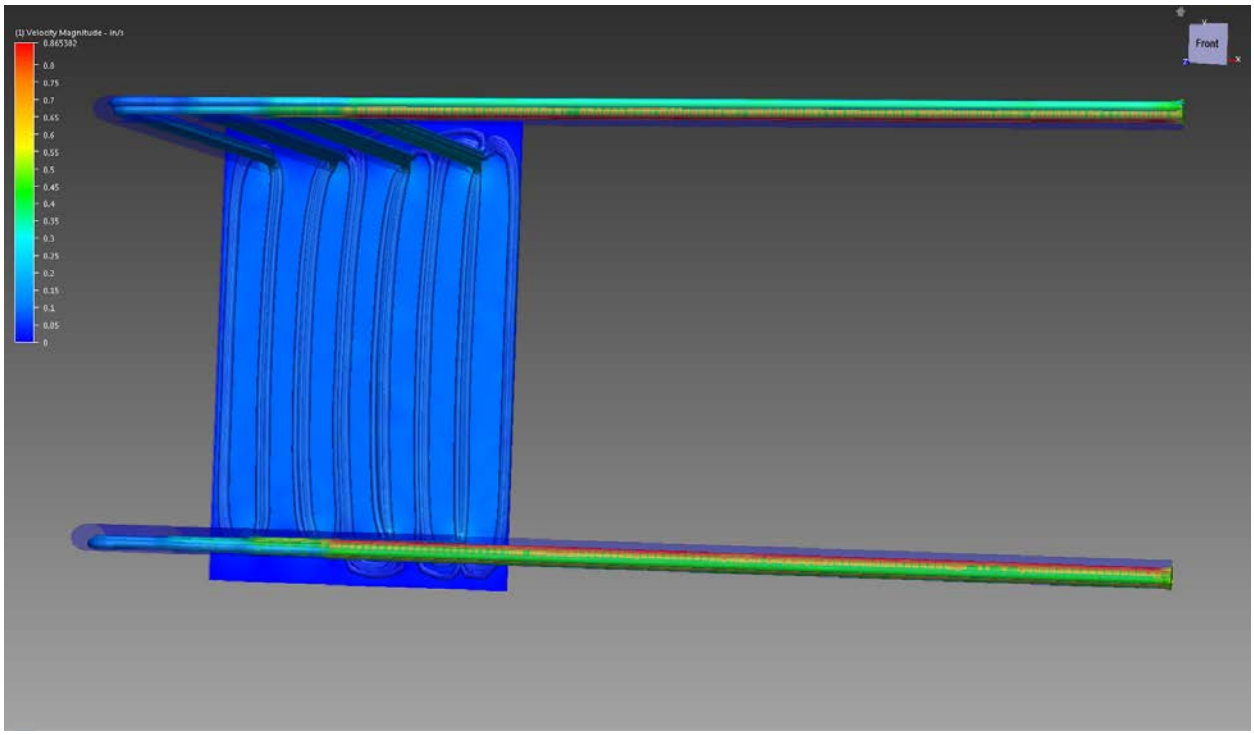

Design # 1 with flow trace

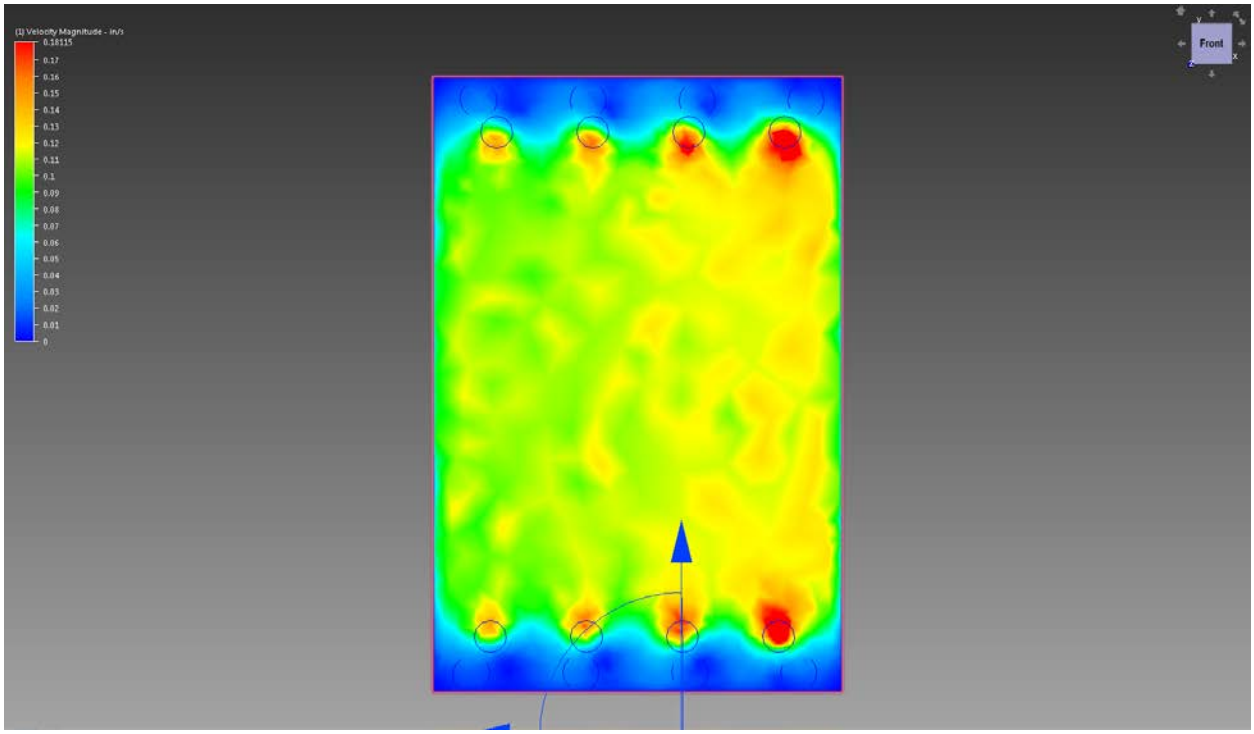

Design #1 electrode-liquid interface

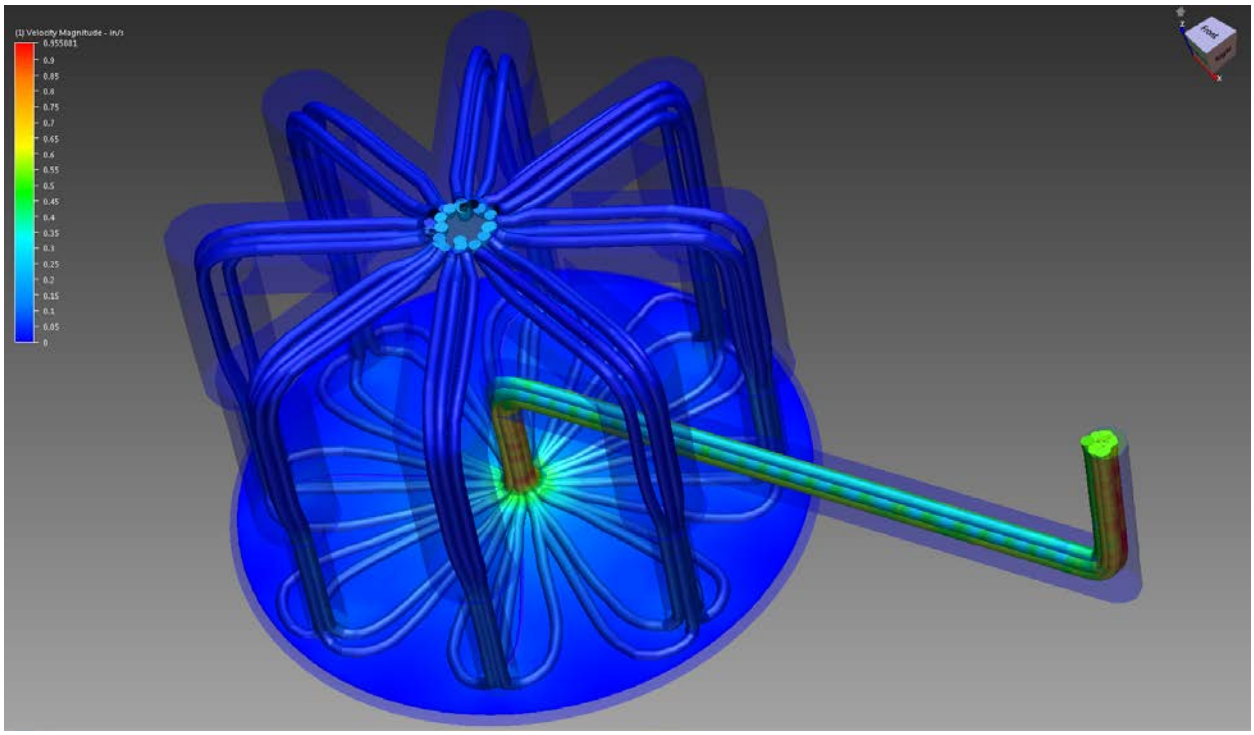

Design # 4 with flow trace

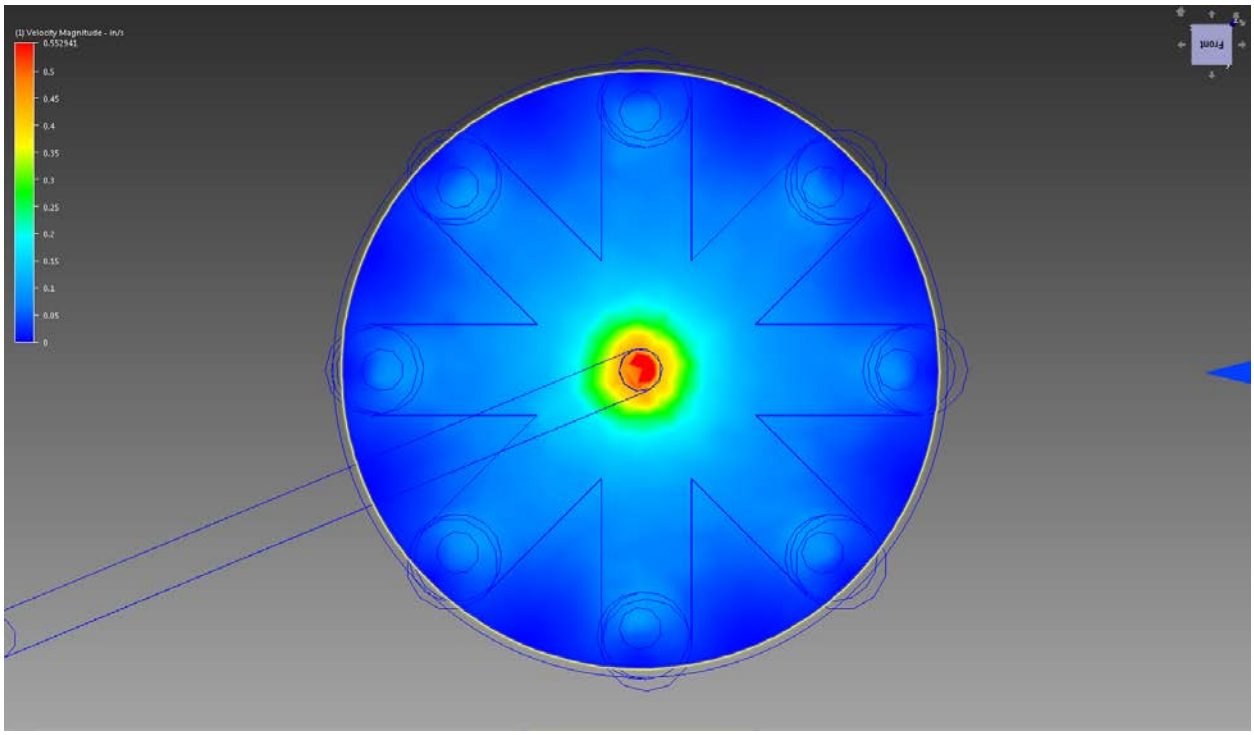

Design #4 electrode-liquid interface

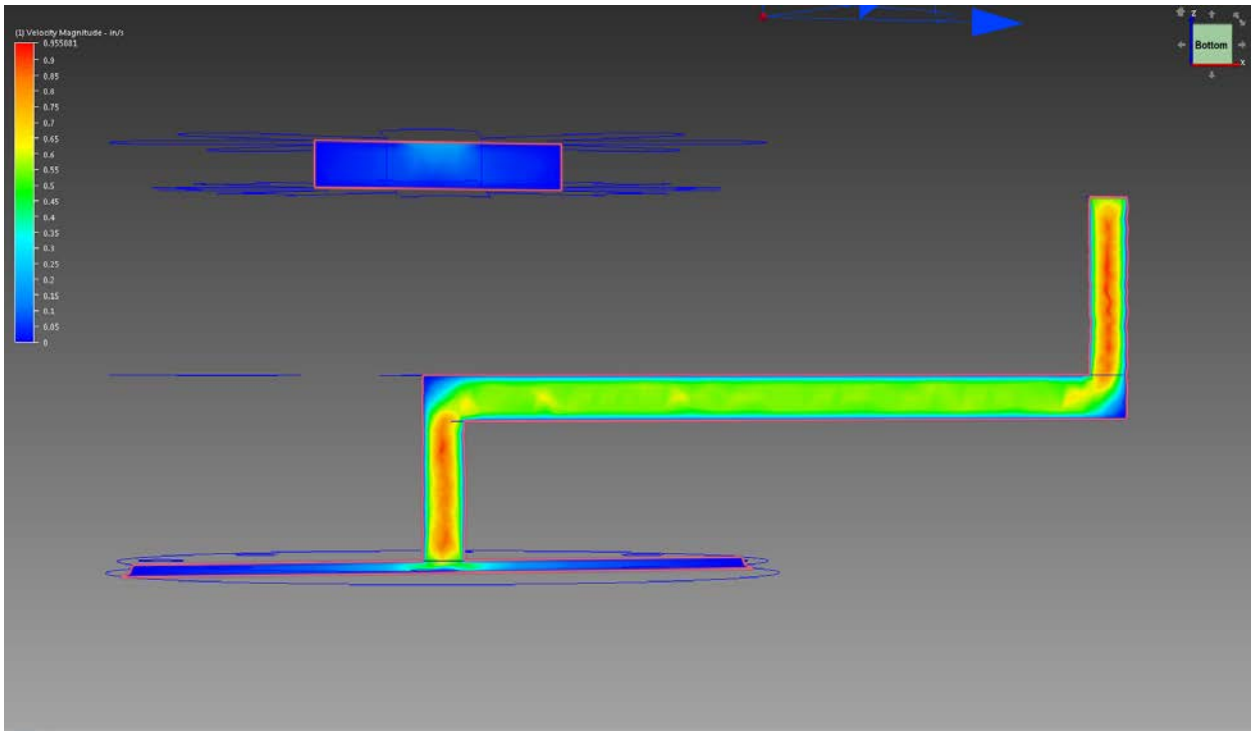

Design #4 inlet stream profile

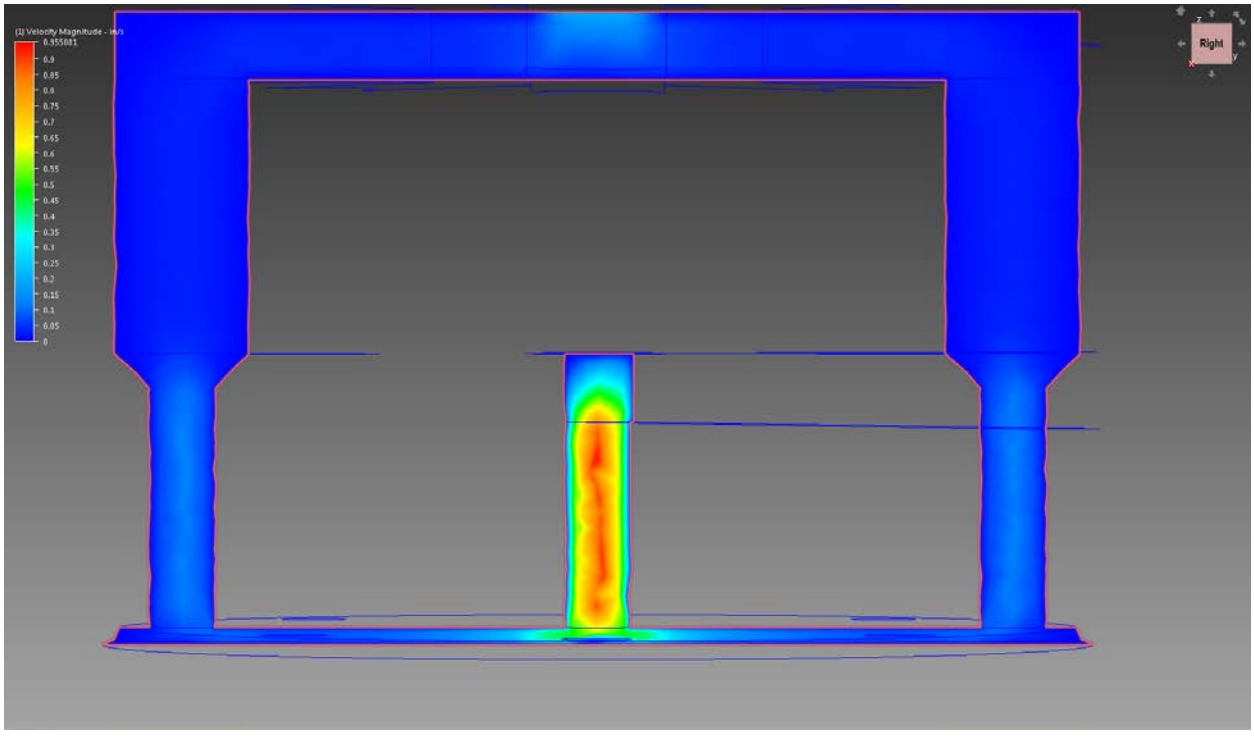

Design #4 inlet/outlet stream profile

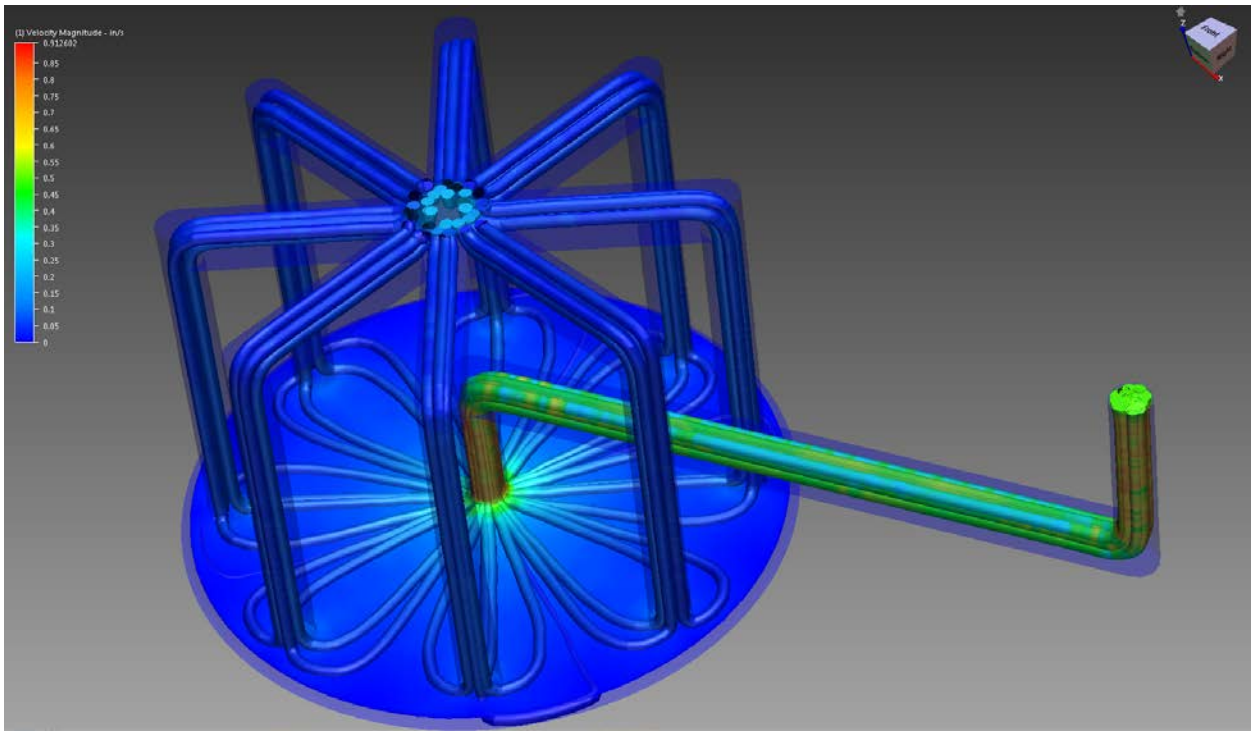

Design # 4 with flow trace

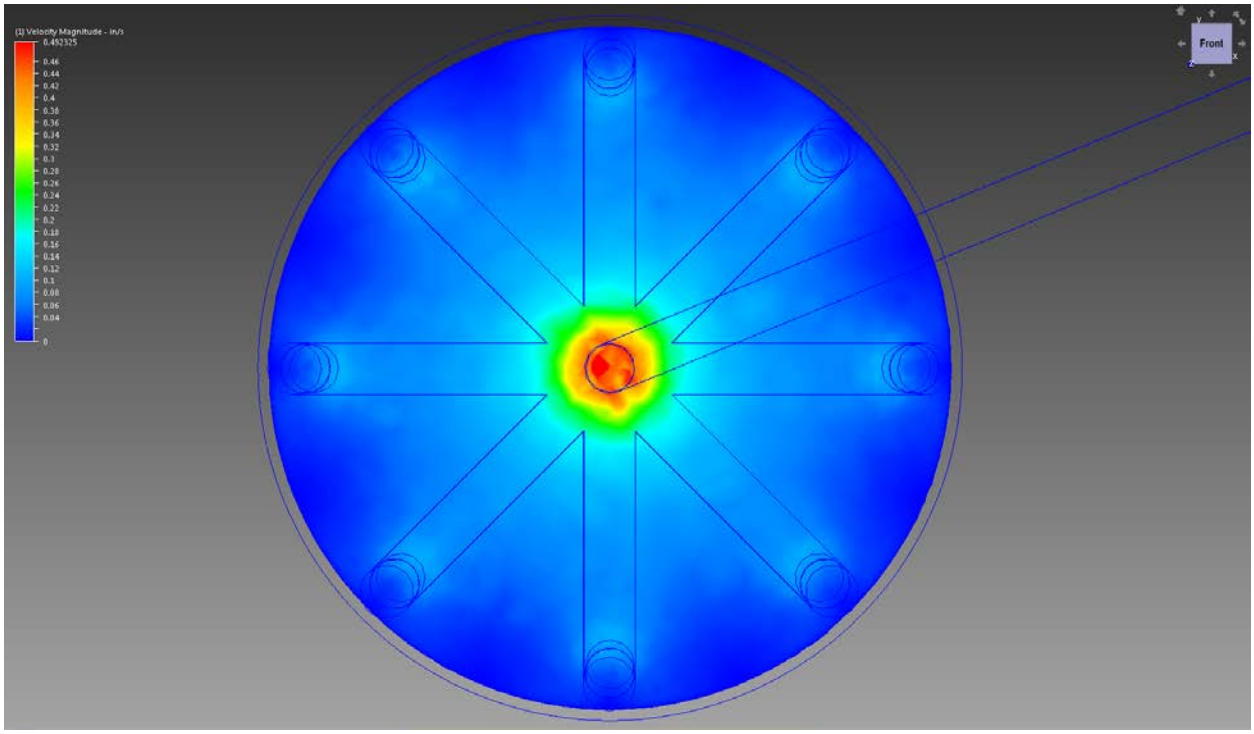

Design #4 electrode-liquid interface

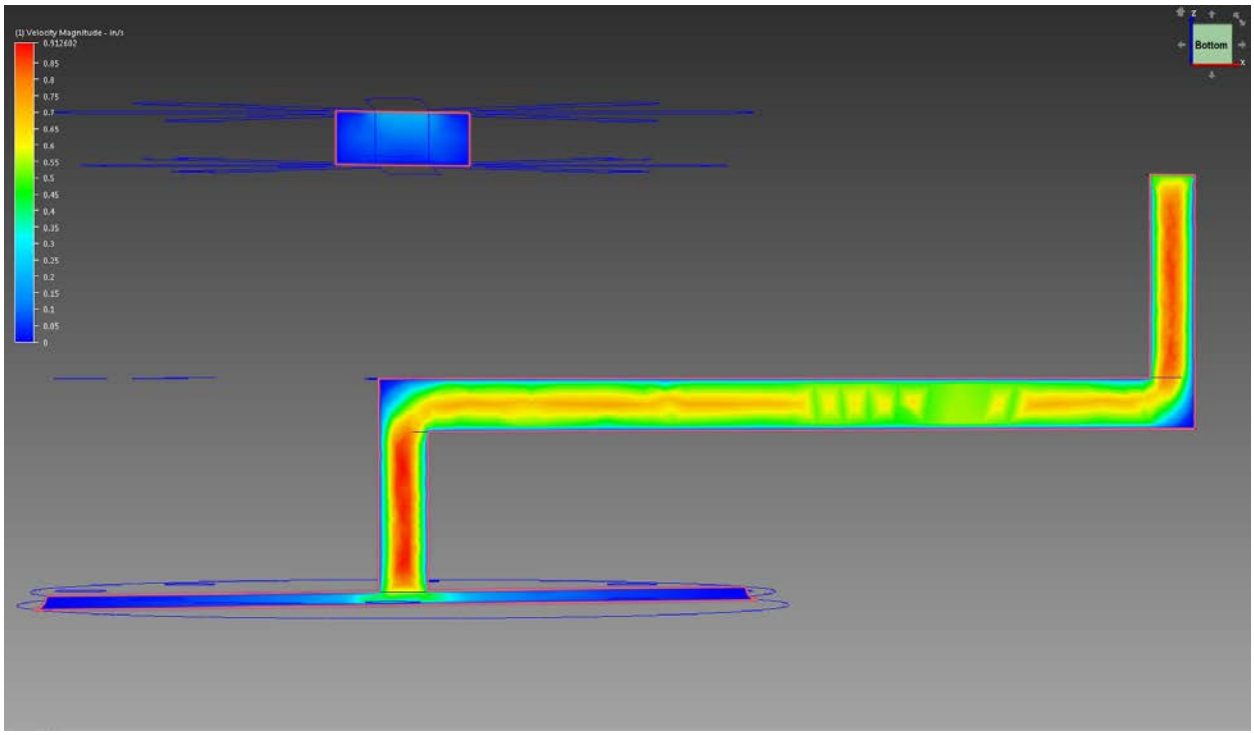

Design #4 inlet stream profile

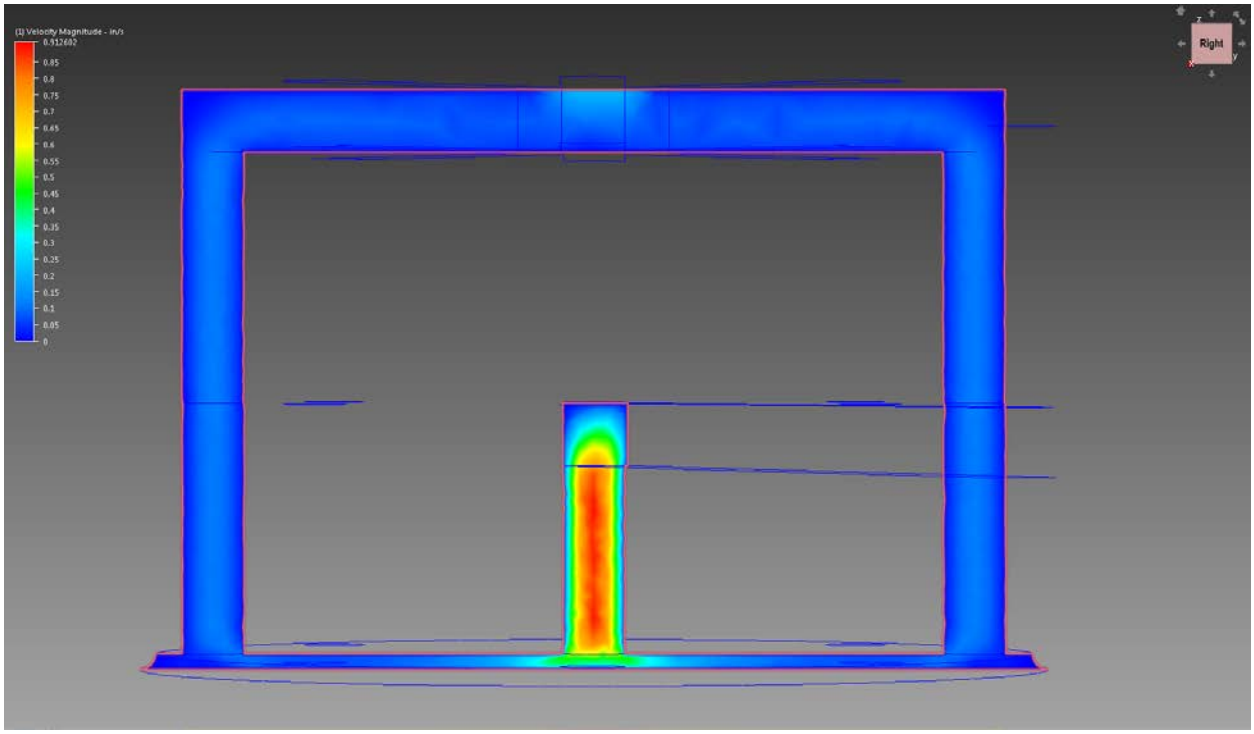

Design #4 inlet/outlet stream profile

FLOW CELL ASSEMBLY: FRONT 4:1

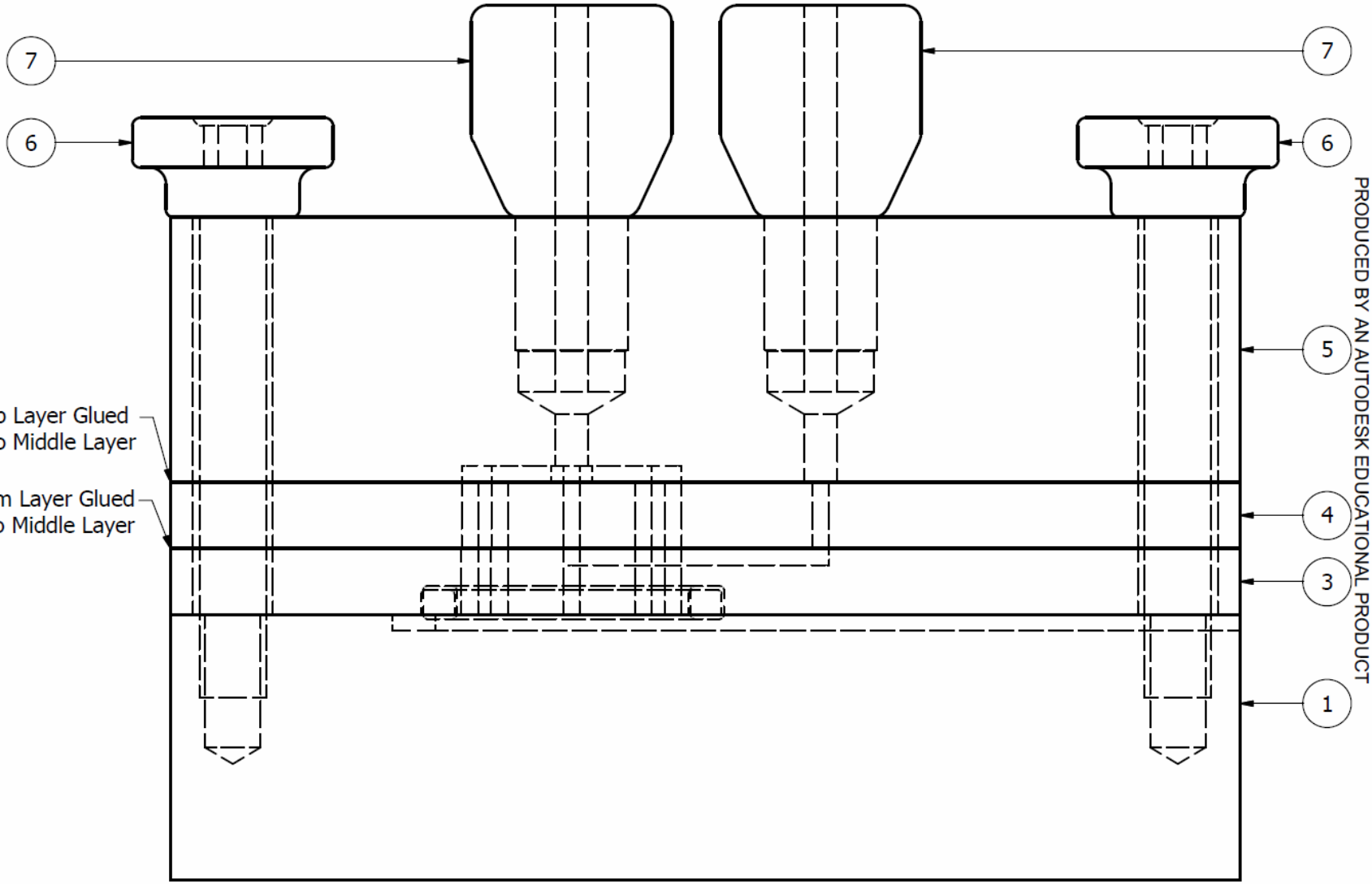

FLOW CELL ASSEMBLY: TOP VIEW 3:1

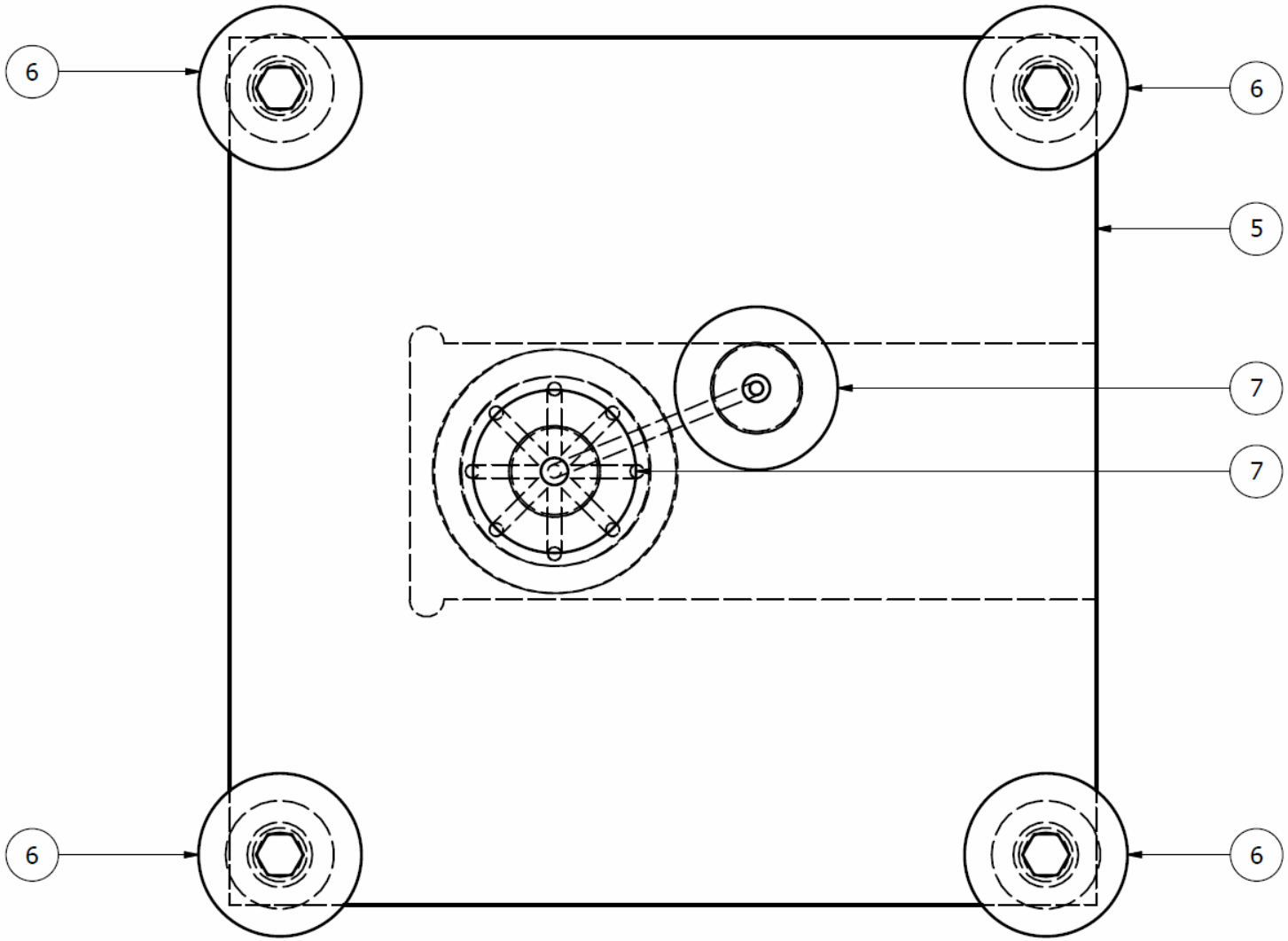

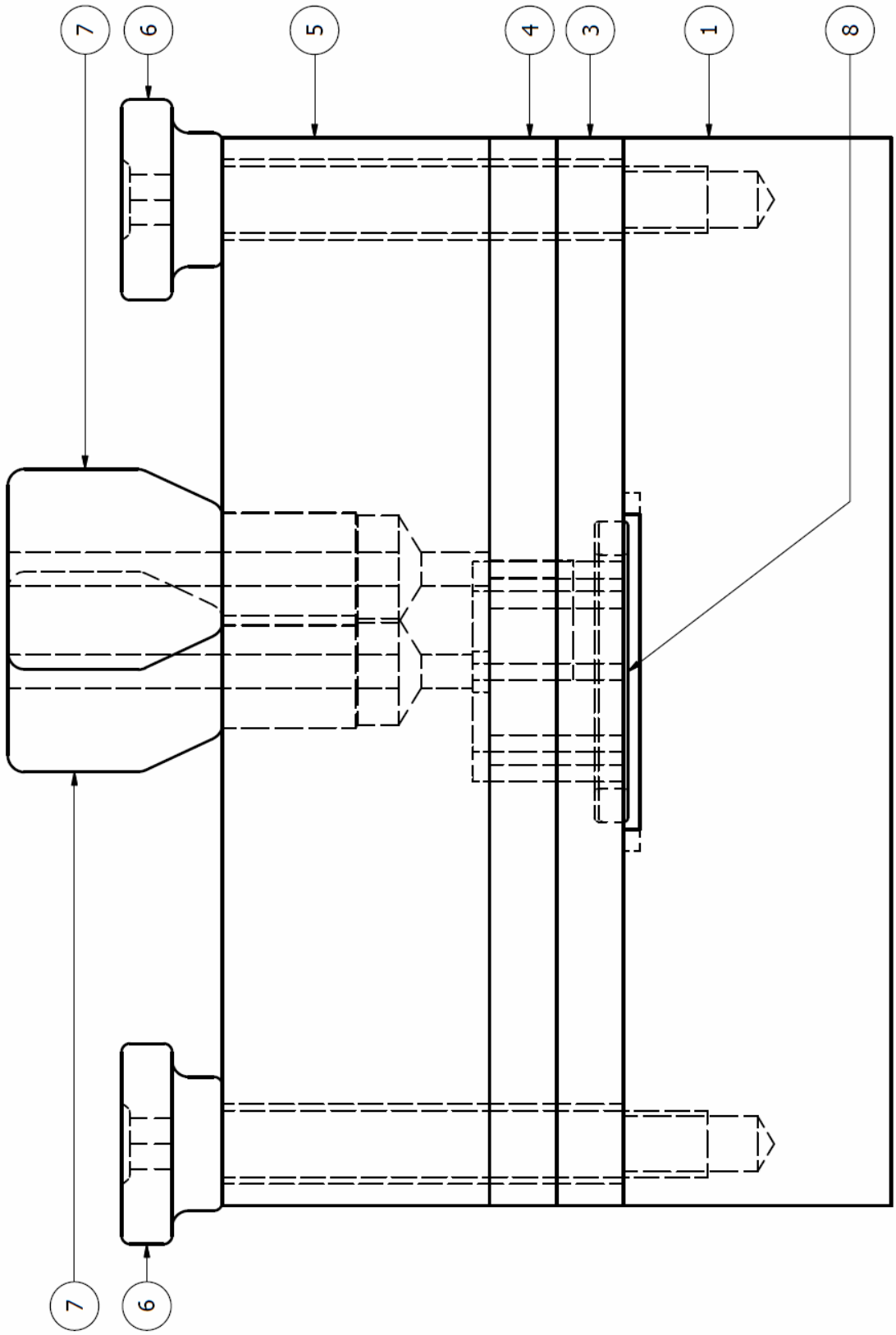

FLOW CELL ASSEMBLY: RIGHT VIEW 4:1

PRODUCED BY AN AUTODESK EDUCATIONAL PRODUCT

PRODUCED BY AN AUTODESK EDUCATIONAL PRODUCT

FLOW CELL ASSEMBLY: ISOMETRIC TOP RIGHT 2:1

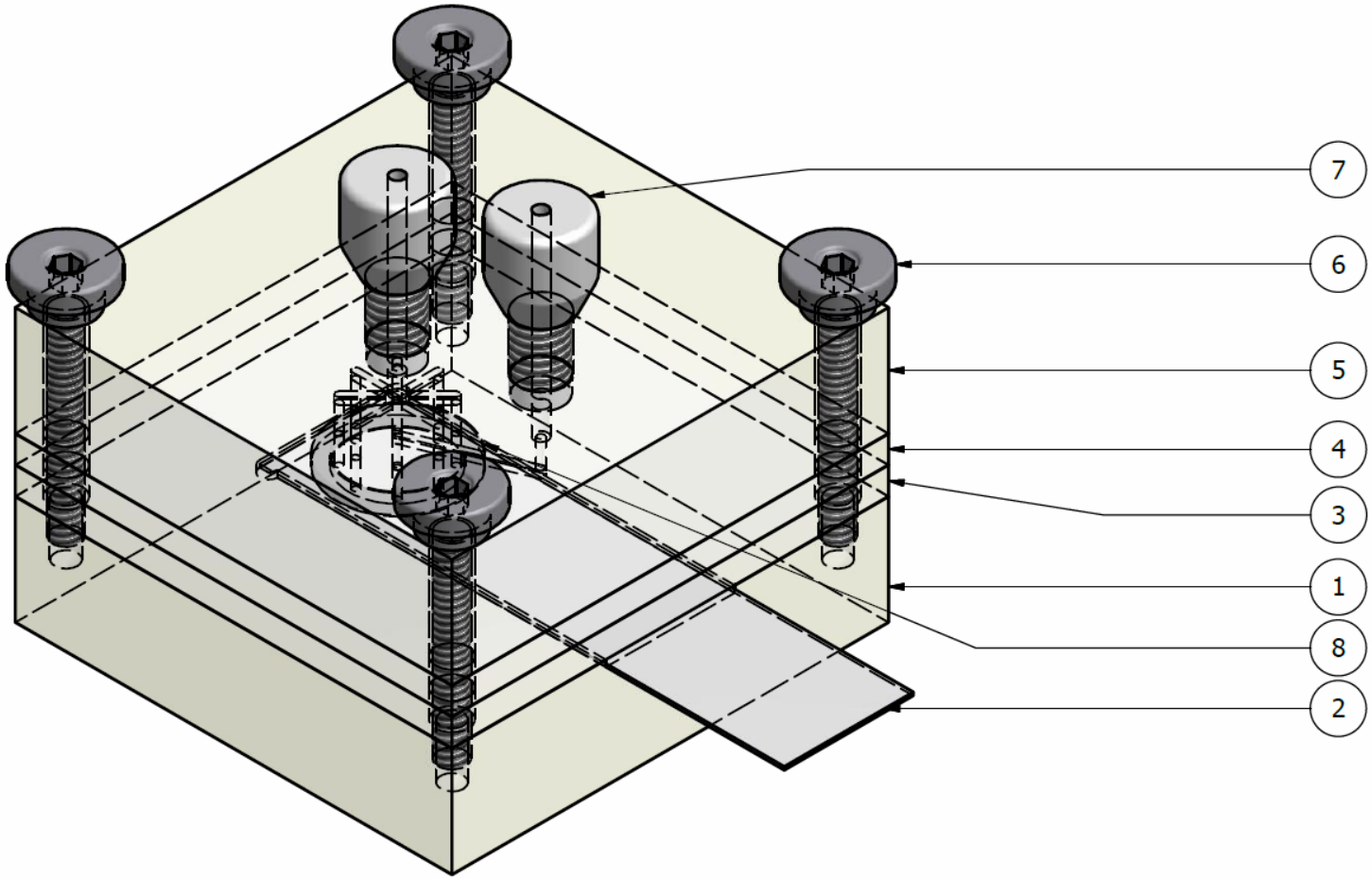

PARTS LIST			
ITEM	QTY	PART NUMBER	DESCRIPTION
1	1	Bottom Piece	Polycarbonate .5" MMC
2	1	Electrode	Part#: RRPE1001C PI
3	1	Bottom Layer	Polycarbonate .25" MMC
4	1	Middle Layer	Polycarbonate .25" MMC
5	1	Top Layer	Polycarbonate .5" MMC
6	4	Thumbscrew	Part#: 98704A335 MMC
7	2	PEEK Nut	Part#: 50345 Valco
8	1	O ring	Part#: 4061T118 MMC

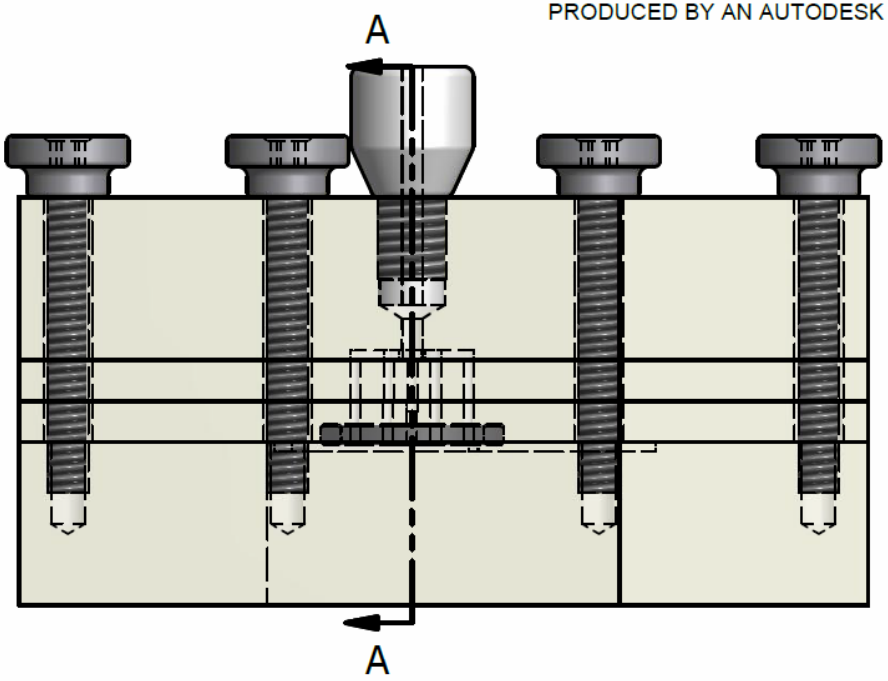

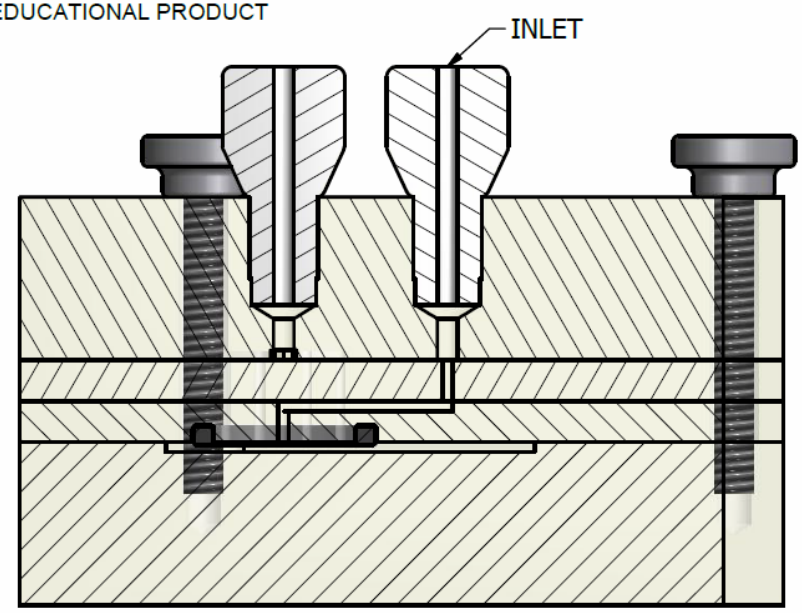

SECTION A-A
SCALE 2 : 1

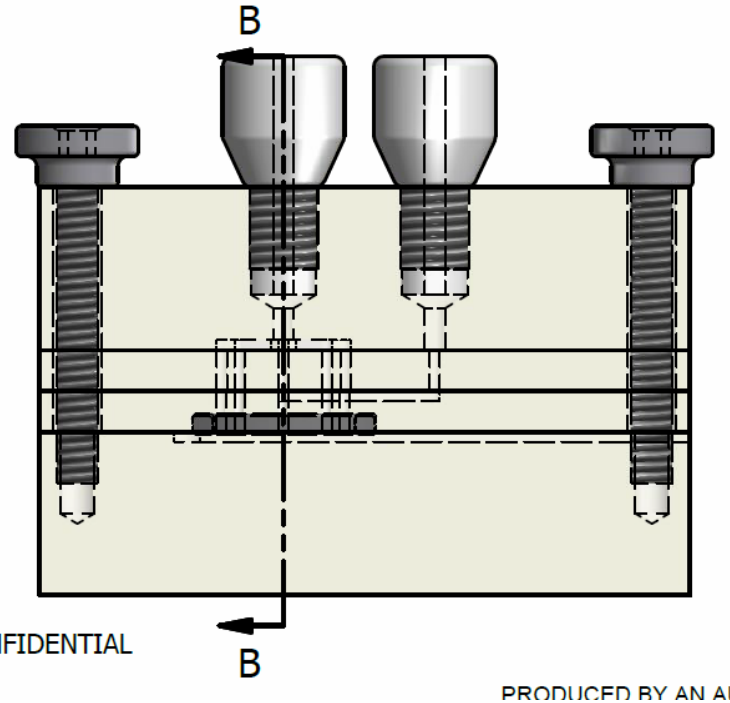

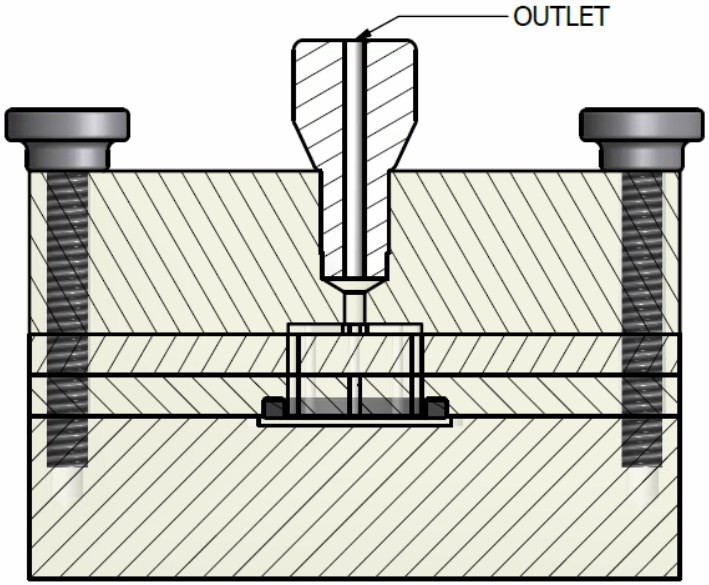

SECTION B-B
SCALE 2 : 1

BASE: FRONT 5:1

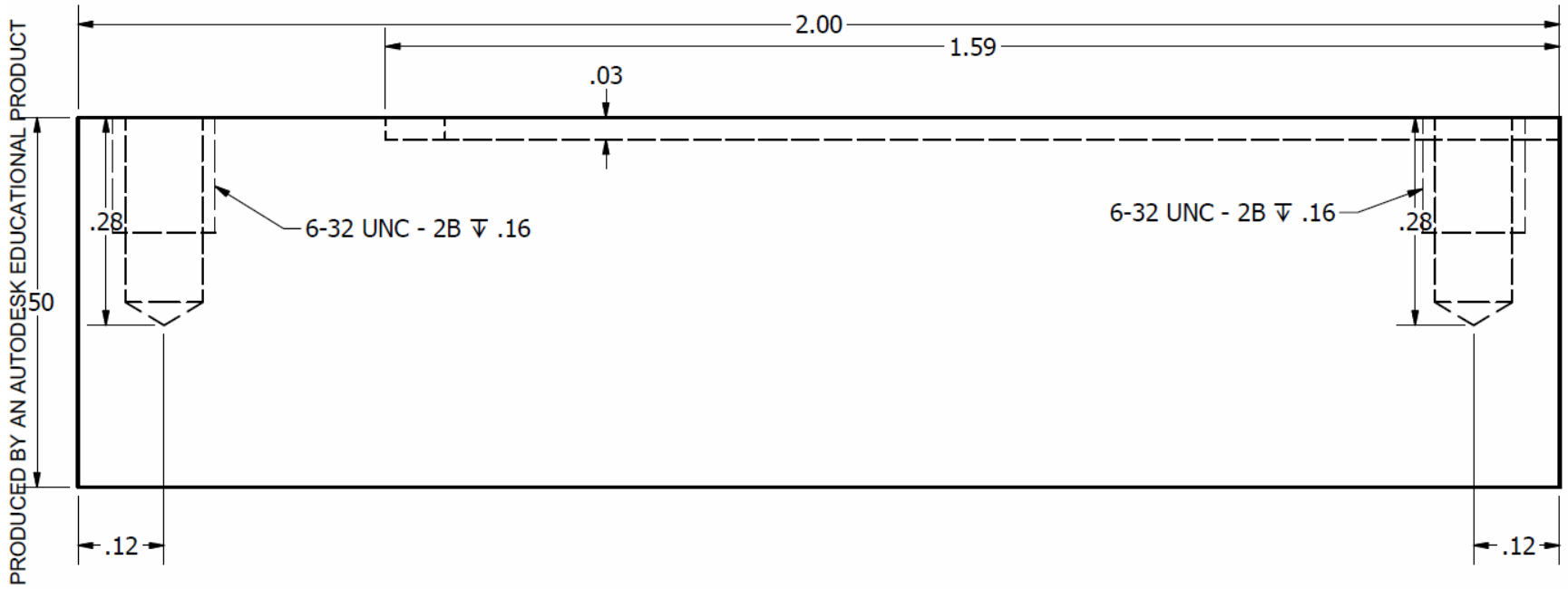

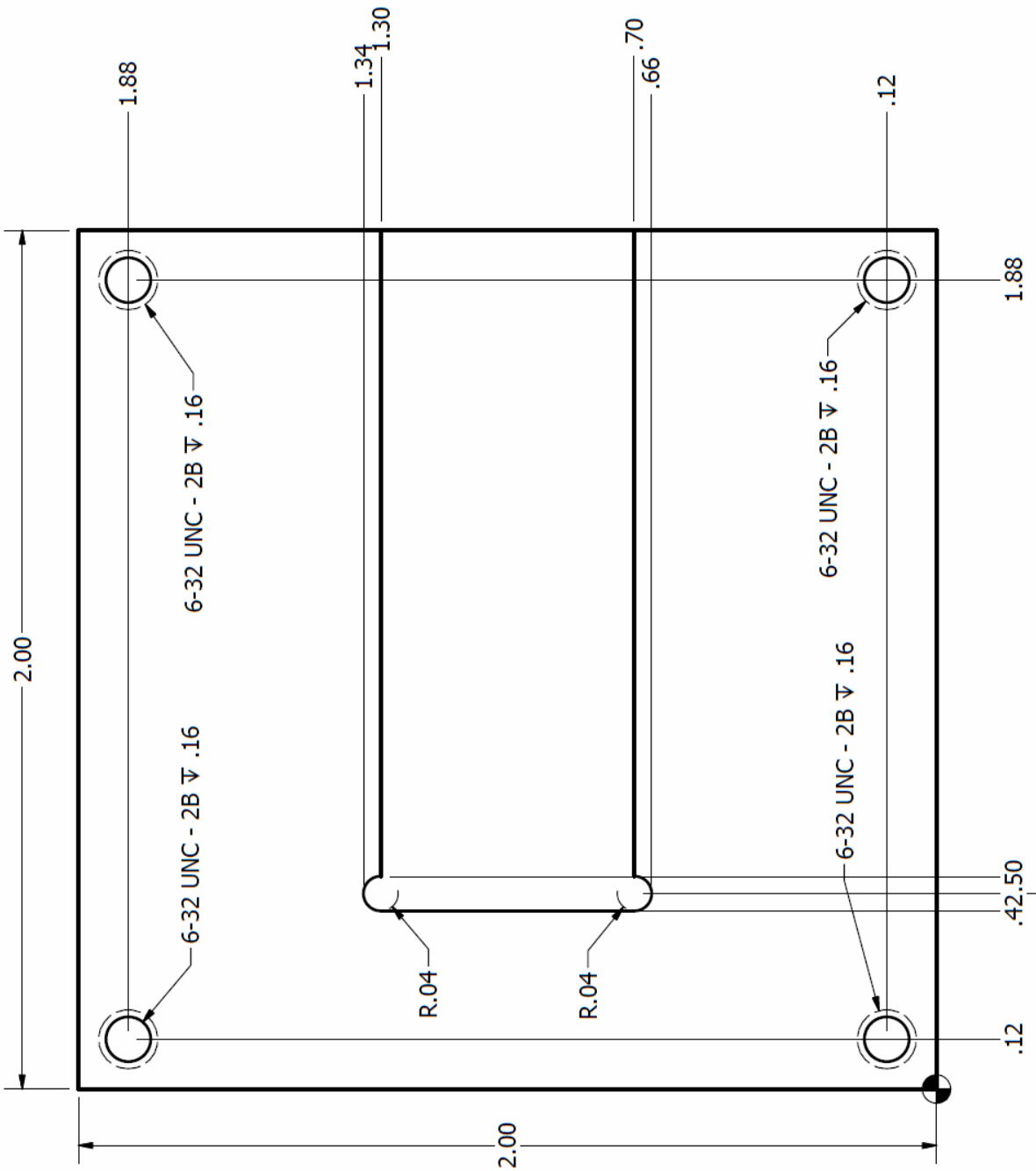

BASE: TOP VIEW 3:1

CONFIDENTIAL

BASE: RIGHT 5:1

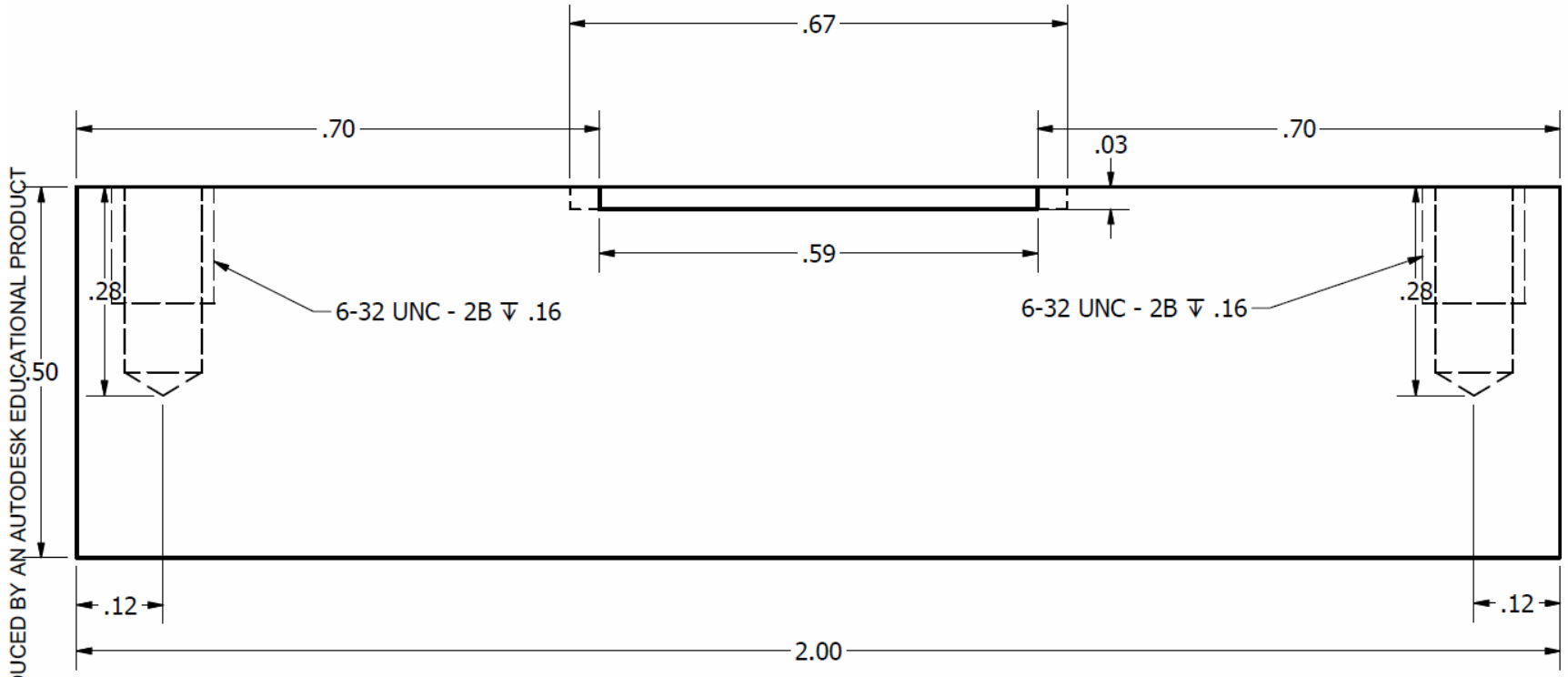

BASE: ISOMETRIC TOP RIGHT 3:1

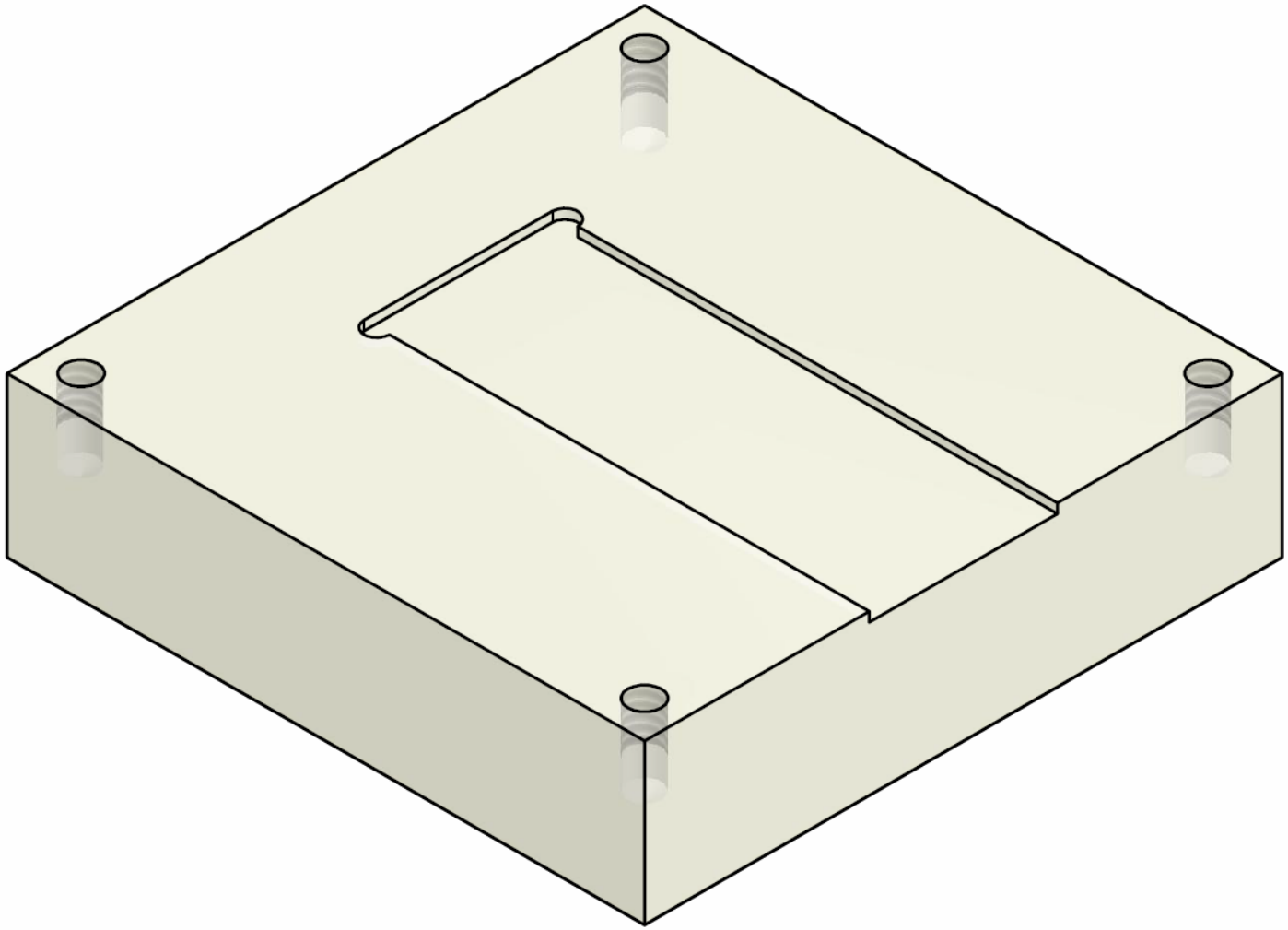

CONFIDENTIAL

BOTTOM LAYER: TOP 3:1

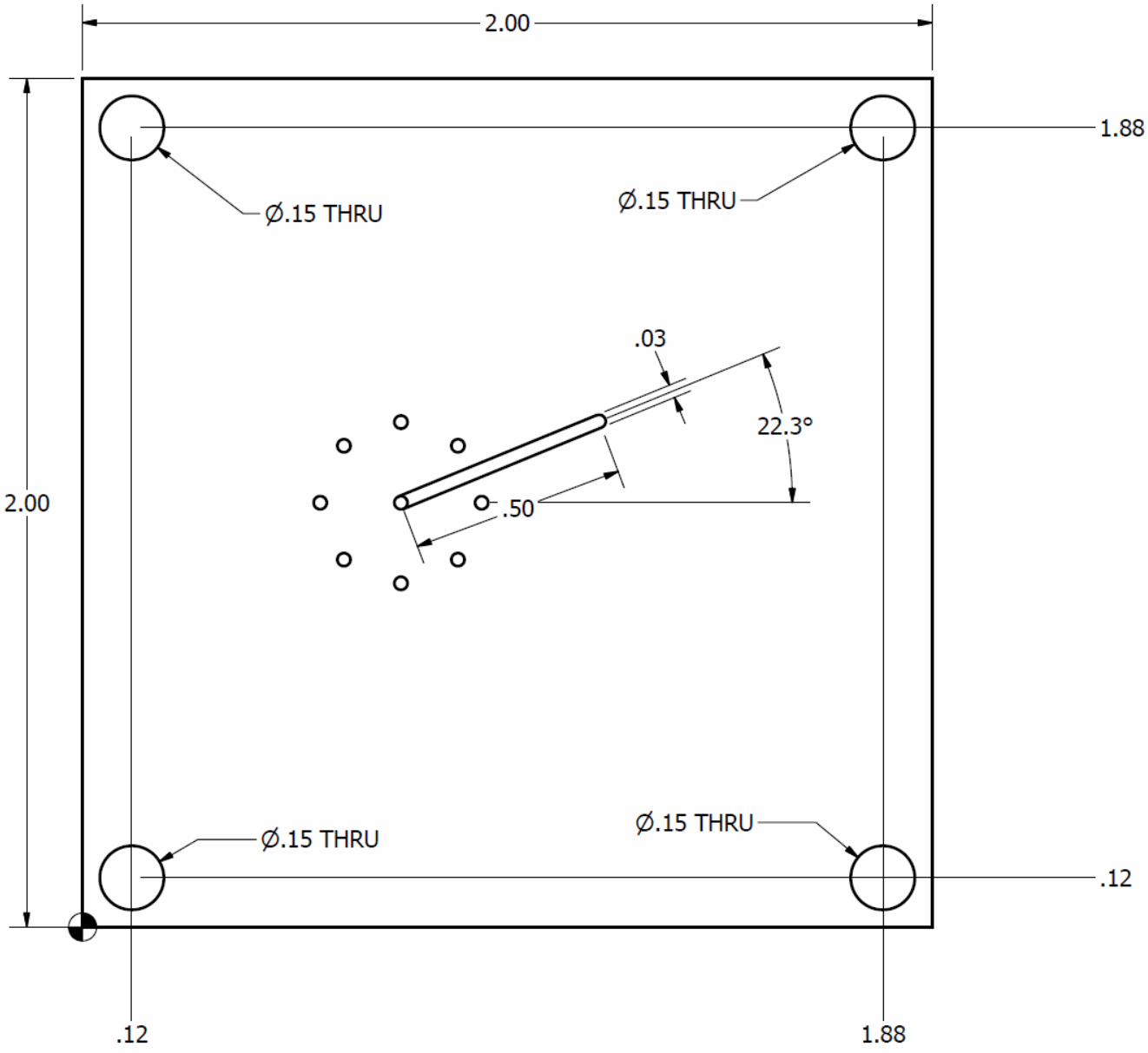

BOTTOM LAYER: BOTTOM 3:1

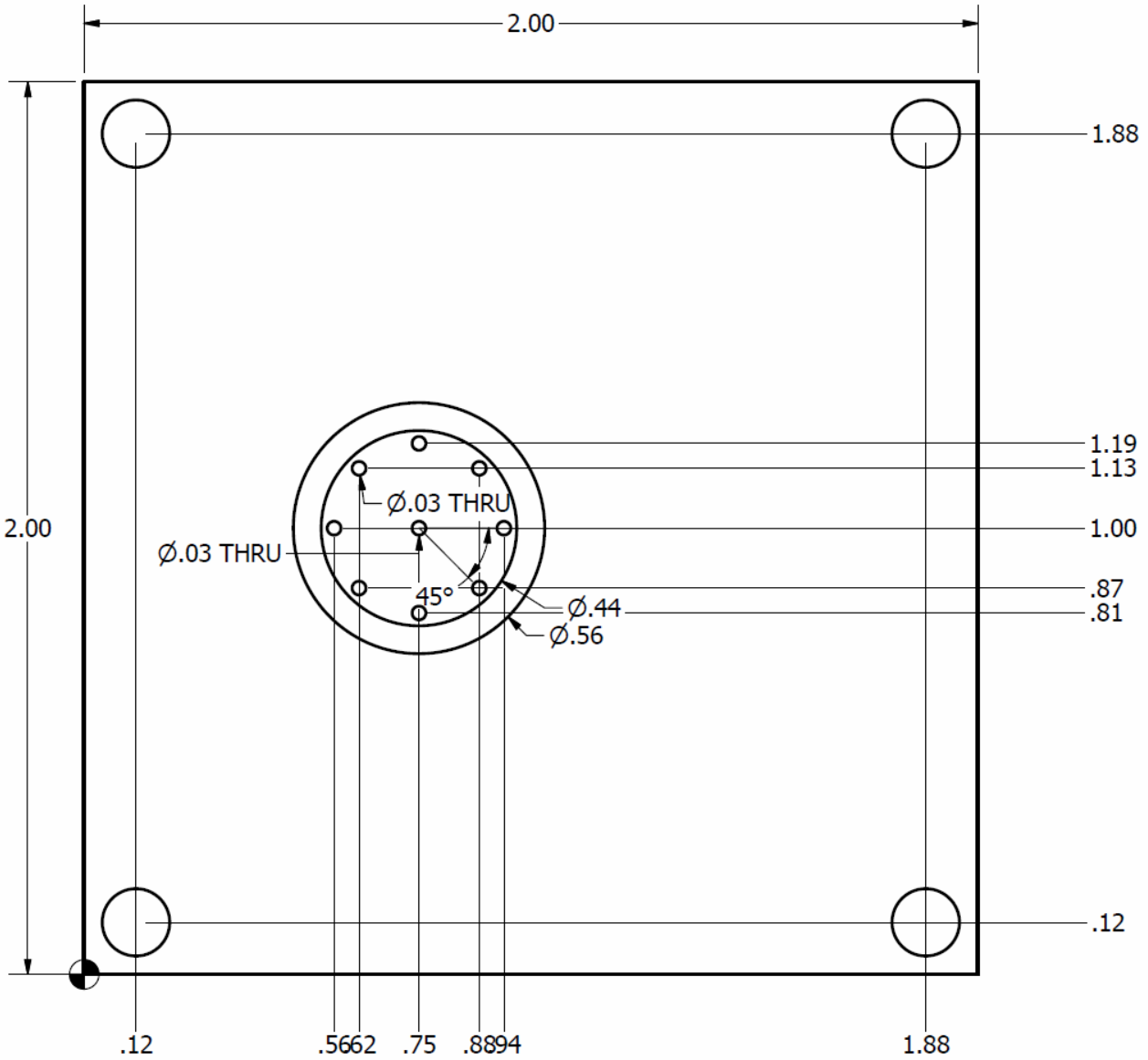

CONFIDENTIAL

PRODUCED BY AN AUTODESK EDUCATIONAL PRODUCT

PRODUCED BY AN AUTODESK EDUCATIONAL PRODUCT

PRODUCED BY AN AUTODESK EDUCATIONAL PRODUCT

BOTTOM LAYER: FRONT 5:1

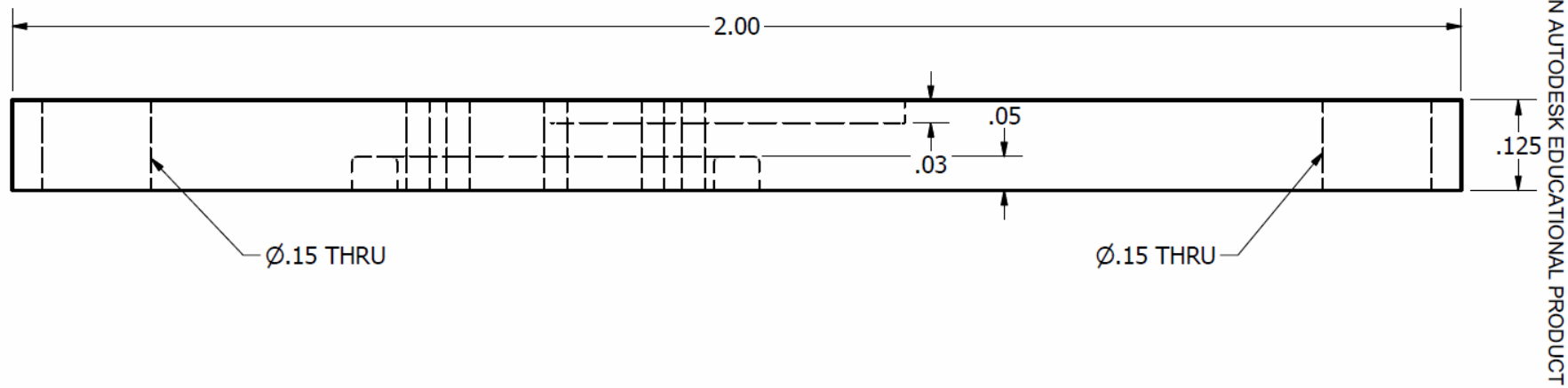

BOTTOM LAYER: ISOMETRIC TOP RIGHT 3:1

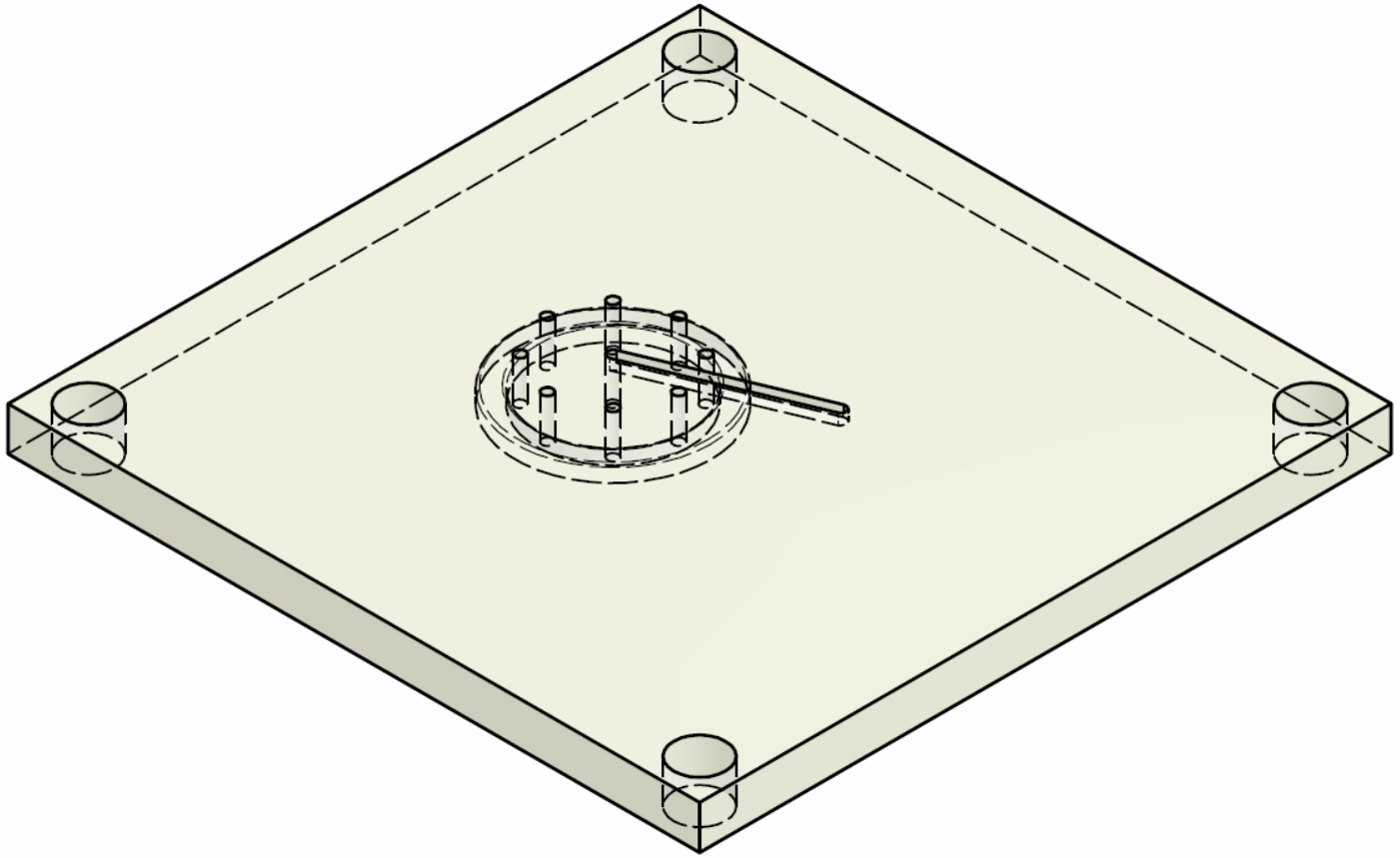

MIDDLE LAYER: FRONT 5:1

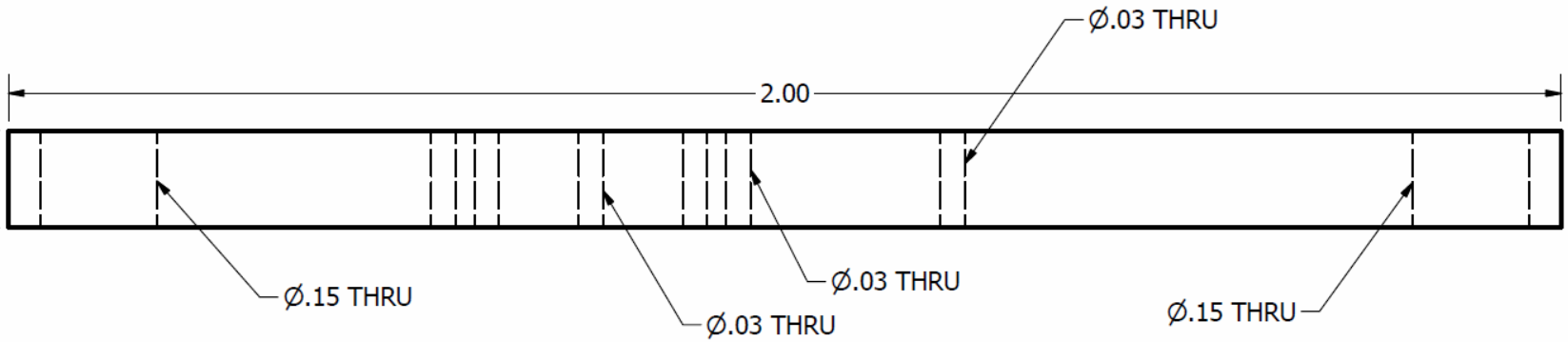

CONFIDENTIAL

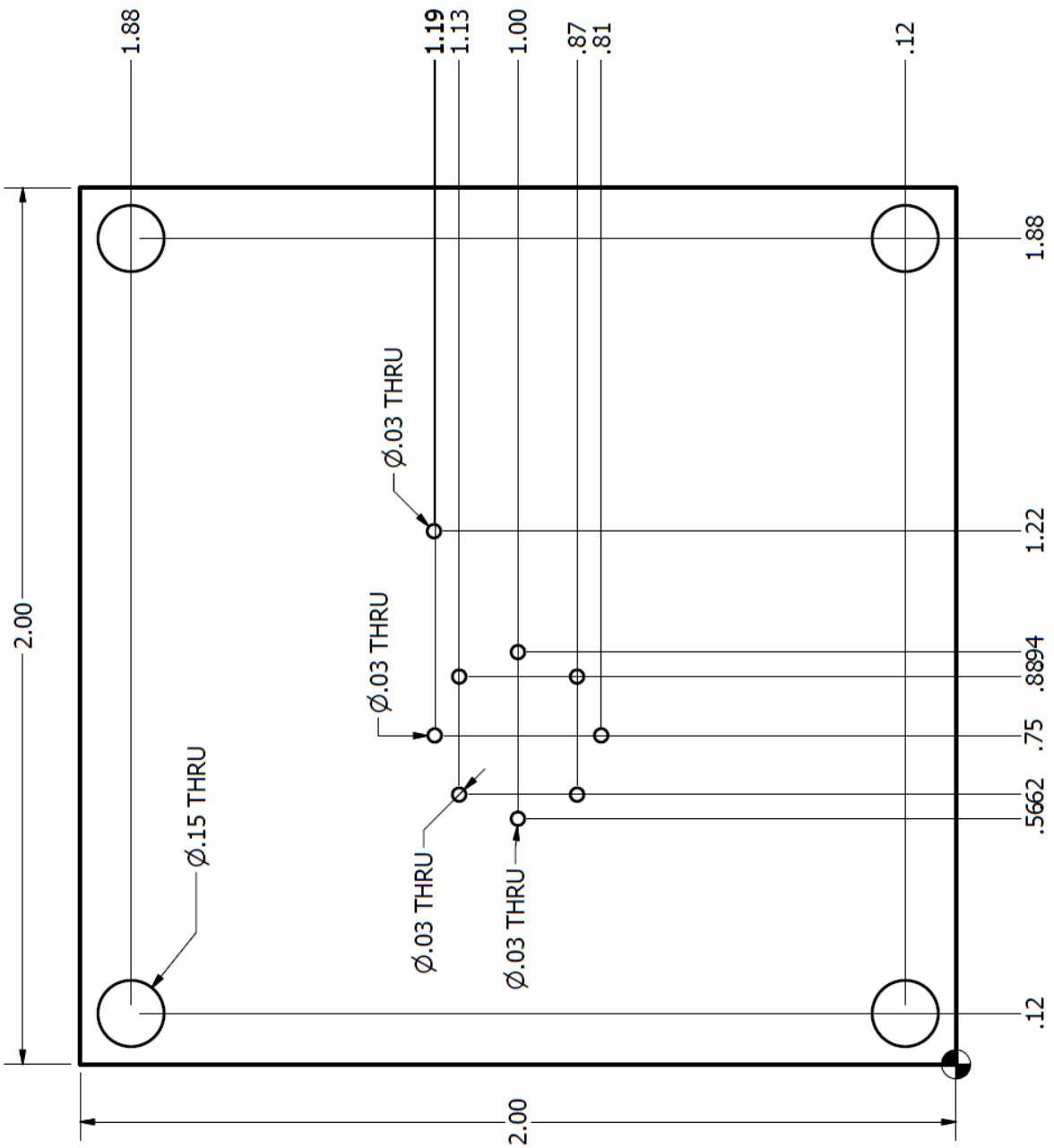

MIDDLE LAYER TOP 3:1

MIDDLE LAYER RIGHT 5:1

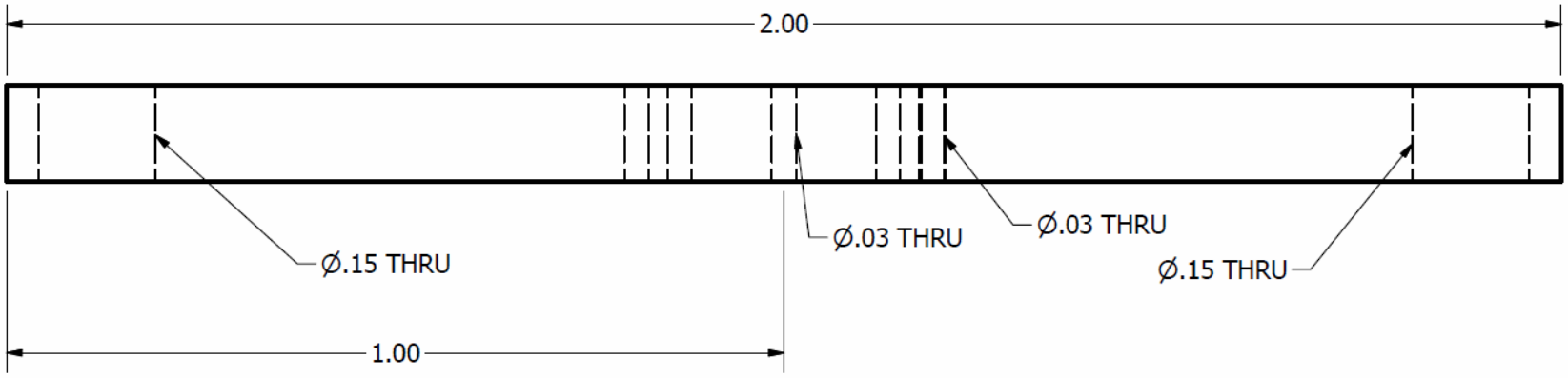

CONFIDENTIAL

MIDDLE LAYER: ISOMETRIC TOP RIGHT 3:1

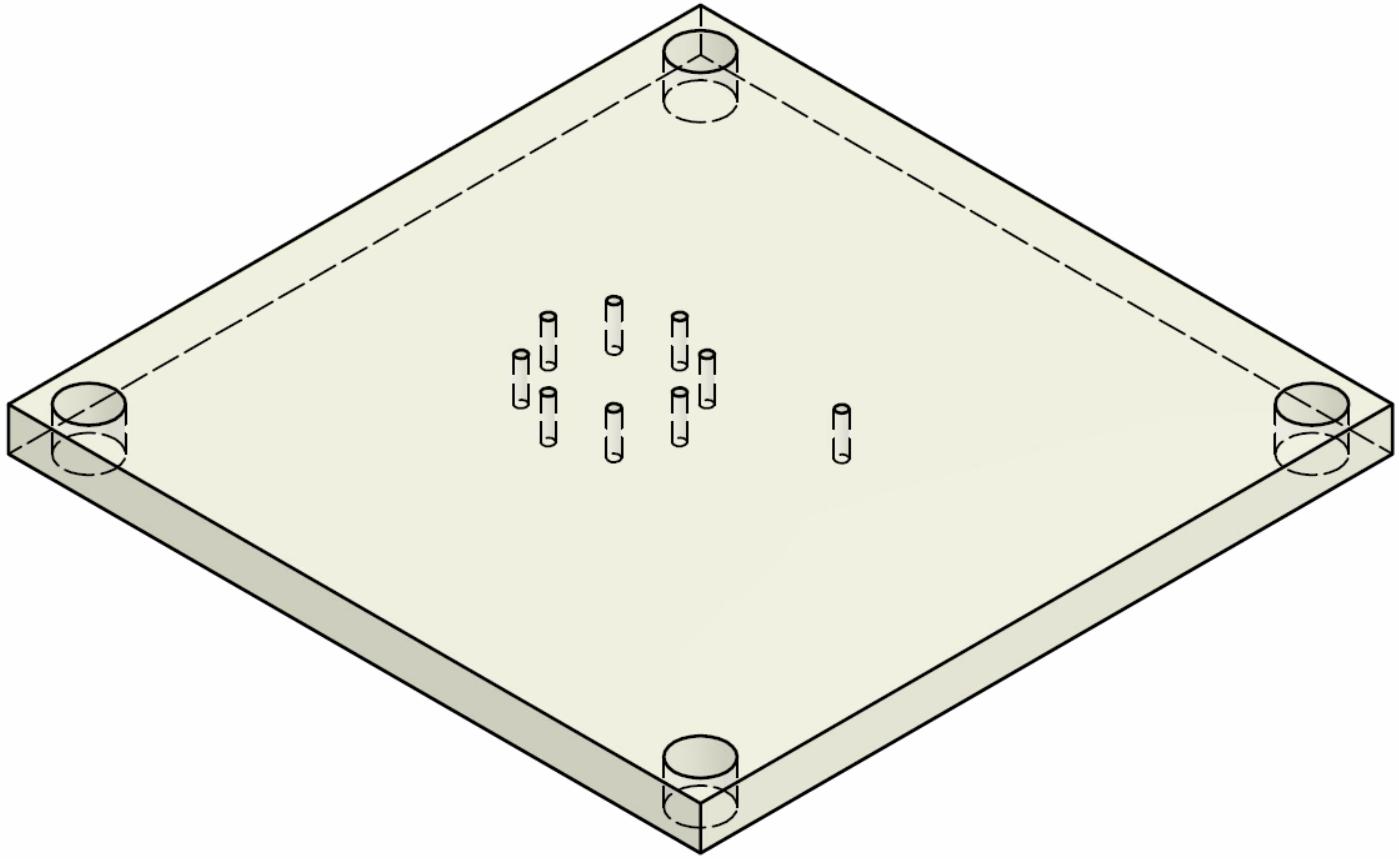

TOP LAYER: FRONT 5:1

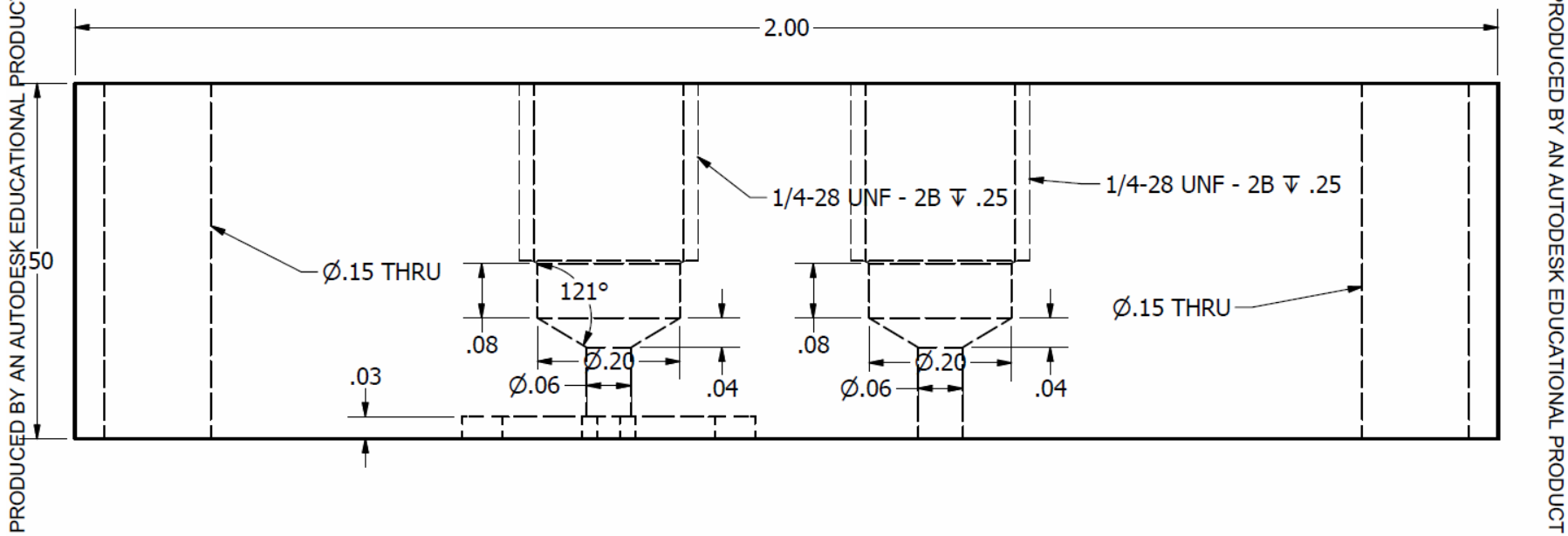

CONFIDENTIAL

TOP LAYER: TOP 3:1

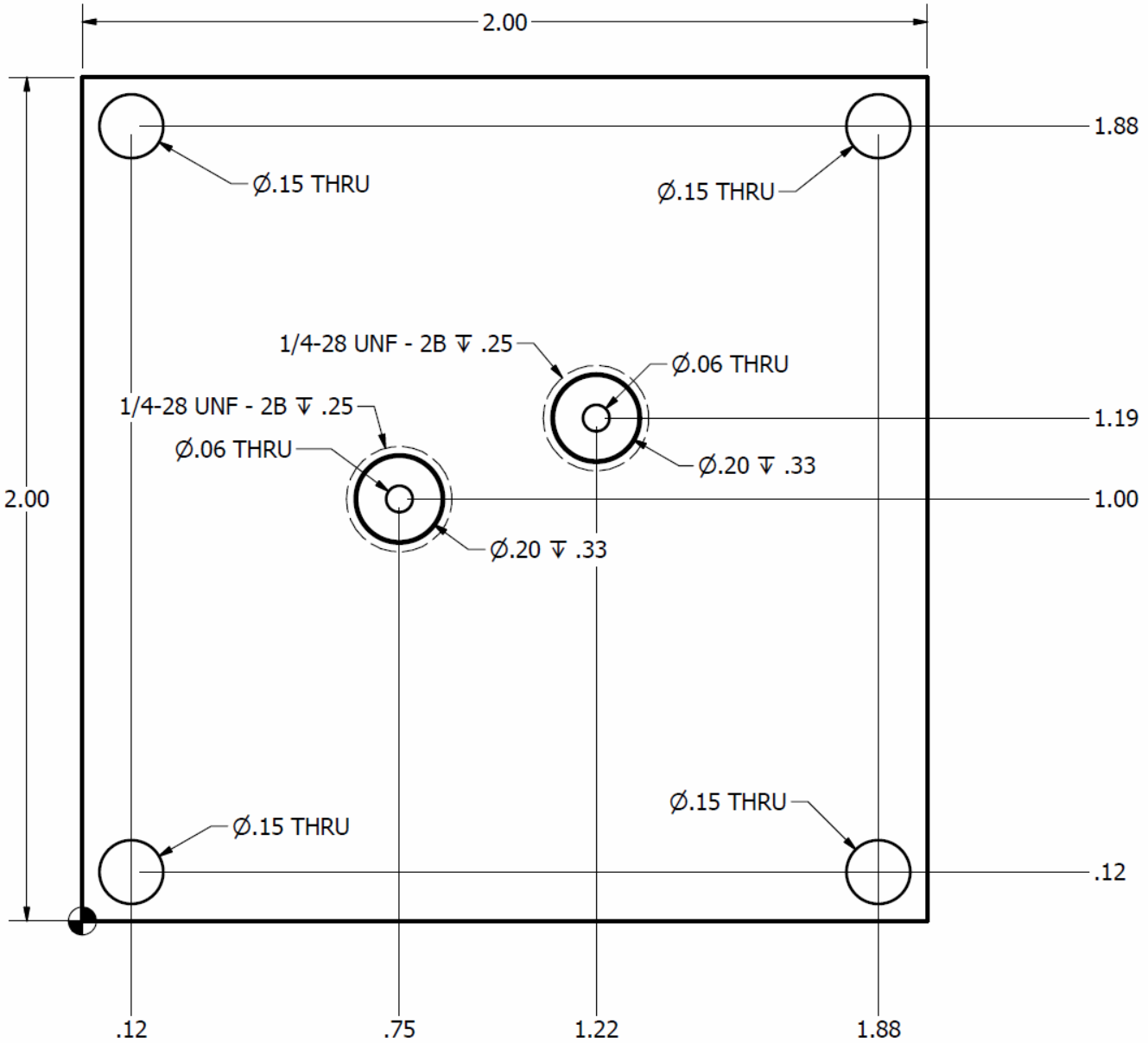

TOP LAYER: BOTTOM 3:1

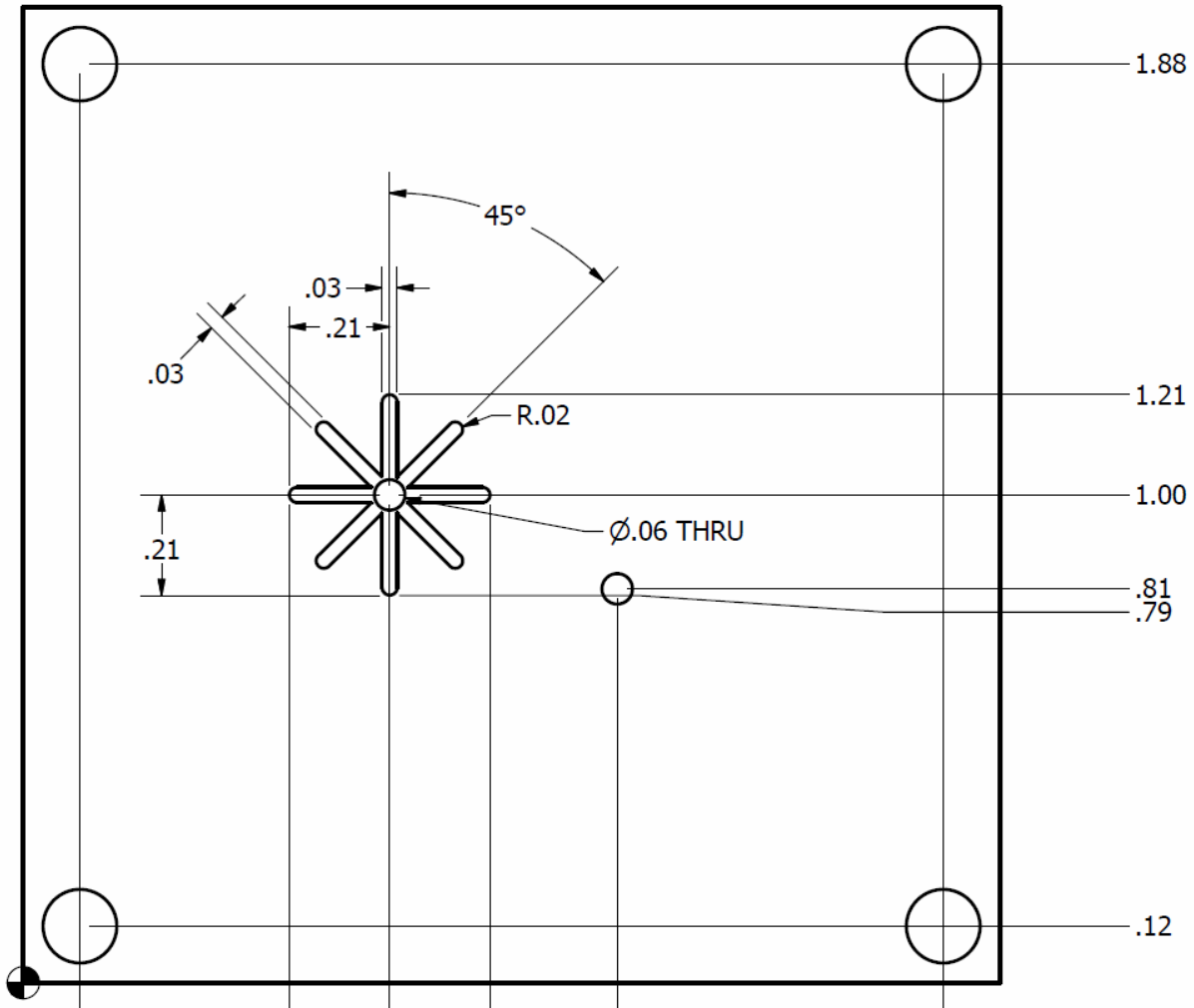

CONFIDENTIAL

TOP LAYER: ISOMETRIC TOP RIGHT 3:1

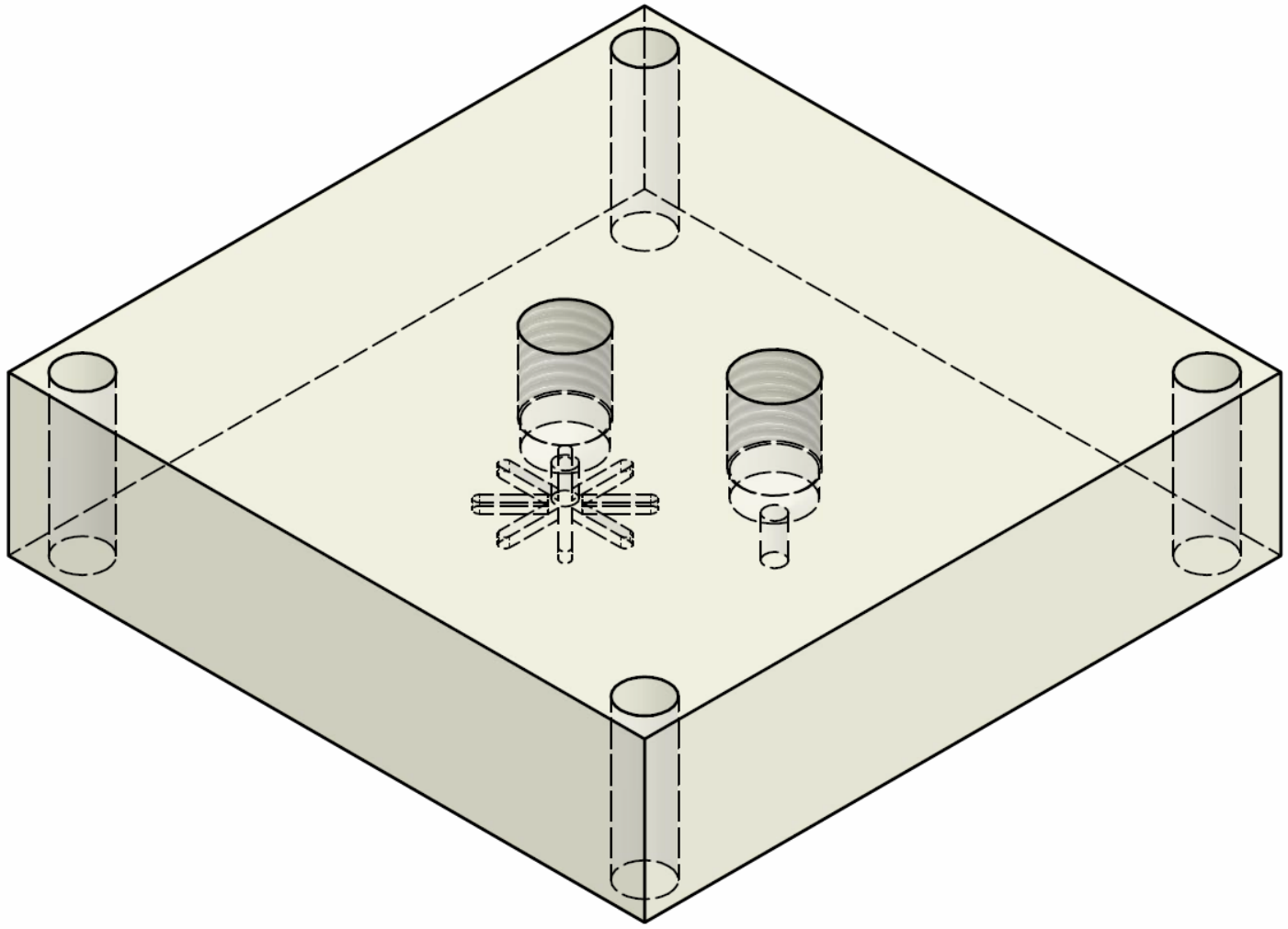

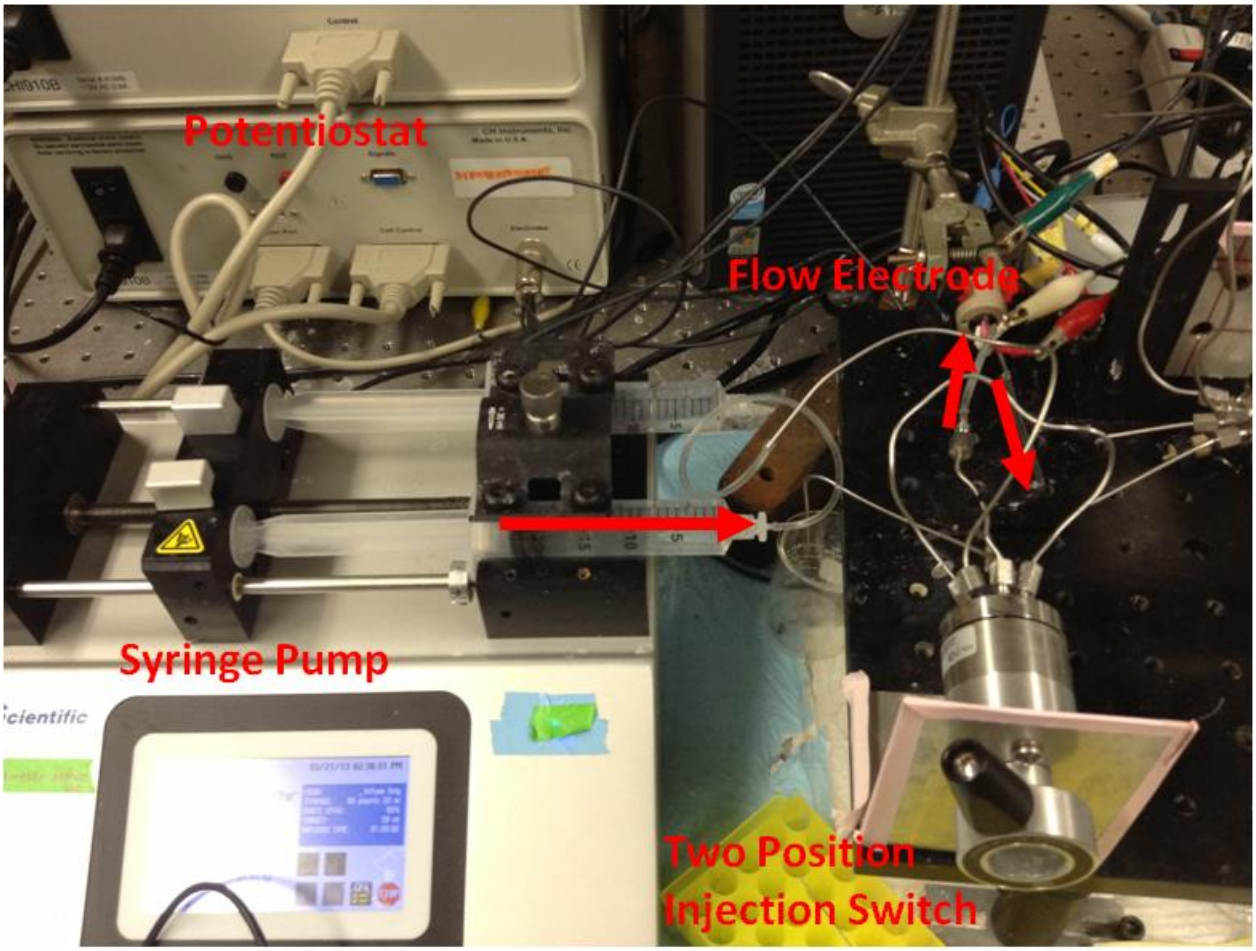
Potentiostat
Flow Electrode
Syringe Pump
Two Position
Injection Switch

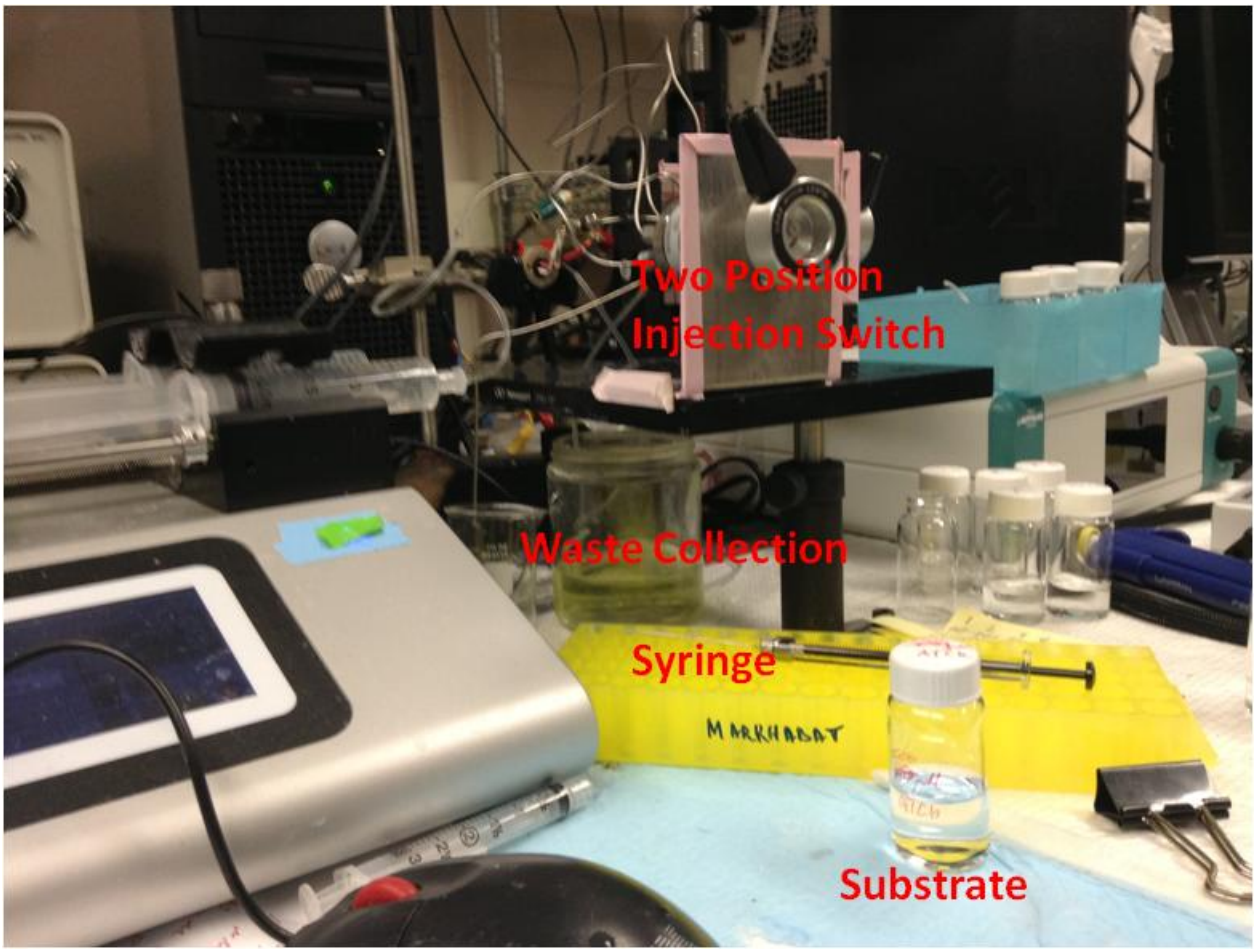
Two Position
Injection Switch
Waste Collection
Syringe
Substrate

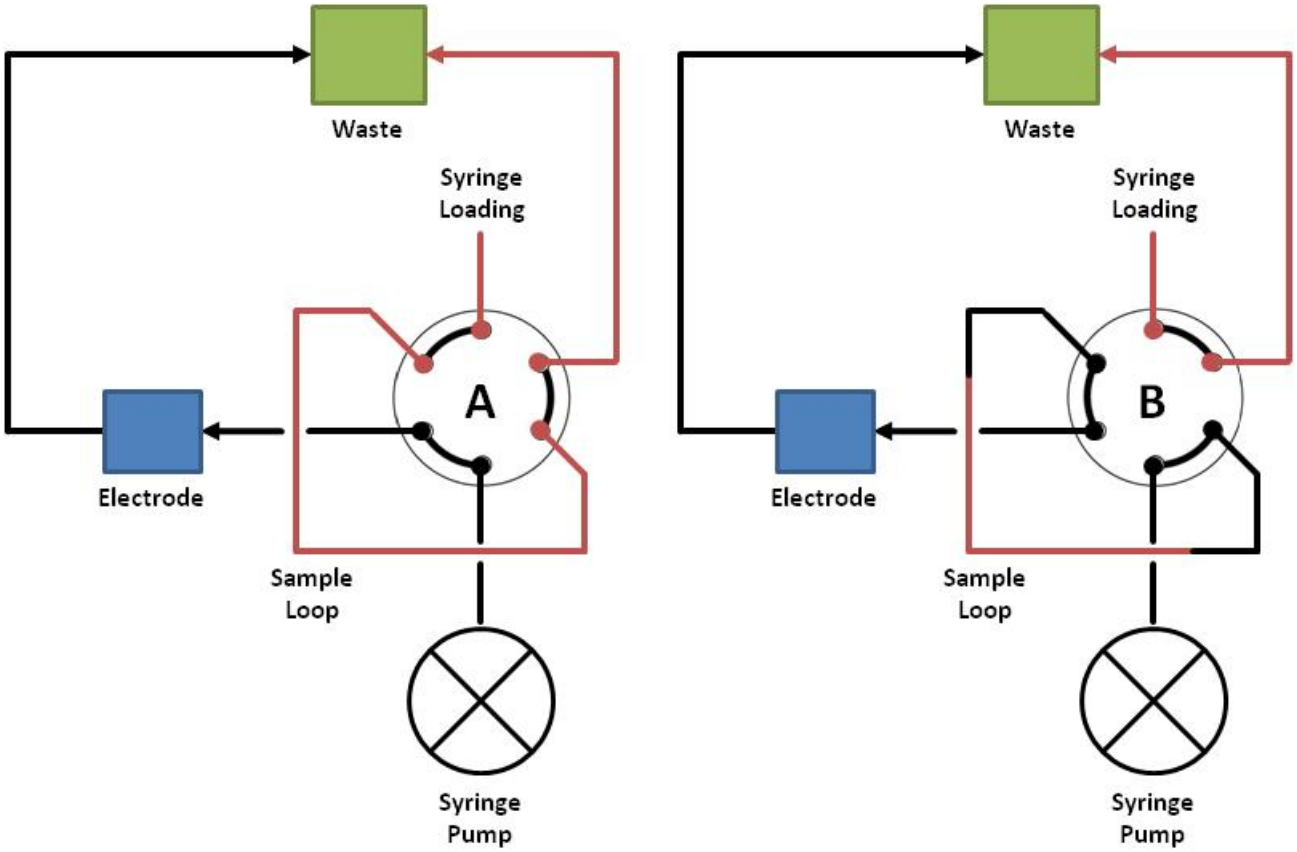
Waste
Syringe
Loading
A
Electrode
Sample
Loop
Syringe
Pump
Waste
Syringe
Loading
B
Electrode
Sample
Loop
Syringe
Pump

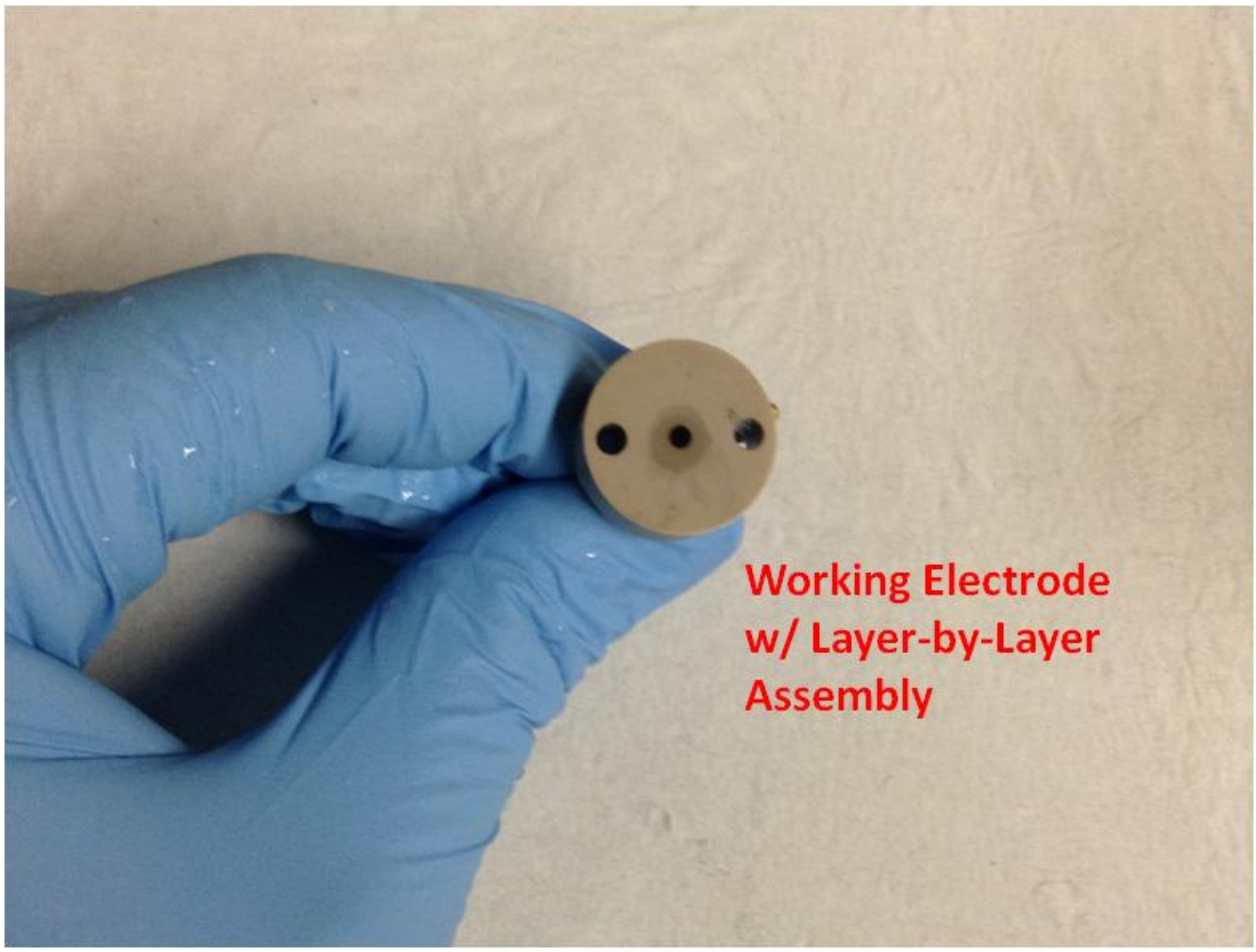
Working Electrode
w/ Layer-by-Layer
Assembly